UCRL-16231

UNIVERSITY OF CALIFORNIA

Lawrence Radiation Laboratory
Berkeley, California

AEC Contract No. W-7405-eng-48

SEMICONDUCTOR DETECTORS for NUCLEAR SPECTROMETRY*

Fred S. Goulding

July 30, 1965

*Lectures to be given at Herceg-Novi, Yugoslavia, August, 1965.

COMPTON DETECTORS

UCRL-16231
Errata

UNIVERSITY OF CALIFORNIA
Lawrence Radiation Laboratory
Berkeley, California

AEC Contract No. W-7405-eng-48

September 24, 1965

ERRATA

TO: All recipients of UCRL-16231

FROM: Technical Information Division

Subject: UCRL-16231, "Semiconductor Detectors for Nuclear Spectrometry," by Fred S. Goulding, dated July 30, 1965.

Please make the following corrections on subject report.

Figures 3-2 and 3-3 should be replaced by the attached figures.

Page 91, line 12 should be changed to read
"The Fano factor established by these measurements is .30 ± 0.03 which is entirely consistent with the approximate value of 0.32 derived from Van Roosbroeck's curves."

111 LABORATORY LIBRARY
298 LECONTE HALL

UNIVERSITY OF CALIFORNIA
Department of Physics
BERKELEY 4, CALIFORNIA

RETURN POSTAGE GUARANTEED

SEMICONDUCTOR DETECTORS FOR NUCLEAR SPECTROMETRY

Table of Contents

List of Figures v

Foreword vii

1.1 Introduction 1

1.2 Properties of Solid-State Detector Materials 4

1.3 Semiconductor Properties of Silicon and Germanium 7

1.3.1 Intrinsic Material Properties 7

1.3.2 Extrinsic Material General Properties 10

1.3.3 More Detailed Behavior of Carriers in Extrinsic Material . . 13

1.4 Junctions in Semiconductors 17

1.4.1 Descriptive Junction Theory 17

1.4.2 Reverse Biased Junction 19

1.4.3 Junction Capacitance 20

1.4.4 Junction Leakage Currents 21

1.4.5 P-I-N Junctions 24

1.4.6 Metal to Semiconductor Surface Barrier Junctions 25

Lecture 1. Figure Captions 29

2.1 Introduction 39

2.2 Discussion of Purity of Semiconductor Materials 40

2.3 Diffused Silicon Detectors 41

2.3.1 Elementary Considerations 41

2.3.2 Surface Properties 45

2.3.3 Preparation of Diffused Detectors 49

2.4 Compensation by Lithium Drifting 53

2.4.1 General Principles 53

2.4.2 Secondary Effects in Lithium Drifting 57

2.4.3 Surface Effects in Lithium-Drifted Devices 60

2.4.4 Preparation of Lithium-Drifted Silicon Detectors 60

2.4.5 Preparation of Lithium-Drifted Germanium Detectors 64

2.5 Detectors Not Employing Junctions 67

2.6 Making The Choice Between Detector Types 69

Lecture 2. Figure Captions 72

3.1 Introduction 87

3.2 Statistical Spread in the Detector Signal 88

3.3 Electrical Noise Sources 91

3.4 Effect of Amplifier Shaping Networks 95

3.5 Vacuum Tubes as the Input Amplifying Device 103

3.6 Alternative Lou Noise Amplifying Elements 107

3.7 Additional Sources of Signal Amplitude Spread 113

3.7.1 Noise Contribution of Main Amplifier 113

3.7.2 Gain Drifts 114

3.7.3 High Counting Rates 114

3.7.4 Finite Detector Pulse Rise Time 115

Lecture 3. Figure Captions 118

4.1 Detector Pulse Shape 138

4.1.1 Pulse Shape Due to a Single Hole-Electron Pair in P-I-N Detector 139

4.1.2 Pulse Shape Due to a Single Hole-Electron Pair in a p-n Junction Detector 141

4.1.3 Pulse Shape Distribution for Gamma-rays in Germanium P-I-N Detectors at 77°K 146

4.1.4 Pulse Shape Distribution for Protons and Alpha-Particles Stopping in a Lithium-Drifted Silicon Detector 149

4.2 Radiation Damage in Detectors 150

4.2.1 Damage Mechanism 150

4.2.2 Consequences of Damage in p-n Junction Detectors 153

4.2.3 Consequences of Damage in Lithium-Drifted Silicon Detectors 156

Acknowledgements 159

Lecture 4. Figure Captions 160

References . . . . , ... 169

Table 1.1 Some Properties of Silicon and Germanium 27

Table 1.2 Impurities in Ge & Si 28

Table 3.1 Noise Integral and Peak Response of Several Networks . . 116

Table 3.2 Input Pulse Shape Dependancc of Several Shaping Networks 117

LIST OF FIGURES

Fig. 1.1 Unit Cell of Single Crystal Si and Ge 30

Fig. 1.2 Variation of Mobility with Temperature in Pure Samples . . . 31

Fig. 1.3 Resistivity - Impurity Concentration for Si 32

Fig. 1.4 Resistivity - Impurity Concentration for Ge 33

Fig. 1.5 Effect of Impurities on Mobility 34

Fig. 1.6 Resistivity Temperature Relation for an Extrinsic Silicon Sample 35

Fig. 1.7 Diagram of a P-N Junction in Equilibrium 36

Fig. 1.8 A Reverse Biased P-N Junction 37

Fig. 1.9 An N^+ PP^+ Punch-Through Diode 38

Fig. 2.1 Depletion Layer Thickness Curves for N and P-Type Silicon . 73

Fig. 2.2 Illustration of Charge Injection at Rear Contact 74

Fig. 2.3 Models of Surface Layers at Junction Edge 75

Fig. 2.4 Effect of Ambients on Leakage Current of a Junction 76

Fig. 2.5 Guard-Ring Structure 77

Fig. 2.6 Typical Leakage Curve for Guard-Ring Detector 78

Fig. 2.7 Steps in Preparing a Planar Junction Device 79

Fig. 2.8 Distribution of Lithium at States of Lithium Drift 80

Fig. 2.9 Drifted Region Thickness - Time Relationship for Silicon . . 81

Fig. 2.10 Drifted Region Thickness - Time Relationship for Germanium . 82

Fig. 2.11 Illustration of Silicon Wafer Prior to Drifting 83

Fig. 2.12 Cutaway View of Lithium-Drifted Silicon Detector 84

Fig. 2.13 Germanium-Lithium-Drift Unit 85

Fig. 2.14 Diagram of Germanium Detector Holder and Cryostat 86

Fig. 3.1 Diagrammatic Representation of Energy Loss Process 119

Fig. 3.2 Calculated Yield and Fano Factor 120

Fig. 3.3 Resolution-Energy Relationship Data for Germanium 121

Fig. 3.4 Typical Electronics for Spectroscopy 122

Fig. 3.5 Simplified Input Equivalent Circuits 123

Fig. 3.6 Typical Shaping Networks and Their Frequency Response . . . 124

Fig. 3.7 Pulse Response of Several Networks (Unit Function Input) . 125

Fig. 3.8 EC-1000 Preamplifer 126

Fig. 3.9 Noise Performance Curves for EC-1000 Preamplifer 127

Fig. 3.10 EC-1000 Preamplifer: Effect of Double Integrator 128

Fig. 3.11 EC-1000 Preamplifer 129

Fig. 3.12 EC-1000 Preamplifer Rise Time Curves 130

Fig. 3.13 Bulk Field-Effect Transistor (N-Channel Type Illustrated) . 131

Fig. 3.14 General Purpose Field Effect Transistor Preamplifer 132

Fig. 3.15 Predicted Noise Behavior of Field-Effect Transistor at 300°K 133

Fig. 3.16 Predicted Noise Behavior of Field Effect Transistor at 77°K 134

Fig. 3.17 Circuit for Low Temperature Tests on Field-Effect Transistors 135

Fig. 3.18 Noise Performance of TIS-05 Field Effect Transistor 136

Fig. 3.19 Noise Performance of Amelco 2N3458 Field-Effect Transistor. 137

Fig. 4.1 Collection of Hole-Electron Pair in a p-i-n Detecotr . . . 161

Fig. 4.2 Signal Output Due to a Single Electron Hole Pair in a p-i-n Detector 162

Fig. 4.3 Collection of Hole-Electron Pair in a P-N Junction 163

Fig. 4.4 Signal Output due to a Single Electron-Hole Pair in a P-N Junction Detector 164

Fig. 4.5 Expected Range of Pulse Shapes from p-i-n Germanium Detector at 77°K 165

Fig. 4.6 Distribution in Triggering Delays of a Discriminator set to β-Peak Pulse Amplitude from a Germanium Detector 166

Fig. 4.7 Detector Pulse Shape for Alphas 167

Fig. 4.8 Frenkel Defect Production by Alphas and Protons (Silicon) . 168

SEMICONDUCTOR DETECTORS FOR NUCLEAR SPECTROMETRY

Fred S. Goulding

University of California
Lawrence Radiation Laboratory
Berkeley, California

July 30, 1965

FOREWORD

These lectures were prepared for presentation at the Summer School for Physicists to be held in Herceg-Novi, Yugoslavia, August, 1965. For the most part they constitute a collection of essential information on the detectors and associated systems. Although some important contributions by other groups to the topic are discussed, no effort has been made to present a detailed review of the voluminous literature on the subject. Therefore, the notes given here must be regarded largely as an account of the work of one group in this field. Very few experimental results obtained with semiconductor detector spectrometers are included as this material should be covered by other speakers at the meeting.

LECTURE 1. DESCRIPTIVE THEORY OF SEMICONDUCTORS

Fred S. Goulding

Lawrence Radiation Laboratory
University of California
Berkeley, California

July 30, 1965

1.1 INTRODUCTION

Much of nuclear physics research is concerned with the measurement of the energy of radiation emitted by nuclei undergoing energy transitions. Consequently, the development of nuclear structure studies has depended largely upon techniques of accurate energy measurement. The most precise energy measurements are based on the effect of magnetic fields in bending the path of electrically charged particles. However, the poor geometrical efficiency and the inability of such devices to allow simultaneous measurenents over a wide range of energies restrict the usefulness of these techniques except for primary standard energy measurements. The high data accumulation rate of a pulse amplitude analyzer fed by a detector which totally absorbs photons or particles to produce a signal linearly proportional to the energy absorbed has made these techniques very useful for general nuclear energy measurements. Gridded ionization chambers and scintillation detectors have been used in such systems and, in recent years, semiconductor detectors have assumed increasing importance.

In our laboratory, semiconductor detectors have almost completely replaced scintillation and gaseous detectors in all nuclear structure work ranging from work with natural alpha, beta and gamma radiations to nuclear reaction studies in the 10 to 100 MeV range. The reason for this sudden change lies primarily in the improvement in energy resolution obtained by

use of these detectors, an improvement which ranges from about 2:1 for low-energy alpha particles to 10:1 for high-energy (~100 MeV) alpha particles and 20:1 for gamma-rays of medium energy (~600 keV). As compared with gaseous detectors the small size of semiconductor detectors and their ability to totally absorb the energy of fast electrons and other particles are additional factors in favour of semiconductor detectors. When compared with NaI (Tl) and other scintillator crystals, the gamma-ray efficiency of presently available semiconductors is poor, in general, but our experience is that good energy resolution is more important than very high efficiency which can usually be compensated for by using more active sources.

While a detailed examination of the problems of energy spread in detector systems will be made in Lecture #3 it is desirable that we briefly review here the basic reasons for the improved energy resolution in semiconductor detectors. In gaseous detector systems electrical noise in the pulse amplifier and statistical fluctuations of ion-pair production in the detector both limit the accuracy of energy measurements. For a 5 MeV alpha-particle (a typical particle in ion chamber applications) about 2×10^5 ion pairs will be produced assuming that 25 eV are required on the average to produce an ion pair. If normal statistical variations existed in this number, an RMS fluctuation of about 500 ion pairs might be expected. As pointed out by Fano[1,2] RMS fluctuations will be less than this by a factor of about 0.6.* Therefore, RMS fluctuation will be about 300 ion pairs. The electrical noise in existing high quality amplifiers contributes an effective RMS input signal fluctuation of about 300 ion pairs also and by adding these two sources of spread in quadrature we find that the total effective fluctuation should be about 420 ion pairs RMS or 1000 ion pairs** full width at half maximum (FWHM is used in the

*The Fano factor (= $\frac{\text{Mean Square Fluctuation}}{\text{Av. No. of Ion Pairs}}$) is assumed here to be 0.4.

**For Gaussian noise the ratio of FWHM/RMS is about 2.3.

remainder of this text). The theoretical FWHM energy resolution for gaseous ion chambers is therefore about 20 keV. In most practical situations this result is not realized and 30-40 keV is more common.

Scintillation detectors suffer from quite different sources of signal spread. The inefficiency involved in the scintillation mechanism, light collection and photo-emission from the cathode of the photomultiplier, results in large statistical fluctuations in the number of photo-electrons emitted by the photo-cathode for a given amount of energy absorbed in the scintillating crystal.* In the case of a NaI (T1) scintillator-photomultiplier system, at least 300 eV of energy is absorbed in the crystal for every photo-electron released. For a 300 keV gamma-ray this results in a FWHM spread of about 25 keV or almost 10%. The energy distribution of electrons produced in the scintillatar by one gamma-ray may differ considerably from that produced by another and since the scintillator light output is not a linear function of electron energy a further spread in light output for gamma-ray interactions is introduced.[4,5] This effect becomes important for high gamma-ray energies, Fortunately the phototube is a noiseless amplifying device and, apart from minor contributions due to statistical variations in the numbers of electrons released by the secondary emission surfaces, it does not further degrade the output signal.

Detectors employing direct collection of ionization in certain solids possess one striking fundamental advantage over scintillation and gaseous detectors. In single crystal semiconductors of the types considered here, a hole-electron pair is produced for about every 3 electron volts (on the average) absorbed from the radiation. This figure is almost a factor of 10 smaller than the equivalent quantity for gaseous detectors and a factor of 100 smaller than

---

*We will not deal here with the details of the scintillation mechanism. Refer to Ref. 3 for details.

that for scintillation detectors. For this reason, statistical fluctuations in the charge prdouction process in the detector are small. Moreover, since the charge flow in the detector is almost 10 times larger than in the gaseous detector, the effect of pulse amplifier noise is reduced by a similar factor. Unfortunately collection of ionization in solids is, in general, a difficult process and some rather rigid requirements must be placed upon the character of the solid. Our next section will discuss these requirements and the characteristics of suitable material.

1.2 PROPERTIES OF SOLID-STATE DETECTOR MATERIALS

We will assume initially that the detector consists of a rectangular block of material with electrodes in good electrical contact with two opposite faces of the block. A potential is applied to the electrodes to produce an electric field in the solid which will (hopefully) sweep out any electrical carriers produced by an ionizing event. Carriers of both polarities (negative electrons and positive holes) will be produced in equal numbers by the ionizing event. As we wish to measure the quantity of ioniaation produced (which is proportional to the energy absorbed from the radiation) it is important that the charge flow in the external circuit of the detector be equal to the total ionization or to some definite fraction of it. In practice the latter possibility is impossible and we are forced to meet the first condition.

The material properties of importance are as follows:

(a) The average energy required to produce a hole-electron pair should be as small as possible. The reasons for this requirement are apparent from the previous discussion. A portion of is used to lift electrons through the band gap from the conduction to valency

band and the remainder is wasted in thermal losses (principally to optical modes of vibration) in the solid. As a general rule this factor favors materials with small band-gaps but the situation is complicated by other factors.

(b) The material should contain few free carriers at the operating temperature as such carriers will be swept to the electrodes in the same way as those produced by the ionizing events and will tend to spread and conceal the wanted signals. This requirement immediately eliminates conductors from consideration and since, in semiconductors and insulators, the thermal activation of electrons across the band-gap is a mechanism for production of free carriers, it, favors wide band-gap materials. Since this conflicts with property (a) a compromise is necessary and the ideal compromise will depend upon the operating temperature. To be of interest materials must produce thermal generation currents in the volume of the detector smaller than 10^{-7} amperes. For some applications even smaller currents than this are required.

(c) The previous requirement suggests that an insulator might be ideal if a rather high value of   is tolerable. However, it is very important that the material used should not contain significant numbers of trapping centers capable of holding electrons or holes produced by the ionizing events. If this were to happen we would lose part of our signal with disastrous consequences. This requirement immediately narrows down the choice of materials to those available as almost perfect single crystals (free of impurities to levels of about 1 part in 10^9 or better and free of crystal imperfections). Moreover materials having wide band-gaps tend to contain

many deep trapping centers and are therefore eliminated on this count. We will characterize the trapping process by the trapping lifetime of a carrier $_T$ which is the average time a carrier exists in a free state before being trapped

(d) Recombination of holes and electrons during the charge collection process must be very small. In practice, recombination occurs primarily through the intermediary of trapping at energy levels near the middle of the band-gap. It is of interest to note that this is related to the property (b) as the primary source of thermally generated conduction electrons in semiconductors is a double-jump process whereby an electron in the valency band is excited info a trapping level near the middle of the band gap and then re-excited into the conduction band. Recombination in a semiconductor is characterized by the carrier lifetime $_R$ and we desire this to be large compared with the charge collection time.

(e) The effect of both trapping and recombination must be related to the carrier collection time $_C$ if the magnitude of the carrier loss is to be evaluated. Ideally the collection time $_C$ should be very short which demands that both holes and electrons should be highly mobile in the lattice. Also the material should be able to support high electric fields without secondary ionization resulting. In most cases, surface effects limit the applied voltage more than bulk effects.

(f) The nuclear properties of a material are also important in its application for detectors. Other things being equal one would like to use materials containing elements of high atomic number to

improve the absorbtion properties of the detector. These requirements are secondary to the electrical requirements discussed in the previous paragraphs which must be met if satisfactory detection is to be achieved. However, the nuclear requirements will certainly influence future work on materials and have already resulted in the use of germanium for gamma-ray detectors in preference to silicon which, in most other respects, is a preferable material.

1.3 SEMICONDUCTOR PROPERTIES OF SILICON AND GERMANIUM

Only two materials are known to approach the requirements of the previous section. Early work in the semiconductor device area (e.g., transistors) was based largely on using germanium and the extensive program of research and development on this material resulted in it becoming available in the form of highly pure single crystals. Later, emphasis on higher temperatures of operation for semiconductor devices resulted in silicon becoming available with quality equal or even superior to germanium. These two materials are now the only ones we are able to use for accurate nuclear spectrometry. We will now digress from our main topic to consider the properties of silicon and germanium as examples of a general class of semiconductors.

1.3.1 Intrinsic Material Properties

Both silicon and germanium crystals are particularly simple in their structure. Fig. 1.1 shows the arrangement of the atoms in a simple valency bond model of a pure crystal of silicon or germanium. Each atom (valency 4) is seen to have its valency bonds oriented equally in space and to donate a single electron to each bond with its four neighbors. Each bond therefore contains a pair of electrons giving a particularly stable structure.

At very low temperatures all valency electrons are bound into the structure and no electrons are available to take part in electrical conduction. Therefore these materials are insulators at these temperatures. At higher temperatures a small number of the covalent bonds are broken by thermal excitation so that electron-hole pairs are produced in the material. In the energy band model, electrons are said to be thermally excited from the valency to conduction band. The quantities of such electron-hole pairs clearly depend upon the temperature and the band-gap (binding energy in the valency bond model). Under normal conditions the number n_i of conduction electrons in the material (called intrinsic since no impurities are present) is given by:

$$n_i = A\, T^{\frac{3}{2}}\, e^{-\frac{E_g}{2\,kT}} \tag{1.1}$$

where A is a constant for a given material,

T is the absolute temperature (°K),

E_g is the band gap,

k is Boltzman's constant.

At normal temperatures the exponential term dominates the temperature dependence.

Once an electron is in the conduction band it is influenced by any electric field applied to the crystal. In normal electric fields this influence is small compared with effects due to the fields produced by atoms in the lattice itself but the applied electric field causes a slow drift of the electrons whereas the effects of the crystal atoms are random

in nature. We can characterize the movement of the electrons in the applied electric field by a mobility μ_e defined by the relationship:

$$V_e = \Sigma \cdot \mu_e \tag{1.2}$$

where V_e = average electron drift velocity in the field direction and E is the electric field.

The positively charged hole left in the valency structure is also free to move* in the electric field. Its movement is characterized by a mobility μ_h defined in the same way as that for the electron in equation (1.2). Combining the currents due to electrons and holes we see that the resistivity of the material is given by:

$$= \frac{1}{q\ (n_e\mu_e + n_h\mu_h)} \tag{1.3}$$

where is the material resistivity,

n_h is the number of holes/cc,

n_e is the number of conduction electrons/cc, and

q is the electric charge.

For intrinsic material, every electron excited into the conduction band produces a hole too so that $n_e = n_h = n_i$:

$$\therefore\ _i = \frac{1}{q\ n_i\ (\mu_h + \mu_e)} \tag{1.4}$$

Using the constants listed in Table 1.1 we find that:

$_i$ for germanium is about 65 ohm/cm, and

$_i$ for silicon is about 230 x 10^{-3} ohm/cm,

both values being derived at 300°K. At 77°K virtually no electrons are

*This can be interpreted as a retrograde motion of electrons from filled positions in the band structure to fill the hole or more correctly, as an alternative quantum mechanical behavicur of the electrons in the valency band.

excited into the conduction band and intrinsic silicon and germanium are excellent insulators at that temperature.

The carrier mobility μ, as well as n_i, is temperature dependent. The dependance of μ on temperature in very pure crystals of good quality is dominated by lattice scattering (i.e., interactions of thermal lattice vibrations with the electron wave travelling in the structure). As the temperature is reduced, the mobility increases. For example, μ_h for silicon changes from 480 $cm^2/V.$ sec at 300°K to about 2×10^4 $cm^2/V.$ sec at 77°K. The temperature dependance of μ_e, μ_h and n_i is indicated in Table 1. Fig. 1.2 shows the bahaviour of μ_e and μ_h in silicon and germanium over a wide temperature range.

1.3.2 Extrinsic Material General Properties

In practice, semiconducting materials of sufficient purity to be regarded as intrinsic, particularly at low temperatures, are not available to us. Generally speaking, the term intrinsic is used rather loosely to imply that electrical conduction is dominated by thermally excited electron-hole pairs rather than by electrons or holes produced by impurities. Thus, at high enough temperatures we can refer to any semiconductor as being intrinsic. In the case of germanium it is possible to purify the material to the degree where the material is intrinsic at room temperature. To accomplish this, impurities* must be reduced below about 10^{13} atoms/cc (i.e., 1 part in 5×10^8) which is just possible. For conduction in silicon to be considered intrinsic at room temperature, the impurity concentration* would have to be reduced to about 10^{10} atoms/cc (i.e., 1 part in 5×10^{11}) which is not practicable. Therefore, for most practical purposes, we have

*We refer here only to electrically active impurities.

to deal with materials in which conduction is dominated by electrical carriers introduced by impurities in the silicon or germanium. This is known as extrinsic material and the conduction is termed extrinsic too.

The electrically active impurities most commonly deliberately introduced into semiconductors are elements of valency 3 or 5 which can substitute for silicon atoms at lattice sites. Thinking in terms of the valency bond model we can regard a valency 5 atom (e.g., phosphorous, arsenic, antimony) which replaces a silicon atom in the lattice as supplying the electrons to complete the co-valent bond structure while the fifth electron associated with the impurity atom is only very loosely bound to its parent atom by Coulomb attraction. This attraction is very small partly due to the fact that the atom is embedded in a medium of high dielectric constant (12 for silicon, 16 for germanium). At normal temperatures the spare electron is thermally excited into the conduction band so that we now have a free electron and a fixed localized positive charge embedded in the lattice in the vicinity of the impurity atom. Such impurities are called donors and, since the electrical conduction in such materials is dominated by negative charge carriers, the material is said to be n-type. Conversely, replacement of silicon atoms by valency 3 atoms (e. g., boron, aluminum, gallium, and indium) produces holes and fixed negative charge centers; the material is p-type and the impurity is called an acceptor. In an energy band model the effect of donors is to introduce permitted discrete levels (localized in the vicinity of the impurity atoms) in the forbidden gap close to the conduction band. Conversely the effect of acceptors is to introduce levels close to the valency band. Donors and acceptors such as these are easily ionized. Table 1.2 lists the ionization energy for some of these cases.

In detector technology we are particularly concerned with a number of other types of center in the lattice. For the present we will note that an interstitial atom can act as a donor or acceptor giving free holes and/or electrons. A good example of this is lithium which acts as a shallow* interstitial donor in silicon and germanium. Certain other impurities acting in a substitutional or interstitial role like gold in silicon or copper and nickel in germanium introduce acceptor and/or donor levels near the middle of the forbidden gap. Note that certain impurities can introduce both donor and acceptor levels. We can picture this as depending upon the position occupied by the impurity atom in the lattice. For example, gold introduces both an acceptor and donor level near the middle of the energy gap. As one might expect, a valency 2 substitutional impurity tends to produce a double acceptor while a valency 6 substitutional impurity tends to produce a double donor.

Another matter of concern to us is the number of traps in the material. These traps may arise due to impurity centers or crystal imperfections (vacancies, dislocations, etc.) and may exhibit preferential trapping properties for either holes or electrons. The traps are of interest in that they provide intermediate levels in the forbidden gap through which recombination and generation processes can take place. Moreover, if the traps are selective for holes (or electrons) and the trapped carriers are not easily re-excited, localized storage of electrical charge may occur and this may inhibit collection of carriers in the device. This is particularly important in low temperature operation of devices and is the cause of the phenomena generally referred to as polarization in detectors.

---

*The term shallow implies that the level introduced by the impurity is close to the conduction band (donor) or valency band (acceptor).

1.3.3 More Detailed Behaviour of Carriers in Extrinsic Material.

Considering, for the moment, intrinsic material in equilibrium, an average number n_i electrons occupy the conduction band and a similar number of holes exist in the valency band. We have to remember that this equilibrium results from the balance between excitation of electrons into the conduction band (called generation) and by electrons falling back into holes in the valency band (recombination). The rates of generation and recombination can be increased by introducing traps into the forbidden gap as these traps provide the potential for a double step process which can clearly proceed at a faster rate than if electrons have to jump across the whole energy gap in one step. Traps at the center of the energy gap are most effective in increasing the generation and recombination rate as the two steps are then equal. Despite the increased rate of recombination and generation the equilibrium density of electrons and holes is the same in material containing large or small numbers of such traps. In a non-equilibrium condition, however, in which an applied electric field sweeps out carriers immediately they are produced, the high generation rate induced by traps considerably increases the leakage current and, from this point of view, traps (particularly in mid-band) are undesirable. We will pursue this point later.

Now let us examine the introduction of a small amount of a donor impurity into the semiconductor. This increases the number of electrons from n_i to n. Let the consequent alteration in the hole population be from n_i to p. The recombination rate between hole and electrons must be proportional to the product $(n \cdot p)$ of the numbers of such carriers present in the material. We can assume that the generation rate is only dependent upon valency bonds

which are far more numerous than the impurity atoms. Since the thermal generation rate (at impurity levels commonly encountered) is therefore the same as for intrinsic material and the recombination rate in such material is proportional to n_i^2 we can write:

$$n \cdot p = n_i^2 \qquad (1.5)$$

Thus we see that the effect of increasing the electron population by adding donors is to suppress the hole population to satisfy equation (7.5). Similarly, if we introduce acceptors, the electron population is reduced. These remarks apply at a fixed temperature; if the temperature is changed, n_i must be chosen for the new temperature.

To appreciate the effect of this minority carrier suppression by introducing majority carriers we may examine the case of silicon at room temperature 300°K). In this case, $n_i = 1.5 \times 10^{10}$/cc. Let us now introduce 1.5×10^{11} donors/cc (i.e., about one atom in 4×10^{10}). The hole population will now only be 1.5×10^9 - a factor of 100 smaller than the electron population. Conduction in such a sample is now dominated by electrons and the resistivity is given by:

$$= \frac{1}{n_e \mu_e q} \qquad (1.6)$$

In our example, would be 35000 ohm/cm. In practice removal of impurities to this extent is impractical. However, the float-zone process in silicon can produce material in the 10000 ohm/cm (p-type) region. Figs. 1.3 and 1.4 show the resistivity as a function of donor and acceptor concentration for silicon and germanium.

We must now examine the behaviour of these extrinsic semiconductors as the temperature is changed. At high temperatures (~150°C for very pure silicon and ~60°C for very pure germanium) the value of n_i increases so

that, in the doping range of interest to us (~ 10^{12} to 10^{16} impurity atoms/cc) electrical conduction hecomes dominated by thermally excited carriers and the material is called intrinsic. As the temperature is lowered, conduction is dominated by the majority carriers and the quantity of these remains essentially the same down to temperatures at which the donor or acceptor centers become unionized (i.e., ~ 10 to 50°K). In lightly doped material the mobility is determined by lattice scattering and the mobility-temperature relationships shown in Table 1.1 apply. However, as the lattice scattering becomes smaller the effect of the Coulomb attraction of impurity atoms becomes more important and mobility becomes determined by impurity scattering. Even at moderate doping levels this effect causes the mobility to level off or decrease below about 200°K. Fig. 1.5 shows the mobility temperature relationship for some samples. In closing these remarks on mobility we must point out that, since the number of carriers remains essentially constant in extrinsic semiconductors over a wide range of temperatures while the mobility increases as the temperature decreases in the range where lattice scattering is dominant, the result is that the material exhibits a high positive temperature coefficient of resistance as seen in Fig. 1.6 over part of the temperature range. This is a surprising result on the basis of traditional views of semiconductors.

In the preceeding discussion we assumed that the extrinsic semiconductor was produced by adding either an acceptor or donor to intrinsic material. Usually, however, we are dealing with materials containing both donor and acceptor atoms. Since we have seeen that the addition of donors to a material produces the hole population so that equation (1.5) is satisfied, it is obvious that addition of donors compensates for acceptors.

If N_a = number of acceptors and N_d = number of donors and $N_a = N_d$ the material behaves very much like intrinsic material. However, the impurity scattering effect mentioned earlier in this section will still occur and the mobility-temperature relationship will not behave as it would for intrinsic material. The departure would be especially noticeable if N_a and N_d were large. An exception might occur if the donor was lithium. In this case, the positively charged lithium atoms may be mobile enough to migrate close to the acceptor atoms and to pair (i.e., be tied by Coulomb attraction) with the negatively charged acceptors. At distances of a few lattice constants the electrical effect of the electrical dipole containing the two atcns might well be negligible and the effects of impurity scattering on carriers is much reduced.

One final concept which must be discussed is that of minority carrier lifetime. For this purpose, we will assume that we are dealing with p-type material in which electrons are the minority carriers. We will suddenly introduce a number ne electrons into the conduction band. Clearly these electrons must eventually disappear by recombining with holes in the valency band. The number of electrons remaining at time t will be given by:

$$n_t = n_e \, e^{-t/ {}_R} \tag{1.7}$$

where $_R$ is the recombination lifetime.

The probability of the electron making the direct jump to recombine with a hole in the valency band proves to be very small (lifetimes of many seconds would occur in silicon if this were the only mechanism whereas the very best silicon exhibits lifetimes in the 1 to 10 msec range). As mentioned earlier, the presence of traps at or near the center of the band gap speeds up recombination. The statistics of the electron capture and emission process

at traps and the same processes for holes has been studied by Shockley[6] and we do not need to consider the details here. However, one can intuitively see that the lifetime will be reduced in the presence of large numbers of traps and that the availability of large numbers of holes* (i.e., heavily doped p-type material) also reduces the lifetime. In practice, high temperature treatments tend to produce lattice irregularities which act as traps and reduce lifetime. The presence of gold in very minute quantities in silicon introduces trapping levels with high cross-section in the center of the band gap and thereby reduces carrier lifetime by many orders of magnitude. In view of these factors it is surprising that carrier lifetimes in the range 20 to 2000 μsec are normal in fully processed detector materials.

1.4 JUNCTIONS IN SEMICONDUCTORS

1.4.1 Descriptive Junction Theory

We have so far discussed only homogeneous semiconductor materials. While the properties of such materials are interesting, practically all applications of semiconductors to detectors and other devices rely on discontinuities between regions of a semiconductor having different properties. The most important discontinuity is that existing between two regions, in cne of which the host lattice is doped with a donor (n-type) while the other is doped with a acceptor (p-type). We must examine a p-n junction of this type in some detail if the operation of semiconductor devices and particularly detectors is to be understood.

---

*This argument must be reversed if we are talking of the lifetime of holes in n-type material. Here the hole lifetime is reduced in heavily doped n-type material.

In Figure 1.7(A) the case of a junction with the n side more heavily doped than the p side is illustrated. The acceptor and donor centers are fixed in the lattice and cannot move. However the free holes and electrons can move and, at temperatures above absolute zero, diffusion of these carriers across the junction takes place. This, in turn, results in the dipole charge layer shown in Fig. 1.7(B) which produces the potential distribution shown in Fig. 1.7(C). The potential hill at the junction is such as to resist the carrier diffusion process and, therefore, its height depends upon the temperature, doping levels, etc. The p-type material contains some free electrons and, in the n-type material, some holes are produced by thermal excitation of electrons from the valency to conduction bands of the silicon host lattice. Since, in our case, the doping of the n-type material is much heavier than that of the p-type material, the density of minority electrons in the p-region will be large compared with that of minority holes in the n-region. In equilibrium a detailed balance must exist both for holes crossing the junction and for electrons. This means that the hole currents to left and right must equal each other and the electron currents each way must also equal each other. In our case the absolute value of the electron current will be very much larger than that of the hole current as illustrated in Fig, 1.7(D). The individual hole or electron currents in a junction can well be in the range of many amperes.

The equilibrium conditions are greatly disturbed if: we apply an external voltage to the junction. For example; applying a negative voltage to the n side of the junction (called forward bias) causes a large increase in the flow of electrons from the n side of the junction (where they are

majority carriers) into the p side where they are minority carriers. This process is called minority carrier injection. At the same time an increase in the number of holes injected from the p to n sides occurs. As the doping on the p side is very light the hole current will be negligible compared with the electron current. The phenomena of minority carrier injection is of major importance at the emitter junction of a bipolar transistor.

1.4.2 Reverse Biased Junction

In detector technology we are more concerned with reverse biased operation of junctions. Examining Fig. 1.8 we see what happens in this situation in our example of a junction with a lightly doped p-region. Free carriers are swept from a depletion layer of thickness W by the electric field and the dipole layer consists almost entirely of fixed donor and acceptor atoms (fully ionized). Since the charge density in the lattice is constant in each region (but different between the regions) it is easy to see that the electric field must be linear as a function of distance either side of the true junction. This results in the parabolic potential distribution shown here. In a case where the n-region doping is very heavy almost the entire junction voltage drop appears in the p-region as seen in Fig. 1.3. In this simplified case, which applies to almost all radiation detector situations, the width W is given by:

$$W = \frac{(V + V_o)^{1/2}}{2 \quad q \quad N_a} \qquad (1.8)$$

where is the dielectric constant of the material.

N_a is the net density of electrically active centers in the lightly doped region (if the material is compensated N_a is the difference between acceptor and donor concentrations).

V_o is the junction built-in potential in the equilibrium situation (~ 0.7 V for Si, 0.3 V for Ge).

The value of the maximum electric field E_p in a junction of this type is given by:

$$E_p = 2 \frac{(V + V_o)}{W} \tag{1.9}$$

This value may be of interest for two reasons. If E_p reaches values greater than 2×10^4 V/cm secondary ionization may arise. Although this would not be expected on the basis of theoretical values for the avalanche breakdown field (~ 250 kV/cm) experience has shown that most junctions, particularly of the large area type used in detectors, are not completely uniform. This results in peak fields far exceeding the value calculated from equation (1.9). A second factor also arises at high field strengths. If the carrier velocity ($= E \cdot \mu$) reaches a value close to the velocities of thermal agitation of electrons in the lattice (~ 10^7 cm/sec) the carrier velocity tends to become independent of the electric field. This may be important in collection time calculations. The limiting velocity for electrons in germanium has been studied[16] but information on holes in germanium and holes and electrons in silicon indicates that the saturation effect is not so apparent in these cases.

1.4.3 Junction Capacitance

When an ionizing particle passes into the depletion layer of a reverse biased junction a specific amount of charge is collected by the electric field. The voltage pulse developed across the junction is inversely proportional to the sum of the junction capacitance and the input capacitance at the input of the pre-amplifier used to amplify the signal. It is obvious that the signal-to-noise ratio of the system is determined by the input signal voltage and is therefore degraded if the detector capacity is large. For this reason we need to determine the junction capacitance.

The depletion layer of a reverse biased junction behaves much like an insulator with metal electrodes at either side of it. If the thickness of the depletion layer is W cm and its area A cm^2, its capacitance is given by:

$$C_D = 1.1 \frac{A}{4\ W} \text{ pf} \qquad (1.10)$$

where   is the dielectric constant of the material.

For silicon:

$$C_D \approx 1.1 \frac{A}{W} \text{ pF} \qquad (1.11)$$

For germanium:

$$C_D \approx 1.37 \frac{A}{W} \text{ pF} \qquad (1.12)$$

1.4.4 Junction Leakage Currents

Leakage currents in reverse biased p-n junctions arise from three sources. In the junction of Fig. 1.8 the three sources are:

(a) Minority holes from the n region which diffuse from a region near to the edge of the depletion layer into the depletion layer. If a hole enters the depletion layer, the electric field causes it to move rapidly across into the p-region.

(b) Minority electrons in the p-region which diffuse from a small layer at the right hand edge of the depletion layer. Once in the depletion layer the electrons travel rapidly into the n-type material. The mathematical treatment of the hole "diffusion" current and that for electrons is the same. It will be clear that the relatively heavy doping of our n-region means that the hole population in it is very small and that the electron current from the p-region will dominate as far as these diffusion currents are concerned. We will therefore only analyze its behaviour. The symbols used are shown in Fig. 1.8.

The electron current arises from thermal excitation of carriers within a diffusion length L_e of the edge of the depletion layer. The volume of material involved in generating the electron diffusion current is therefore $A \cdot L_e$. In equilibrium this volume would contain $A \cdot L_e \cdot n_p$ electrons and since each of these would exist, for an average time $_e$ the recombination current would be $\frac{A \cdot L_e \cdot n_p \cdot q}{e}$
In the case we are now concerned with, these electrons flow into the infinite sink which the depletion layer forms for electrons We therefore have:

$$\text{Diffusion current } i_D = A \cdot q \cdot n_p \cdot \frac{L_e}{e} \tag{1.13}$$

(Note that we assume that the average occupancy of the recombination centers by holes is not significantly affected by the removal of the small number of electrons which would be present in the equilibrium situation.)
Other forms of equation (1.13) can be derived using Einstein's relationship. The most useful is:

$$i_D = A \cdot n_i^2 \cdot \mu_h \cdot \rho_p \cdot q^2 \quad \frac{kT}{q} \frac{\mu_e}{\tau_e} \tag{1.14}$$

Where $_p$ is the resistivity of the p-type material.

If the constants for silicon at room temperature are inserted in this equation we obtain:

$$i_{D(Si-25^\circ C)} = \frac{16 \quad _p}{_e^{1/2}} \text{ nA/cm}^2 \tag{1.15}$$

where $_p$ is expressed in K · cm.
and $_e$ is μsec.

In a typical case for a diffused silicon junction detector $_p$ = 1 K · cm and $_e$ = 50 μsec. Here we see that i_D is 2.3 nA/cm^2 of junction area.

(c) In junctions operated with very thin depletion layers (e.g., signal diodes, transistors) the diffusion current will constitute the main bulk leakage current. However, for obvious reasons, thick depletion layers are necessary for radiation detectors. Here the generation current of electrons and holes in the large volume of the depletion layer may well become dominant as the electric field existing in this layer causes the carriers to be collected before they have the opportunity to recombine. Unfortunately, knowledge of the position of traps in the band-gap is required if an accurate calculation of this generation current is to be made and knowledge of the lifetime of carriers in the material in equilibrium is not adequate for the purpose.* If the traps are assumed to be at the center of the energy gap and with certain other simplifying assumptions the value of the generation current, i.g., in the depletion layer is:

$$i_g = A \cdot W \cdot q \cdot \frac{n_i}{2} \qquad (1.16)$$

In general this equation will overestimate the leakage current by a factor between 2 and 20 depending on the position of the traps in the band-gap.

We can rewrite equation (1.16):

$$i_g = A \cdot \frac{\cdot \;_p \cdot \mu_h \; (V + V_o)^{1/2}}{2} \cdot q \; \frac{n_i}{2} \qquad (1.17)$$

*In the case of calculating the difffusion current we assumed that the small loss of electrons did not affect the average occupancy of the traps. In a depletion layer, however, holes are removed immediately they are formed and the trap occupancy is quite different from that applying in the undepleted material.

When the constants for silicon at room temperature are included in this equation we obtain:

$$i_g = \frac{1.2\ (\ V)^{1/2}}{_e}\ \mu A/cm^2 \qquad (1.18)$$

where = p-type material resistivity in K · cm.

$_e$ = electron lifetime in the p material in μsec.

If = 1 K cm and $_e$ = 50 μsec and V = 100 V

i_g = 0.25 $\mu A/cm^2$ of junction area.

Note that this is two orders of magnitude higher than the diffusion current calculated earlier.

1.4.5 <u>P-I-N Junctions</u>

Examining Equation (1.9) we note that the depletion layer may be made very thick by reducing N_a (i.e., increasing the resistivity of the p-region in our example) and by increasing the applied voltage V. If the thickness of the slice is suitable, it is possible to "punch through" the wafer or make the depletion layer reach the back of the wafer. If a simple metal contact or an n region vere used as the back contact, electrons would be injected by the contact and be swept up in the field. This would cause a very high junction current. Indeed, even if the depletion layer did not quite reach the back contact injection from the contact would still be serious. For this reason, where the detector is designed for punch-through operation a highly doped (designated p^+) region is deliberately introduced as the back contact (if the basic material is p-type). Such a device is referred to as p-i-n (incorrectly implying an intrinsic region between p and n regions) or p- -n, or more correctly, a $n^+p\ p^+$ punch-through device (the + sign meaning highly doped). Such a device and its electric field, potential and charge distribution is shown

diagramatically in Fig. 1.9. Most of the voltage drop in the device occurs in the p-region and the electric field can be made high through the entire p-region - which is nearly the entire thickness of the wafer. If the p-region is very lightly doped and the electric field is below a value at which carrier velocity saturation occurs, the collection time for a carrier making the complete transit across the depletion layer is given by:

$$T_C = \frac{W^2}{\mu \cdot V} \tag{1.19}$$

For example, if W = 0.1 cm, μ = 500 cm^2/V sec (a hole in silicon) and V = 200 Volts then T_C = 0.1 μsec.

The thermal generation current of a p-i-n diode can be calculated from equation (1.16) with the assumption that traps are at the middle of the energy gap. If the carrier lifetime in our example were 1 msec the generation current would be 0.16 μA/cm^2.

1.4.6 Metal to Semiconductor Surface Barrier Junctions

All the forementioned types of junctions are encountered in radiation detectors. An additional one for which no very satisfactory theory exists is used in many radiation detectors. This is the so-called surface-barrier junction. Certain metals such as gold, when evaporated onto an n-type silicon or germanium surface form a rectifying barrier which behaves in many ways like a true p-n junction. The preparation of the surface prior to and following evaporation involves certain emperical procedures which are believed to form en oxide layer. However, this is not the only factor as studies have shown some relation between

the work function of the evaporated metal and the behaviour of the surface barrier. While the simple processes involved in making surface barrier devices are attractive the lack of basic understanding of the mechanism leads to serious problems. We will not devote any further discussion to this type of device.

Table 1.1. Some Properties of Silicon and Germanium[+]

	SILICON	GERMANIUM	UNITS
Atomic Number Z	14	32	-
Atomic Weight A	28.06	72.60	-
Density (300°K)	2.33	5.33	g/cc
Dielectric Constant	12	16	-
Melting Point	1420	936	°C
Band Gap (300°K)	1.12	0.67	eV
Band Gap (T°K)	$1.205-2.8 \times 10^{-4}T$	$0.782-3.4 \times 10^{-4}T$	eV
Intrinsic Carrier Density (300°K)	1.5×10^{10}	2.0×10^{13}	per cc
Intrinsic Carrier Density (T°K)	$2.8 \times 10^{16}T^{3/2}e^{-6450/T}$	$9.7 \times 10^{15}T^{3/2}e^{-4350/T}$	per cc
Electron Mobility μ_e (300°K)	1350	3900	cm^2/volt sec.
Hole Mobility μ_h (300°K)	480	1900	cm^2/volt sec.
Electron Mobility (T°K)	$2.1 \times 10^{9}T^{-2.5}$*	$4.9 \times 10^{7}T^{-1.66}$*	cm^2/volt sec.
Hole Mobility (T°K)	$2.3 \times 10^{9}T^{-2.7}$*	$1.05 \times 10^{9}T^{-2.33}$*	cm^2/volt sec.
Energy per Hole Electron Pair	3.75**	2.94	eV

[+] Data largely obtained from E. M. Conwell, Proc. IRE 46, 1281 (1958).

* Measured only over a limited temperature range (about 100-300°K for Germanium) and 160-400°K for Silicon).

** Recent measurements in our laboratory. Measurements by some authors indicate a difference between the value of in silicon for electrons and particles, (-3.61, -3.79) but we are inclined to attribute this to a charge multiplication phenomena at the surface barrier employed by these authors.

Table 1.2. Impurities in Ge & Si

ELEMENT	TYPE	IONIZATION ENERGY (eV) In Silicon	In Germanium
Boron	Acceptor	0.045	0.0104
Aluminium	"	0.057	0.0102
Gallium	"	0.065	0.0108
Indium	"	0.16	0.0112
Phosphorus	Donor	0.044	0.0120
Arsenic	"	0.049	0.0127
Antimony	"	0.039	0.0096
Lithium	" (Interstitial)	0.033	0.0093

LECTURE 1. FIGURE CAPTIONS

Fig. 1.1 Unit Cell of Single Crystal Si and Ge.

Fig. 1.2 Variation of Mobility with Temperature in Pure Samples.

Fig. 1.3 Resistivity - Impurity Concentration for Si.

Fig. 1.4 Resistivity - Impurity Concentration for Ge.

Fig. 1.5 Effect of Impurities on Mobility.

Fig. 1.6 Resistivity Temperature Relation for an Extrinsic Silicon Sample.

Fig. 1.7 Diagram of a P-N Junction in Equilibrium.

Fig. 1.8 A Reverse Biased P-N Junction.

Fig. 1.9 An N^+PP^+ Punch-Through Diode.

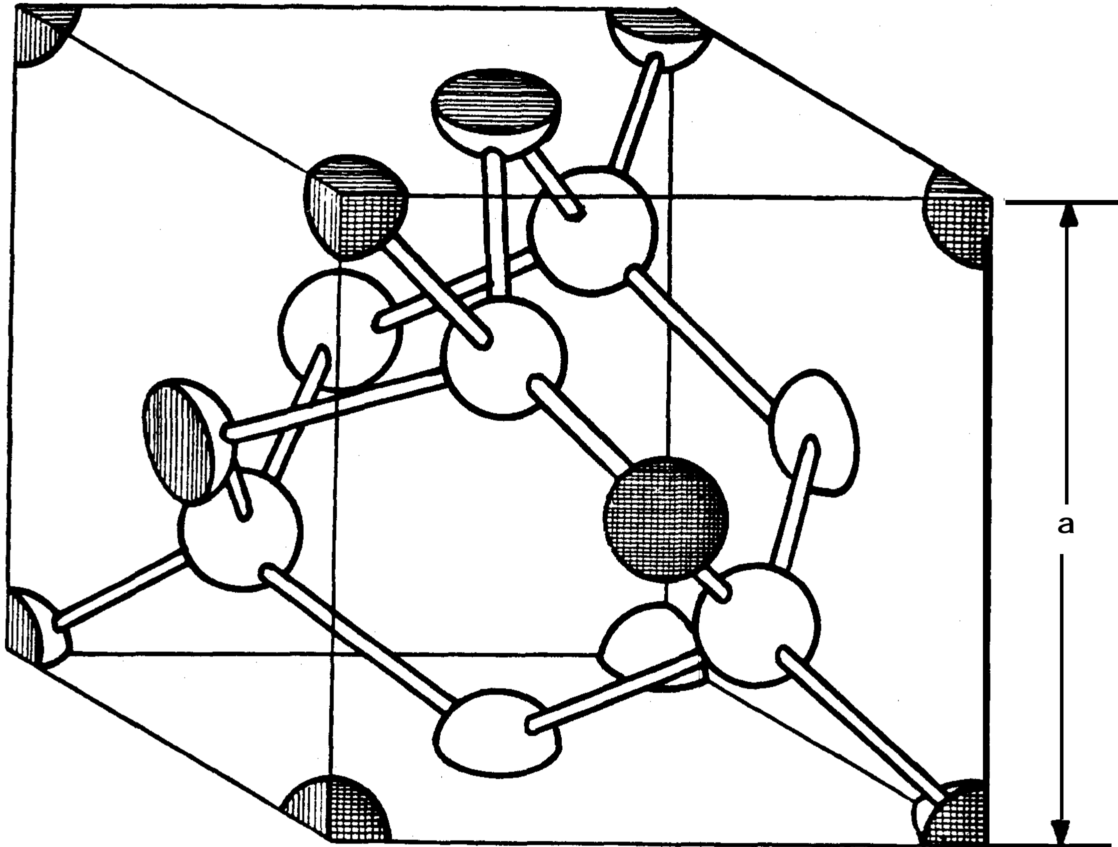

FIG I.I

UNIT CELL OF CRYSTAL OF Si & Ge

NO. OF BONDS/ UNIT CELL = 16

NO. OF ATOMS/ UNIT CELL = 6

VALUE OF a

Si - 5.43 Å

Ge - 5.66 Å

NO. OF ATOMS/cc

Si - 6.22 x 10^{21}

Ge - 5.53 x 10^{21}

MUB-6960

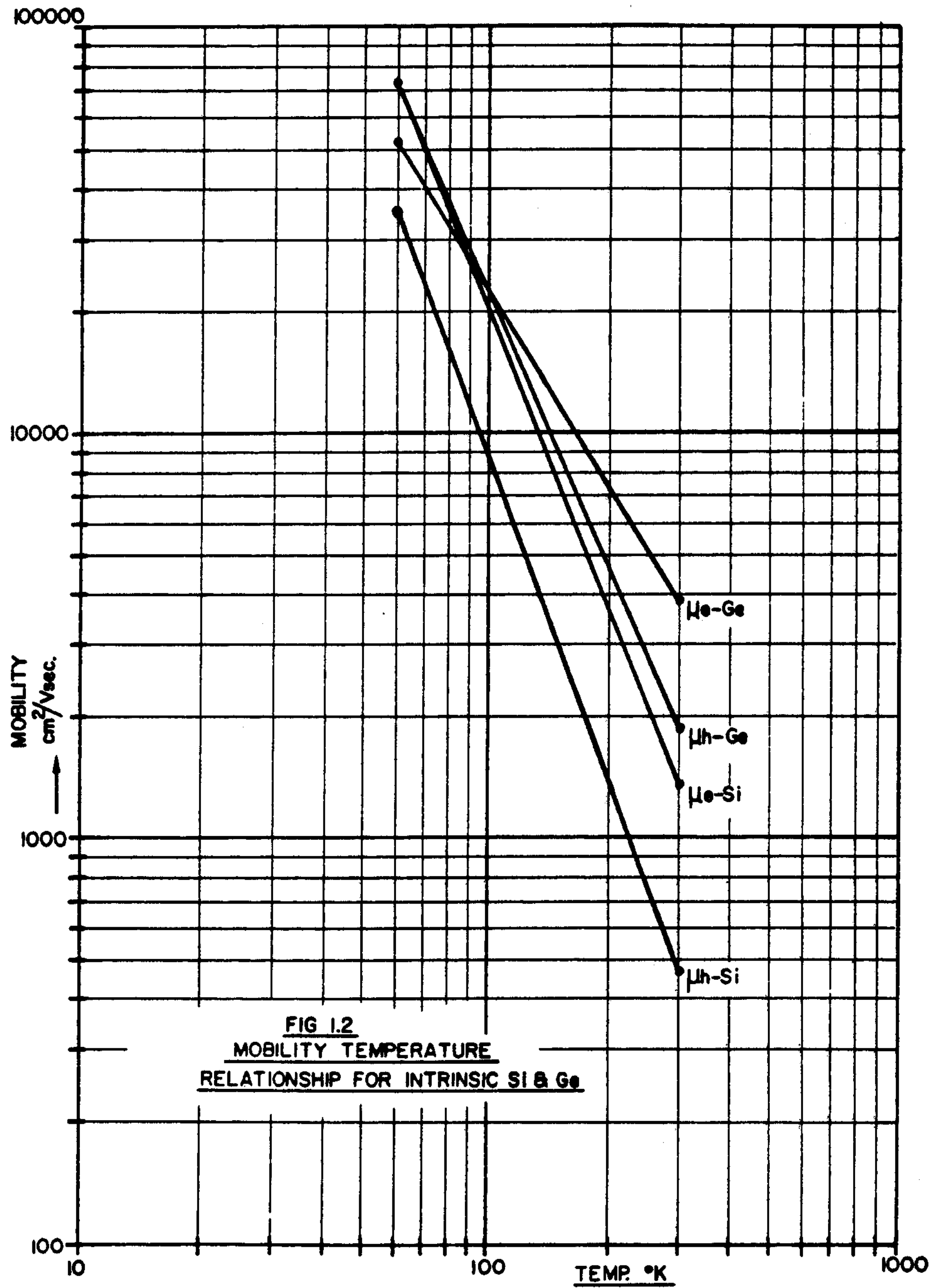

FIG 1.2
MOBILITY TEMPERATURE
RELATIONSHIP FOR INTRINSIC SI & Ge

MUB-6961

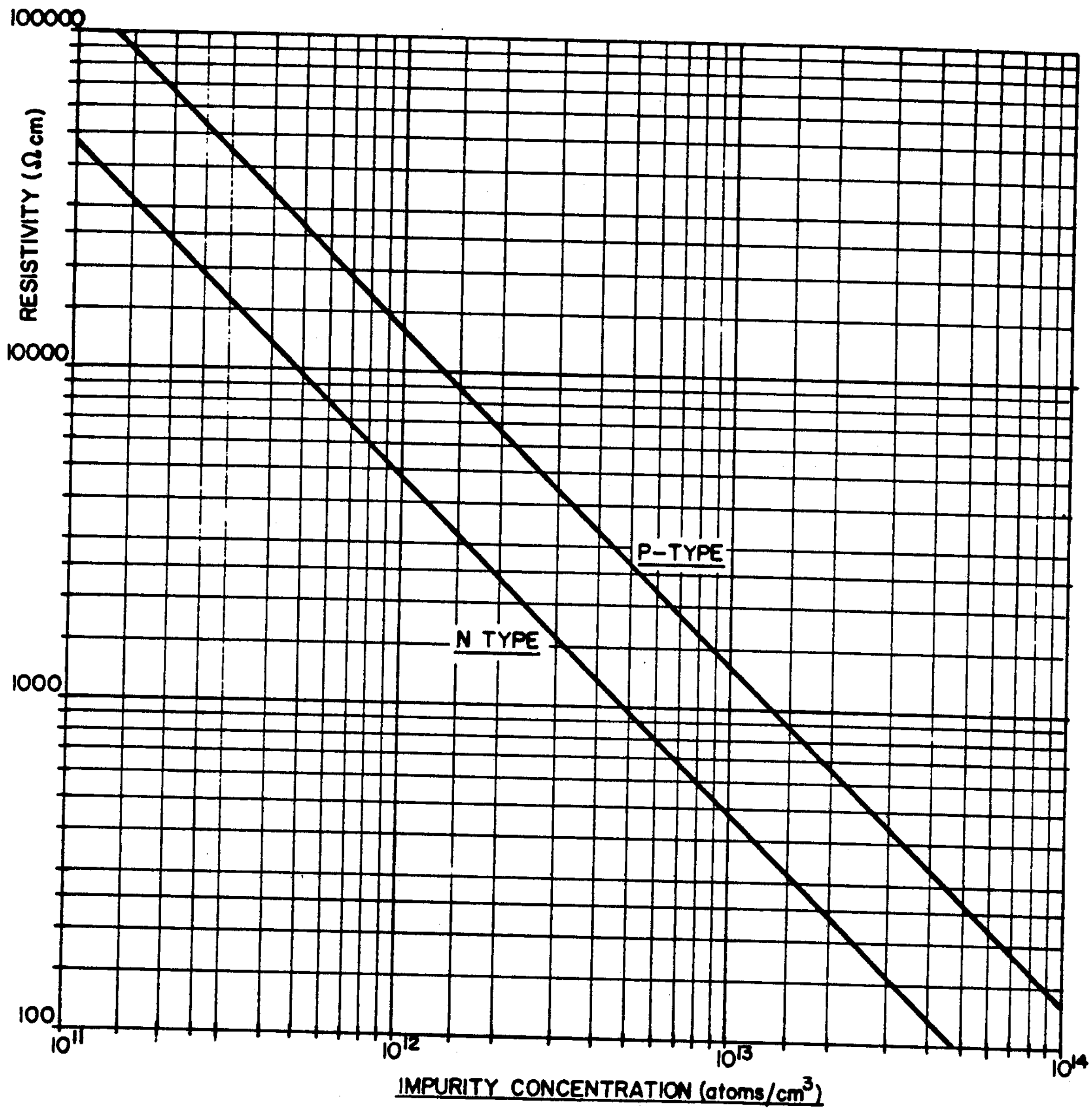

FIG. 1.3

RESISTIVITY CONCENTRATION CURVES FOR SILICON (25°C)

MUB-6962

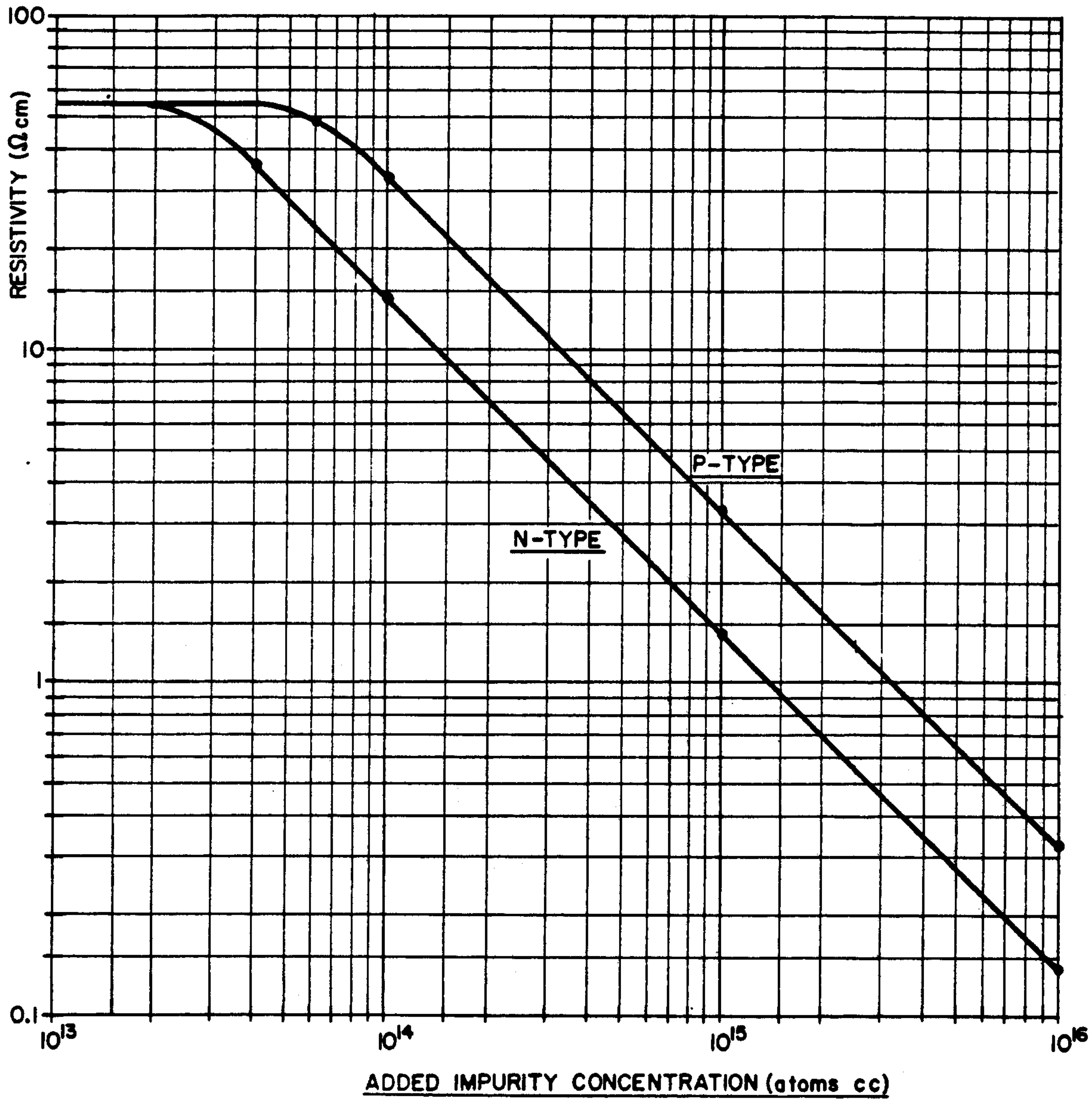

FIG. 1.4

RESISTIVITY CONCENTRATION CURVES FOR GERMANIUM (25°C)

MUB-6963

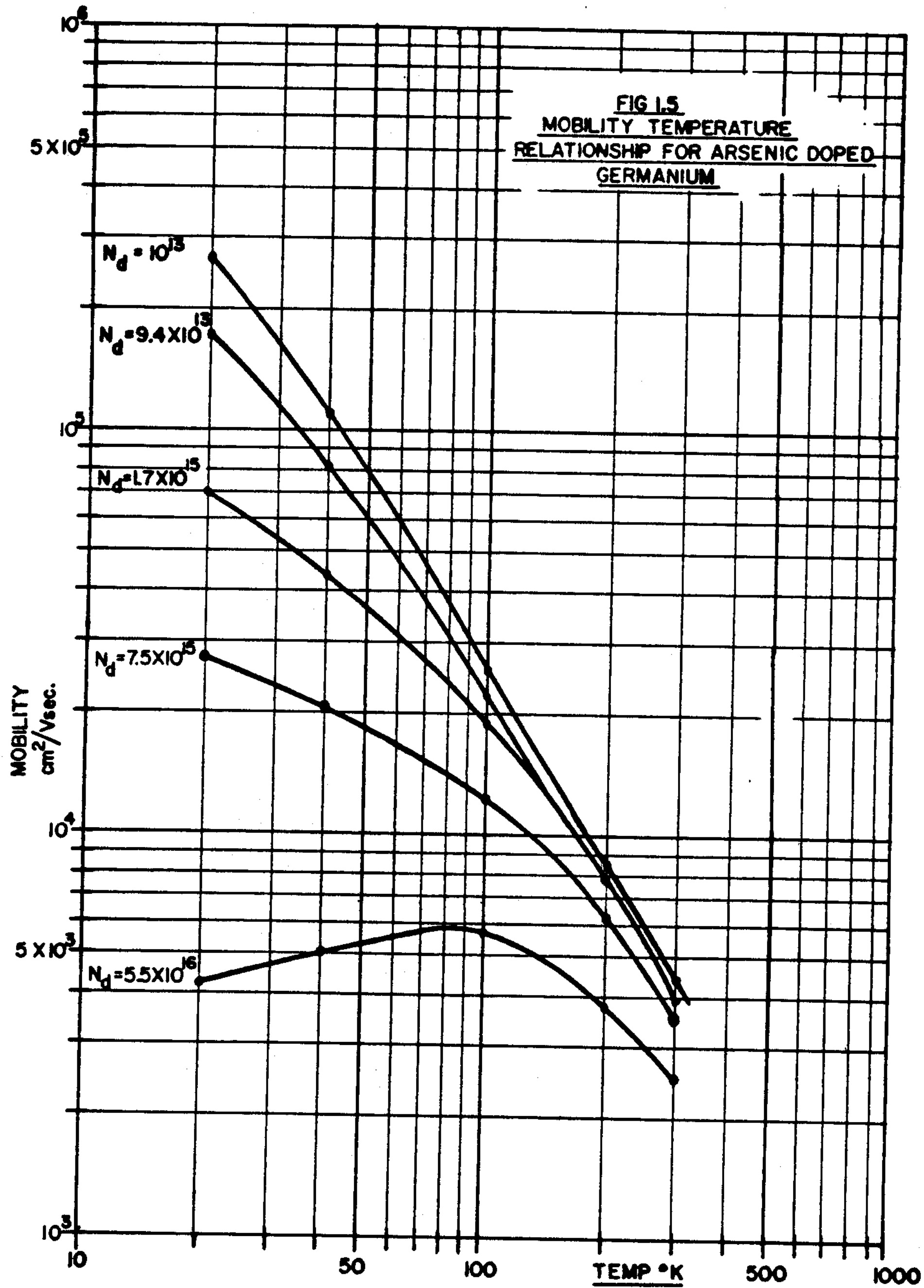

MUB-6964

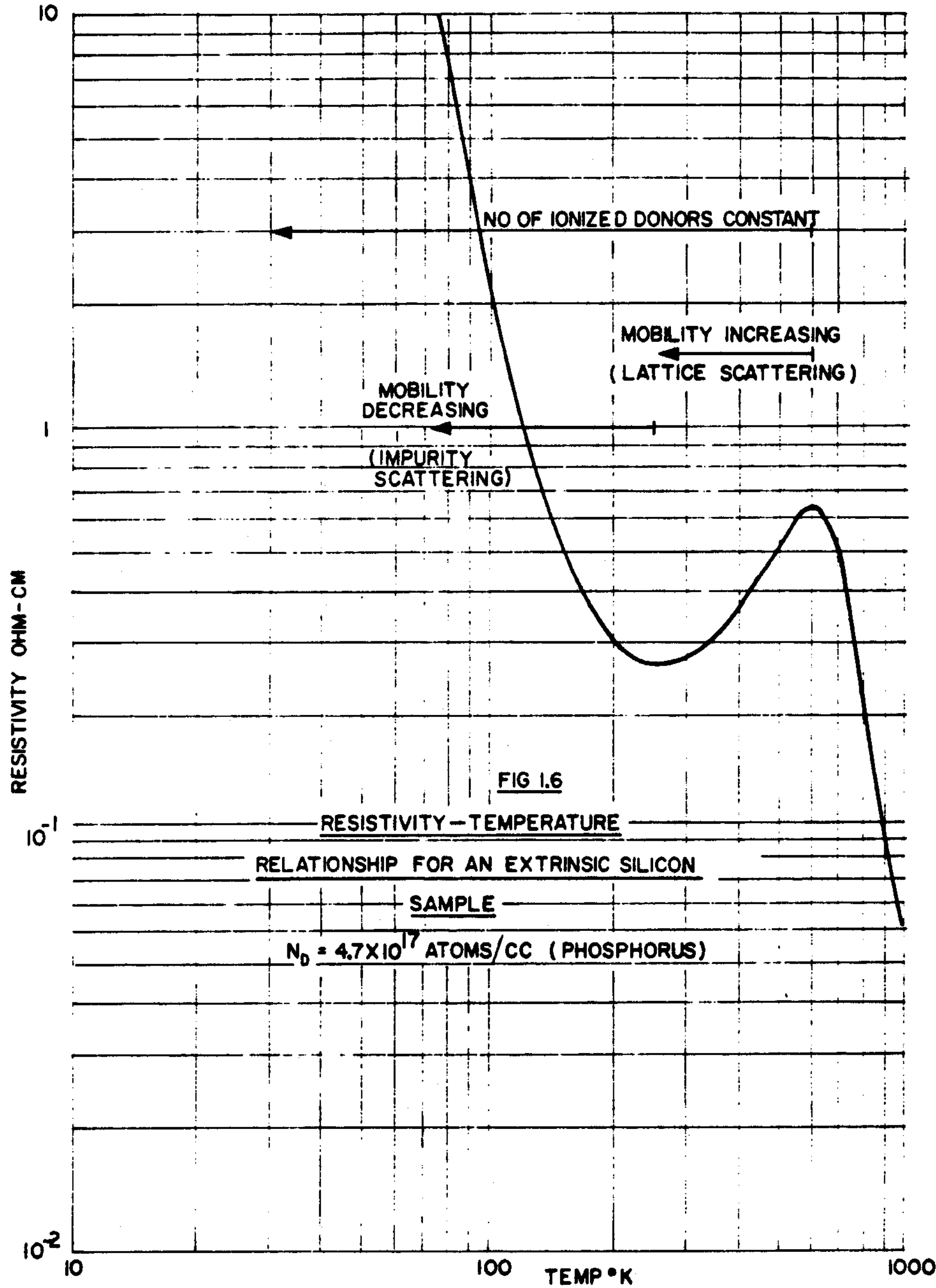

FIG 1.6

RESISTIVITY-TEMPERATURE RELATIONSHIP FOR AN EXTRINSIC SILICON SAMPLE

$N_D = 4.7 \times 10^{17}$ ATOMS/CC (PHOSPHORUS)

MUB-6965

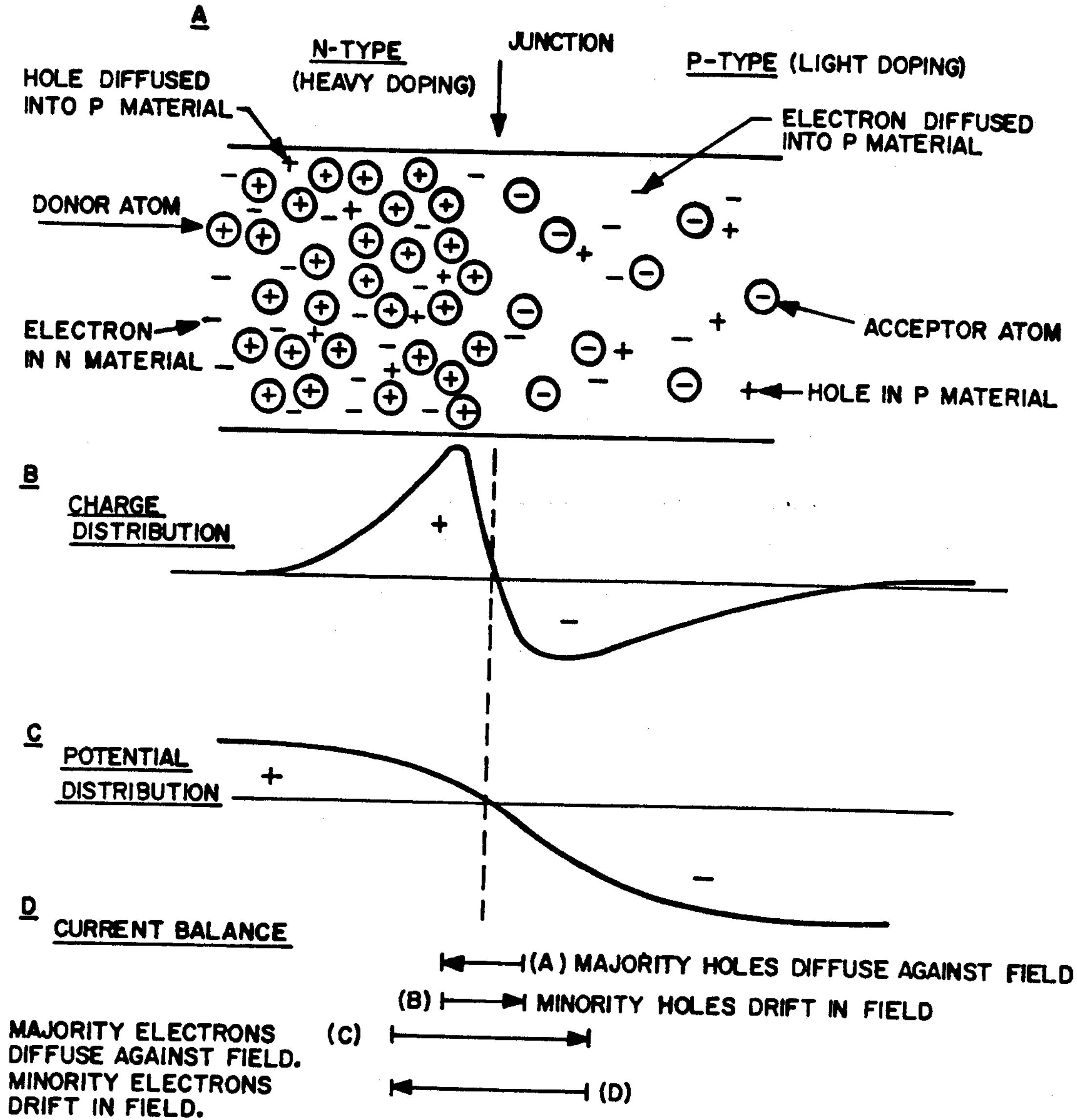

FIG 1.7

A P-N JUNCTION IN EQUILIBRIUM

MUB-6966

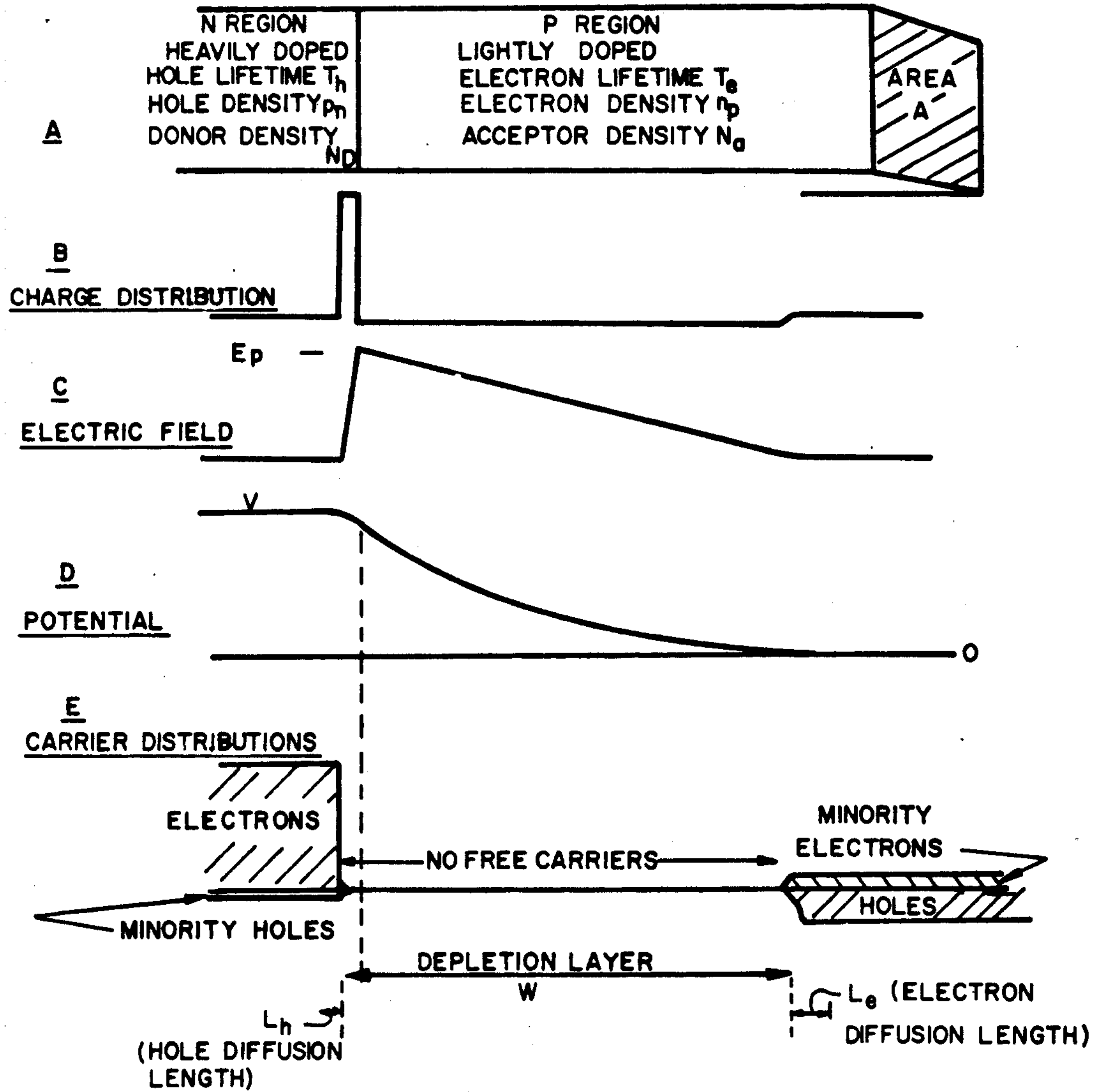

FIG 1.8

A REVERSED BIASED P N JUNCTION

MUB-6967

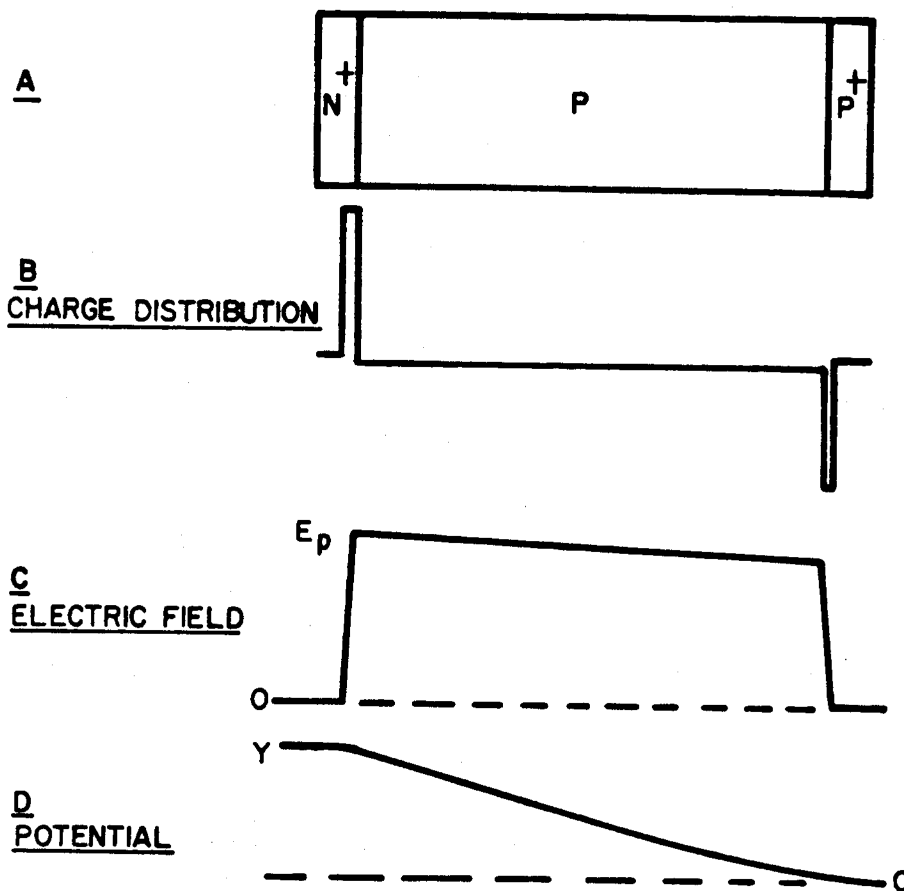

FIG 1.9

A $N^{+}.P.P^{+}$ PUNCH-THROUGH DEVICE

MUB-6968

LECTURE 2. SEMICONDUCTOR DETECTOR TECHNOLOGY AND MANUFACTURE

Fred S. Goulding

Lawrence Radiation Laboratory
University of California
Berkeley, California

July 30, 1965

2.1 INTRODUCTION

Two major differences exist between the problems involved in making semiconductor elements such as transistors and diodes and those encountered in making nuclear radiation detectors. In radiation detectors we are usually dealing with device areas in the region of a few cm^2 while modern transistors have areas in the region of 10^{-4} cm^2. Also, since the particles we detect and measure may have substantial ranges in the material, the thickness of our sensitive region must be in the range of .01 to 1 cm whereas the equivalent region in transistors and signal diodes is only a few microns thick. Thus, our sensitive volume is $\sim 10^8$ times more than that normally encountered in semiconductor technology. It is perhaps surprising that so many of the techniques used in the transistor field have been almost directly applicable to the field of radiation detectors. However, it should not surprise us that limitations not encountered in transistor production do arise in detector technology. The basic semiconductor electronics outlined in the previous paper applies to either situation but, apart from the use of similar techniques such as diffusion processes, the contents of this paper are of major interest mainly in the detector field.

2.2 DISCUSSION OF PURITY OF SEMICONDUCTOR MATERIALS

As we saw in the previous paper the production of thick sensitive regions in semiconductor detectors depends upon the availability of very high resistivity silicon and germanium. The material used in semiconductor detectors is made by a zone-levelling process whereby a floating zone is passed through a crystal several times. Most of the impurities in the silicon or germanium prefer to remain in the liquid phase so that the re-crystallized material behind the zone contains a reduced impurity concentration as compared with that in front of it. By successive passes of the zone along the rod, impurities are concentrated at one end and can be removed by cutting off the end. A limitation exists in this process due to the diffusion of impurities from the crucible material which holds the silicon or germanium. Commercially produced germanium is purified by a zone refining process in a quartz crucible and adequate reduction of impurity concentrations for normal semiconductor devices is achieved. This implies that impurity concentrations of less than 5 parts in 10^8 can be achieved since this corresponds to the carrier concentration in intrinsic germanium at room temperature. However, if such germanium is cooled to 77°K, its carrier concentration will remain close to the value it had at room temperature which is much too high for thick detectors. Similarly with silicon, the impurity concentration which can be produced by zone levelling in a crucible is not adequate to give silicon of sufficiently high resistivity for detector use. A zone-levelling process in which a self-supporting liquid zone is passed through a rod of silicon is used to produce the very high purity silicon now used in radiation detectors. This is known as the floating-zone method and no crucible is required for it.

It is usually carried out in vacuum, heat being supplied by R.F. induced eddy-currents and the walls of the tube surrounding the vacuum are water cooled to reduce contamination.

Unfortunately, with all precautions discussed in the previous paragraph, silicon which is intrinsic at room temperature and germanium which is intrinsic at 77°K are not available from zone-refining processes. In silicon, one limitation arises due to the fact that boron exhibits a very small segregation coefficient between the liquid and crystal phases. For this reason most high quality silicon is p-type. Difficulties are also experienced with removing the last traces of oxygen in silicon and germanium. While oxygen is not electrically active in its normal state in silicon and germanium it can produce electrically active centers when the material is processed at high temperatures and can affect the material properties adversely.

For these reasons there are severe restrictions on the sensitive thickness of detectors made with commercially available silicon and germanium. In fact, germanium in its commercially available form is now never used in detectors. A substantial part of the effort in detector manufacturing processes therefore consists of deliberately compensating the unwanted impurities in silicon and germanium to produce very high resistivity (or nearly intrinsic) material. We will examine the compensation processes later but will now deal with the case of silicon detectors made with no compensation process.

2.3 DIFFUSED SILICON DETECTORS

2.3.1 Elementary Considerations

The p-n junction described in 1.4 provides one method of using zone refined silicon for radiation detection and measurement. In the commonest

form of such a detector a thin n-type surface layer is produced on one face of a high resistivity p-type bulk. The best method of producing the n-type layer is by solid-state diffusion of a donor element (usually phosphorus) from a phosphorus-containing vapor into a silicon wafer which is held at a temperature in the range 800 to 1200°C. While this process is similar to that used in all modern semiconductor devices, the diffusion depth must be made very small in p-n junction radiation detectors as the ionizing particles usually enter the bulk through the surface diffused layer. For this reason diffusion schedules are short and temperatures are low compared with those used in conventional semiconductor technology. The doping level of the surface n-layer produced by this process will be very high and the sheet resistance will, in general, be less than 10 ohm/sq.

To use a p-n junction as a radiation detector, reverse bias is applied to the junction to produce a depletion layer as described in section 1.4.2 The thickness of the depletion layer obeys equation (1.8) and this relationship is shown graphically in Fig. 2.1. Fig. 2.1 also shows the relationship for the case of a heavily doped p-type surface layer on n-type bulk. The depletion layer is expressed in terms of the room temperature resistivity of the bulk silicon and the applied voltage. As silicon of the necessary quality is only relatively readily available in the resistivity range of 100 ohm cm to 10000 ohm cm, depletion layer thicknesses of p-n junction detectors operated at 300 V (which is a typical value for good detectors) are in the range 50 to 500 microns for p-type material or 100 to 1000 microns for n-type material. Material toward the top of the resistivity ranges is difficult to obtain and tends to be highly compensated. High temperature heat treatments usually change such materials considerably. For these

reasons a good practical limit to assume for the thickness of diffused detectors is .05 cm (i.e., 500 microns). This limits their use to measurement of fission fragments, p-particles up to about 500 keV, natural alpha particles and the lower energy range of machine-produced particles.

Due to the relatively small thickness of the depletion layer the capacity of the junction tends to be quite large, which, as we shall see in Lecture 3, places a limitation on the energy resolution which can be obtained. Using a detector of 1 cm^2 area having a depletion layer thickness of 200 microns (detector capacity = 55 pF), electrical noise limits energy resolution to about 7 keV FWHM (using present day preamplifiers). To this figure we must add any signal spread due to other factors such as the statistics of hole-electron pair production in the detector.

So far we have discussed only the elementary principles of a diffused junction detector. Unfortunately the simple model used would not be a good device and several years of development effort have been required to overcome its deficiencies. Before describing a process for making high quality diffused detectors, two major sources of difficulty must be discussed. Surface effects at the junction edge justify a separate section of the paper. However, we will start by dealing with the question of charge injection by the back contact of the device. In Fig. 2.2(A) the simple structure of a n-p junction detector is shown. An ionizing particle entering the depletion layer leaves behind a track of ionization and the electric field due to the applied voltage causes the holes and electrons to separate. The electrons move up to the n^+ contact and disappear into the highly doped region. The holes drift down into the undepleted p-region. Therefore, a localized positive charge is introduced into the p-region. This produces a

slight local positive potential to occur in the region where the pulse of holes enters the undepleted p-material. This situation clearly cannot exist for long,* and, in general, is corrected by a movement of holes in the p-material away from the region and into the evaporated metal contact (process (1) in Fig. 2.2 (B)). However, it is quite possible for a localized n-region to exist at the metal contact as shown in Fig. 2.2(B). In this case a second mechanism (2) exists to correct the potential rise in the p-material. An electron may now be injected into the p-material from the n-region. This electron will then exist as a minority carrier in the p-material and will diffuse in the material until it either recombines with a hole, or until it reaches the boundary of the depletion layer, in which case it will rapidly travel across the depletion layer (3) in Fig. 2.2(B). If this happens, charge over and above the original ionization will flow in the internal circuit and a multiplication effect occurs.

The consequences of this are shown in Fig. 2.2(C). In a detector which does not exhibit this effect, the Am^{241} alpha-particle spectrum has the general form shown as (a). However, a detector exhibiting the charge multiplication phenomena gives a pulse amplitude spectrum as in (b). In severe cases multiple peaks have been observed.

In order to ensure that multiplication of this type does not take place, it is now common to diffuse a p^+ layer on the back surface. We normally use boron as the diffusant and the diffusion depth is made about 2 μ. This ensures that no n-regions exist on the back surface and that the mechanism (2) in Fig. 2.2(B) is eliminated. The virtual absence of electrons in the p^+ layer means that electrons are not available for mechanism (2).

---

*The dielectric relaxation time for the material is equal to $1.1 \frac{}{4} \times 10^{-12}$ sec. For 1000 ohm cm silicon this is 1.1 nsec.

2.3.2 Surface Properties

It would be no exaggeration to say that the least understood and most time-consuming aspect of semiconductor devices is the behavior of the region where a junction intersects the surface of the crystal. The objective of all the work on this problem can be stated simply as being to establish desirable initial surface conditions and to minimize changes in the surface properties during the useful life of the device.

Fig. 2.3 shows two typical surface conditions which can be produced by chemical treatments or ambient effects at the surface of a p-type wafer the front face of which contains a diffused n^+ region. In the first case, the surface behaves as a lightly doped n-type layer and forms a "skirt" (or "channel") on the diffused n^+ region. When reverse voltage is applied to the main junction, the junction between the n-type channel (close to the n^+ region) and the p-type bulk is also reverse biased and a depletion layer forms in this region as well as in the n^+ region. The n-type surface channel is, in general, only lightly doped and the leakage current from it into the bulk must flow through the channel. In consequence a voltage gradient exists along its length and the channel-bulk junction is only reverse biased to a limited distance from the edge of the n^+ region - this distance usually being referred to as the channel length. On high resistivity p-type silicon it can extend for substantial distances - we have measured channel lengths of up to 0.5 cm in reverse-biased diffused junctions. The junction between the n-type surface channel and the bulk is a particularly poor one and produces substantial leakage currents which, in most simple junction diodes, far exceed the bulk generation and diffusion currents discussed in section 1.4.4. As we saw in 1.4.4(B) the diffusion current across a reverse

biased junction arises from minority carriers generated within a diffusion length of either side of the junction. The surface layer contains a high density of traps in the forbidden band-gap and the thermal carrier generation rate is very high. Therefore the lightly doped n-type surface layer acts as a copious source of holes which are injected across the depletion layer. If the layer is made more n-type, the channel extends further and the surface generated current flow in the external increases.

The opposite situation is represented in Fig. 2.3(B). Here we have a p-type surface and the depletion layer does not extend along the surface. However, at the junction between the p-type surface and the n^+ region, only a very thin depletion layer exists. As the reverse bias is increased, the high electric field across this peripheral junction causes avalanche breakdown and high leakage currents. As the surface is not generally uniform the breakdown is not sharp as in avalanche diodes but causes a fairly rapid rise in current as the reverse bias is increased beyond a certain value.

The contrast between the two cases is obvious in the measured characteristics of junction detectors. An n-type surface is characterized by high leakage but no breakdown at high voltages while a p-type surface shows low leakage at low voltages but a rapid increase of leakage above a certain voltage. Curves obtained by T. M. Buck[7] are shown in Fig. 2.4 as an illustration of this behavior. In this case, changes in the ambient atmosphere are seen to produce large changes in the leakage characteristics. A gross difference also exists in the characte r of the electrical noise produced by the leakage current in the two cases. In the case of the n-type surface the noise behaves much as simple current noise with a reasonably flat frequency distribution but, in the p-type case, the noise contains a larger proportion of low frequency noise and tends to be very "spiky" as seen on

an oscilloscope. For these reasons, the ideal surface is lightly n-type and chemical treatments are aimed toward achieving this ideal.

A method of making the diode characteristics less surface dependant is to use the guard-ring structure described by the present author and W. L. Hansen[8] in 1960. Fig. 2.5 shows the structure. Here, a narrow isolation ring is etched through the n-type diffused surface layer thereby dividing it into two regions. The central region is used as the detector and signals are taken from it. The outside region - called the guard ring - is connected to the same bias potential as the central region but its leakage current does not flow in the load resistor and produces no signal. As far as the central region is concerned, its surface channel can only extend out across the etched isolation ring and the surface area of the channel is very small. Thus, by treating the surface to make it lightly n-type, the central region leakage current can be made very small. Fig. 2.6 shows a typical characteristic for the central region. The guard-ring leakage, on the other hand, is similar to that of a normal diode due to the surface channel surrounding it. The impedance between the central and outside regions is very low for small detector bias voltages due to the n-type surface channel across the etched isolation ring. However, increasing the detector bias causes the surface channel to deplete and the inter-electrode impedance becomes very large (~ 1000 M ohm) so that it does not significantly shunt the load resistor R_2:

Unfortunately, as can be observed in the ambient effects shown in Fig. 2.4, an unprotected surface at the edge of a p-n junction is subject to the effects of the prevailing atmosphere and, consequently, such a detector changes its properties over a period of time. Attempts to protect

the surface with various "painted-on" products such as epoxies, silicones, glasses melting at low temperatures, etc., have, in general, proved unsatisfactory partly due to their own adverse electrical effects and partly due to their failure to provide complete long-term protection. For some time, it has been recognized that a thermally grown SiO_2 protective layer offers the best possibilities for surface passivation. This process was first used in making transistors and has been responsible for one or more orders of magnitude improvement in the reliability of semiconductor devices. It is illustrated in Fig. 2.7 which shows the steps used in preparing a junction using a planar technique. Two key features deserve comment:

(a) The phosphorus does not diffuse through the oxide coated surfaces.

(b) The edge of the junction is produced under the oxide and, if the oxide is not removed after this time, the junction edge is never exposed to ambient gases.

Efforts to accomplish oxide passivation of silicon junction detectors have involved a lengthy development program due to the formation of an n-type (inversion on p-type material) layer at the Si-SiO_2 interface. This inversion layer causes a very long surface channel resulting in very large detector leakage.

We have now successfully accomplished an oxide pascivation process and the details of it will be discussed in section 2.3.3. However, before dealing with the process in some detail, we will briefly discuss certain aspects of the behaviour of the Si-SiO_2 interface. The n-type layer observed at the Si-SiO_2 interface in early experiments suggested the possibility of compensating the donors by diffusing an acceptor impurity into

the silicon prior to oxide growth. This was successfully accomplished using gallium as the acceptor impurity[9] (gallium was chosen due to its low surface concentration during diffusion end also because oxide growth tends to deplete it from the bulk) but the temperature-time diffusion parameters were very critical and difficulties were encountered in obtaining good yields from the process. Further investigation of the mechanism involved in the formation of the n-type layer indicated that the "strength" of the layer was not a function of the oxide-growth itself but, instead, was entirely controlled by the ambient atmosphere present in the furnace tube during the phosphorus diffusion and in the cooling period following the diffusion.[10] The presence of oxygen causes strong inversion layers due, probably, to formation of SiO_4 complexes in the Si surface layers. Formation of these complexes is inhibited by the presence of hydrogen. The presence of nitrogen produces many traps at the interface and these, by reducing the carrier mobility in the surface layer tend to reduce the length of the surface channel. Control of these parameters allows the production of excellent diodes without the use of gallium surface compensation.

2.3.3 Preparation of Diffused Detectors.

The process described in this section is one used to produce quantities of detectors in our Laboratory. Different processes exist in other laboratories but the steps described here will serve as a guide to anyone interested in developing his own process.

(i) Wafers are cut on a diamond saw from p-type floating-zone silicon. The resistivity is usually in the range 100 ohm cm to 10000 ohm cm, and typical wafer thicknesses are from 40 to 80 x 10^{-3} cm.

(ii) The wafers are lapped with 10 micron Al_2O_3 lapping compound, either on a lapping machine or by hand on a Pyrex plate. About 13 x 10^{-3} cm is removed from each side in this operation.

(iii) The wafer is etched all over in a standard 3:1 HNO_3-HF etch for 1-1/4 to 1-1/2 minutes. This removes about 5 x 10^{-3} cm from each side thereby taking off the regions damaged by lapping.

(iv) Oxide is removed from the surface of the wafer by immersion in HF for 1 to 2 minutes. The HF is rinsed off with CH_3OH and then with C_2HCl_3 (trichlorethylene).

(v) After this cleaning step, the wafer is immediately put into a tube furnace where the boron diffusion is carried out. The diffusant is BI_3 vapor with a reducing carrier gas* which conists of about 90% nitrogen mixed with about 10% hydrogen. The boron predeposit under these conditions is carried out for 1 hour at 1000°C. The flow of BI_3 vapor is then stopped and diffusion is continued for a further 2 hours in the reducing atmosphere. This schedule produces a boron diffused layer of 2.7 microns thickness. The sheet resistance is in the range 4 - 8 ohm/sq. The furnace is allowed to cool below 700° before removing the wafer.

(vi) One side of the wafer (which will be referred to as the back from now onwards) is painted with a material capable of resisting the etch. We use Picein 80.** The remainder of the wafer is then etched in the 3:1 etch for 45 seconds which completely removes the boron from the unprotected side.

(vii) The Picein is washed off in C_2HCl_3 and the wafer is cleaned as in step (iv). A further cleaning step consists of leaving the wafer in H_2O_2 for a brief period and washing again with CH_3OH and C_2HCl_3.

---

*Gas flow rates in all cases are 1/2 l/min.

**Made by New York Hamburger Gummi-Waaren Compagnie, Hamburg 33

(viii) The wafer is immediately inserted into the tube furnace where oxidation takes place. Oxidation is in a steam atmosphere generated in a quarts boiler and is carried out at 1000°C for 2 hours. The oxide thickness resulting from this is about 0.7 microns. The tube is flushed out with nitrogen for a few minutes prior to allowing steam to enter it and nitrogen is also introduced when the steam is turned off. (Nitrogen flushes through all furnaces at all times to prevent the entry of air into the furnace tubes.) The furnace is cooled to less than 700°C before the wafer is removed.

(ix) The wafer is coated with Picein on the back and the required geometry is painted on the front using Picein (in the case of a simple diode the geometry consists of an uncoated central disc while the region outside it is coated; a guard ring device has a more complex geometry) the oxide in the unprotected regions is now dissolved off by immersing the wafer in ammonium bi-floride for 3-4 minutes.

(x) The silicon surface is then etched in 20:1 HNO_3, HF for 1 minute. This removes about 1 micron of silicon.

(xi) Picein is washed off with C_2HCl_3 and the wafer is thoroughly cleaned as in steps (iv) and (vii).

(xii) The wafer is immediately put into the furnace tube where the phosphorus diffusion takes place. The initial predeposit is made for 40 seconds in an atmosphere of $POCl_3$ in O_2. Nitrogen then flows through the furnace tube for 3 minutes and this is changed to a reducing gas (90% N_2 10% H) for 7 minutes. This is then changed

back to nitrogen for a further 20 minutes. The whole of this process is carried out at 900°C and the furnace is allowed to cool to almost exactly 600° before removing the wafer.* A modification is made to the above process when using materials of resistivity less than 400 ohm cm. In this case the hydrogen step is omitted to achieve the right final surface condition.

(xiii) The front of the wafer is coated with Picein and the oxide is removed from the back by immersing the wafer in HF for 1 minute.

(xiv) The Picein is removed in C_2HCl_3 and the wafer is thoroughly cleaned and dried. It is then dipped for 6-8 seconds in a very weak oxide etchant** to remove a very thin layer off the surface of the oxide.

(xv) We now have a complete detector and evaporation of gold contacts on the n^+ and p^+ areas completes the operations.

The performance obtained from detectors made by this process will be illustrated in a later part of this paper. We will now return to the topic of making detectors having sensitive regions much thicker than those attainable in diffused detectors.

---

*If the furnace is allowed to cool below about 500°C or lower before removing the wafer, a drastic change in the electrical character of the Si-SiO_2 interface takes place.

**The weak etch used for removing a thin layer from the surface of the oxide consists of 60 c.c. of HF mixed into a solution containing 1 lb. of ammonium fluroide in 2 litres of deionized water.

2.4 COMPENSATION BY LITHIUM DRIFTING

2.4.1 General Principles

It is a fortunate circumstance that the behavior of lithium in silicon and germanium lends itself to producing well compensated almost intrinsic regions of substantial thickness. The two important properties which make this possible are the very high mobility of lithium ions in the valency 4 crystals combined with the fact that the lithium atom acts as a singly charged interstitial donor atom with a low ionization energy (.033 eV in Si, .0093 eV in Ge). Other elements have a high mobility in silicon and/or germanium (e.g., Cu in Ge, Au in Si) and exhibit donor or acceptor properties but do not behave in a simple calculable fashion like lithium. Originally this aspect of lithium drifting suggested its use as a tool in the investigation of the interactions between impurities and defects in silicon and germanium and the classical work of Reiss, Fuller and Morin[11] and, later, Pell was concerned with the use of lithium in such investigations. The concept of producing thick compensated regions was first conceived by Pell[12] and has found its greatest application in semiconductor detectors.

Since lithium is a donor, all lithium compensation is done in p-type material. The lithium is usually evaporated onto the surface of the p-type material,* the temperature is raised to about 400°C and lithium diffuses into the silicon. After this step, the lithium distribution in the silicon has the form shown in Fig. 2.8(A) which is represented by the relationship:

$$N_D = N_o \operatorname{erfc} \left(\frac{x}{2\sqrt{D_0 t_0}} \right) \qquad (2.1)$$

where N_D = donor concentration at depth x from the surface,

N_o = lithium surface concentration ($\sim 10^{18}$ atoms/cc),

t_o = duration of diffusion,

D_o = diffusion constant at the diffusion temperature.

---

*A suspension of lithium in oil is sometimes used for this purpose.

If the acceptor concentration in the p-type material is N_A the p-n junction will be at a depth x_o given by:

$$N_A = N_o \text{ erfc } \left(\frac{x_o}{2\sqrt{D_o t_o}} \right) \qquad (2.2)$$

The value of x_o for a 400°C diffusion of 3 minutes duration is about 7×10^{-3} cm for silicon (floating zone). For germanium (almost oxygen free) a typical diffusion depth is 50×10^{-3} cm after a 5 minute diffusion at about 450°C.

If reverse bias is now applied to the p-n junction, the lithium ions, which carry a positive charge, begin to move from the n side of the junction to the p side where they tend to compensate the acceptor atoms in the p-region. At quite moderate temperatures the flow of lithium ions across the junction is large enough to provide enough donors to compensate a substantial volume of p-type material in a short time. Fig. 2.8(B) shows the situation after a short period of drifting. It is seen that lithium has moved out of the n-region to produce an intrinsic region of width W. That the compensation mechanism will be quite accurate is illustrated in Fig. 2.8(C). Here we have imagined a pile-up of donors to occur in a region toward the middle of the intrinsic region. The electric field distribution, shown in Fig. 2.8(D), indicates that a higher electric field exists to the right of the pile-up region than to the left. Therefore the current of lithium ions to the right out of the pile-up region exceeds the current of ions into it from the left. The piled-up donors therefore very rapidly dissipate leaving an accurately compensated region.

It is interesting to calculate the rate of growth of the intrinsic region. For this purpose we will assume that the electric field is high enough for the current of lithium ions to be almost entirely due to the electric field and

for the diffusion current to be negligible. We will also assume that the initial period of drift is completed and the situation illustrated in Fig. 2.8(B) exists. Throughout the intrinsic region $N_A = N_D$ and the electric field is $\frac{V}{W}$ where V is the applied voltage. We then have:

$$\text{Current of Li ions/sq. cm} = J_L = \frac{V}{W} \cdot \mu_L \cdot N_A \qquad (2.3)$$

where μ_L is the mobility of the lithium ions in the semiconductor at the drift temperature.

The number of acceptors which can be compensated in time dt is therefore $J_L \cdot dt$ and, since the acceptor concentration in the uncompensated material is N_A, the increase W in the thickness W of the intrinsic layer in time dt is given by:

$$NA\ dW = \frac{V}{W} \cdot \mu_L \cdot N_A\ dt$$

$\therefore$ by integration; $W^2 = 2\ V \cdot \mu_L \cdot t$

$$W = \sqrt{2\ \mu_L \cdot V \cdot t} \qquad (2.4)$$

For practical purposes this relationship suffices for nearly all detector drift calculations. It breaks down only at short times when W is of the same order as the thickness of the lithium diffused n-region. Fig. 2.9 shows this relationship for silicon (V = 500 V) and Fig. 2.10 gives similar information on germanium (V = 600 V). We note, from equation (2.4) that the drift rate is independent of the resistivity of the starting material and that the drift rate can be increased by raising the temperature (since the Li ion mobility increases as temperature rises) or by increasing the applied voltage. The value of the latter is usually dictated by diode surface breakdown problems and voltages in the range 500 to 1000 volts are generally employed. The temperature is subject to an absolute upper limit above which the material becomes intrinsic and the junction ceases to behave as a diode.

Lower resistivity materials allow higher temperature operation but such materials, in general, produce poorer quality devices. Moreover, a drift temperature well below the intrinsic temperature is desirable due to the fact that a considerable bulk leakage current flows in the device at higher temperatures. Sufficient lithium resides in any part of the drifted region to produce electrical neutrality in that region at the drift temperature. As the holes and electrons produced thermally in the drifted region, during their transit across the depletion layer, constitute charge in the bulk the lithium concentration adjusts itself to a value determined by this charge as well as the acceptor charge. This results in the lithium distribution not being correct to compensate the acceptors. Drifting at a lower temperature for at least the final part of the drift operation (this is called levelling) reduces the overcompensation to a negligible amount.*

Typically our silicon detectors are drifted at 130°C and 500 V (see Fig. 2.9) which means that a 3 mm detector requires about 60 hours to drift. Germanium detectors are usually drifted at about 40°C and 600 V. An 8 mm thick germanium detector therefore requires 300 hours to drift.

We see that the drift times involved are quite long and some thought has been given to reducing these times. One interesting method which has not yet been employed is to largely compensate a piece of p-type material by diffusion of lithium in a tube furnace (a closed box system would be required to prevent the reaction between the lithium and the quartz tube). We might aim to introduce a fraction F of the lithium required to achieve complete compensation by this method. The material is then used for a normal lithium drift process. Examining equation (2.3) we see that the

*This effect can easily be estimated; it is about 1 part in 10^3 for drifting a 3 mm thick silicon detector made with 1 K ohm cm material drifted at 500 V and 1 mA leakage (~125°C).

current of lithium ions across the compensated region is unaltered for the same width W, but the region dW now contains only $(1-F)N_A \cdot dW$ acceptors which require compensating. Equation (2.4) then becomes:

$$W = \sqrt{\frac{2\ \mu_L \cdot V \cdot t}{(1-F)}} \qquad (2.5)$$

If F = 0.9, the value of W achieved in a given drift time would be about 3 times larger than in silicon (or germanium) not treated by the partial compensation by diffusion method prior to drifting.

2.4.2 Secondary Effects in Lithium Drifting

A number of secondary effects which occur in the lithium-silicon and lithium-germanium systems can have very significant effects in lithium drifting operations and, as these complicate the process, we must deal with these here in a general way. The effects which lead to complications all arise from reactions between the lithium and defects in the material such as vacancies and other impurities. The most important ones are:

(a) Oxygen Content of the Semiconductor.

In both silicon and germanium concentrations of oxygen in the crystal in the range of 1 part in 10^9 have a serious effect in reducing the drift rate of lithium. This is caused by a reaction between the lithium ions and oxygen atoms forming LiO^+ which is less mobile than the Li^+ ion. It has been suggested that this effect might be useful in preventing the movement of lithium in detectors for use at higher temperatures but its effect in slowing down the drift process is more important in detector technology. In order to drift successfully it is necessary to obtain silicon and germanium almost completely free of oxygen. Silicon produced by the vacuum floating zone process is suitable

material. In the case of germanium satisfactory results have been achieved with material made by carrying out the zone levelling process in a reducing atmosphere.

(b) Fairing Reactions between Lithium and Acceptors.

The drifting process results only in compensation of any charge existing in a volume of the material of the order of the Debye length. No direct association between the acceptor atoms (e.g., boron) and the lithium ions is necessary for this. However, as the positively charged lithium ions diffuse they will tend to be attracted by Coulomb forces to the negatively charged acceptor atoms. A close association between acceptor and lithium atoms may therefore result. At high temperatures this "pairing" effect will be negligible due to thermal agitation processes, but at low temperatures, if sufficient time is allowed to elapse, the pairing will be complete and each atom of lithium will be closely tied to an acceptor atom.

The effects of pairing may be important in detectors from two points of view. In the first place the binding of lithium atoms to the acceptor centers can inhibit the movement of these atoms and thereby stabilize the characteristics of the device. A second possible advantage accrues from the reduction in impurity scattering due to the pairing process.* As pointed out in 1.3.3, this has the effect of increasing the carrier mobility at low temperatures.

*Close pairing of a lithium and acceptor atom results in negligible electric field due to these atoms at a distance and, therefore, little effect on carriers passing through the material.

(c) Precipitation of Lithium at Vacancies.

In order to compensate for a concentration Na of acceptors, N_a atoms of lithium per cm^3 must be introduced into the material. If N_a is larger than the maximum solubility of lithium at room temperature (or the detector temperature) the material is super-saturated with lithium and precipitation of the excess lithium will occur if the lithium atoms can find suitable precipitation sites. Vacancies in the material provide such precipitation sites, and when the lithium atoms precipitate they lose their electrical activity.

This situation is particularly important in germanium. The initial diffusion process gives a lithium surface concentration of the order of 10^{18} atoms/cm^3 while the equilibrium solubility of lithium in intrinsic germanium at 25°C is 6.6×10^{13} atoms/cm^3. Particularly in the material used in early detectors (probably due to oxygen and surface damage) difficulty was experienced due to the lithium precipitating in the surface n-region to leave a p-type surface. A further difficulty can, in principle, arise in the bulk compensated region. Studies have shown that the equilibrium solubility of lithium in germanium is smaller than the value required to compensate material of less than 30 ohm/cm. Therefore, one must anticipate possible precipitation problems when using starting material of lower than 30 ohm · cm resistivity.

For lithium precipitation to occur, precipitation sites must exist and the quantity of these is greatly dependant upon the quality of the material. It is possible, under certain circumstances,

to fill the precipitation sites with atoms of another element and thereby to inhibit precipitation of lithium at a later-time. We once used copper for this purpose[13] but, as material quality has improved, this has ceased to be necessary.

Lithium precipitation does not appear to be a significant problem in floating zone silicon.

2.4.3 Surface Effects in Lithium Drifted Devices

Unfortunately the planar oxide passivation technique described in section 2.3.2 has not yet proved to be applicable to either lithium drifted germanium or silicon detectors.* The failure to develop oxide passivation is due to the fact that high temperature processing required in oxide growth introduces impurities and defects in the material which give large generation (leakage) currents in thick lithium drift detectors. We must therefore resort to chemical treatments for adjustment of surface states and to paint-on varnishes for surface protection. Typical treatments are described in the following sections in which the steps in our production processes for lithium-drifted silicon and germanium detectors are detailed.

2.4.4 Preparation of Lithium Drifted Silicon Detectors**

(i) Wafers are cut to the required thickness from floating zone p-type silicon in the resistivity range 500-5000 ohm cm.+ Wafer thicknesses range from 0.5 to 5 mm.

---

* One commercial manufacturer produces oxide passivated lithium drifted silicon detectors but the oxide is not thermally grown.

** This process is the one used in our laboratory and might be termed a low temperature process as contrasted with methods which use much higher temperatures. It is to be regarded as illustrative of a general method; variants are used in other laboratories.

+ We find that leakage currents are lower and device performance better at low temperatures if material in the top half of this resistivity range is used. One might attribute this to the general poorer quality of the low resistivity material.

(ii) Wafers are lapped with 10 micron AL_2O_3 lapping compound removing about 10 x 10^{-3} cm from both sides. They are thoroughly cleaned in detergent, methyl alcohol and triclorethylene.

(iii) Wafers are placed on a heater plate in a vacuum evaporator and heated to 350°C. Lithium is then evaporated from a lithium metal source onto one side for 30 sec. We continue to hold the wafer at 350°C for a further 1-1/2 minutes. The hot plate is then cooled rapidly by passing water through a cooling coil. This process gives a very uniform lithium diffused region 7.5 x 10^{-3} cm thick.

(iv) Wafers are removed from the evaporator and washed with CH_3OH to remove free lithium on the surface. They are then given an overall 1/2 minute etch in 3:1 HNO_3 - HF etchant. This removes any traces of lithium which may have strayed onto the wrong side of the wafer.

(v) In preparation for drifting on the automatic drifting apparatus, a pattern is evaporated (gold) on the back of the wafer (i.e., the face opposite to the lithium side). The purpose of this pattern, which consists of a central disc of 3 mm diameter surrounded by a 1 mm space then by a completely gold-covered outer region, is to allow the drift apparatus to monitor the approach of the drifted region to the back.

(vi) The central region of the lithium face is masked with Picein to give a junction of the required area and the whole of the back is masked too. A 6 minute etch in 3:1 etchant removes all the lithium diffused region {etch depth about 15 x 10-3 cm) except the central masked area. The etch is quenched in running distilled water and

the Picein is then washed off with C_2HCl_3 and the wafer thoroughly cleaned with CH_3OH and C_2HCl_3. The two sides of the wafer are now as illustrated in Fig. 2.11; on the back is the gold evaporated structure while the front has the lithium diffused region in a mesa form.

(vii) The wafer is now put into the drift apparatus where drifting takes place at about 130°C with an applied voltage of 500 V. A detailed description of this apparatus has been given by the author and W. L. Hansen.[4] For the purpose of this outline we may say that the principal feature of interest in the drift apparatus is that it controls the wafer temperature to maintain the device leakage current during drift at a preselected value in the range 0.5 to 5 mA and constantly monitors the approach of the drifted region to the back of the wafer. For completely automatic operation the drift can be terminated by the apparatus when the drifted region reaches a pre-determined distance from the back. In practice we allow nearly all our devices to reach the back and over-drift for a short time.

(viii) When drifting is complete, the back of the wafer is lapped to a depth of about 10^{-3} cm and a staining procedure* is used to reveal the location and size of the intrinsic region's intersection with the back. If the size is adequate (usually about equal to the mesa area on the front) and the region is uniform, the drifting is considered to be satisfactory. Occasionally it is necessary to lap a short distance from the back to satisfy the test.

(ix) The whole front of the wafer and a ring around the periphery of the back is masked with Picein and the remainder of the back is etched

*Immersion in a $CuSO_4$ solution containing a small amount of HF. A bright light is necessary to obtain a good stain.

for 3 min in 3:1 etchant and quenched in running distilled water. This produces a well in the back about 7.5 x 10-3 cm deep. The Picein is now removed with C_2HCl_3 and the wafer is washed with CH_3OH and C_2HCl_3. A final clean up overall etch of 1/2 minute in 3:1 etchant water is then given to the wafer and the etch is quenched with running distilled water.

(x) The wafer is now thoroughly cleaned by scrubbing with a cotton swab immersed first in C_2HCl_3 then in CH_3OH and washed in CH_3OH and C_2HCl_3. It is then soaked in HF for about 1 minute, washed briefly with CH_3OH and dried in a jet of dry nitrogen. It is then left in room air in a covered dish for about 16 hours.

(xi) Gold is now evaporated over the entire back of the wafer and also onto the contact region on the lithium diffused front.*

(xii) The wafer is now ready for final setting of surface states. To carry this out we first scrub the periphery of the mesa with a cotton swab dipped in CH_3OH then wash briefly with CH_3OH. The front of the wafer is then covered with HF for 30 seconds. This removes all oxide on the surface and leaves a very n-type surface. Washing with CH_3OH for about 15 seconds produces a neutral or lightly n-type surface. In all cases we measure the characteristics of the diode at this stage and rewash with CH_3OH until the desired surface is achieved.**

---

*The gold back to the intrinsic region produced by this process is usually regarded as a surface barrier. However, in our case we believe that the gold only contacts a shallow p-region produced by the etching process at the surface. This belief is supported by the fact that scratching the gold does not affect performance and also by the observation that use of a slow etch in step (vii) produces a thick dead layer at the surface.

**As was seen in 2.3.2 an n-type surface is characterized by fairly high leakage hut no breakdown at high voltages and a p-type surface by the opposite situation.

(xiii) The periphery of the mesa is now coated with a polyurethane varnish which is allowed to dry for about 24 hours before the device is used. The polyurethane provides good protection and has negligible effect on the surface properties established in step (xii).

2.4.5 Preparation of Lithium-drifted Germanium Detectors

NOTE: Partly due to the size and mass of the pieces of material used (often ~ 6 cm^3) and also due to the brittle nature of germanium, the handling of this material is much more difficult than that of silicon. For this reason all heating and cooling operations are made slowly to avoid thermal shock. Also sawing operations are made in several steps -- we slice 0.5 cm at each pass.

(i) Horizontal single crystal zone-levelled material obtained from Sylvania is employed. This is supplied in the form of an ingot of up to about 12 inches length with a cross section which is not rectangular but is about 4 cm wide at the bottom, 3 cm at the top and 2-1/2 cm high.

(ii) Cut the detector blocks from the ingot on a diamond saw. (Here, for example, the material and the pitch used to cement it onto the ceramic mount are heated quite slowly to avoid thermal shock.) We usually cut the blocks a little over 1 cm thick except for special thin detectors.

(iii) Lap the faces of the block with 10 μ Al_2O_3 lapping compound. This is done manually with light pressure using a pyrex lapping plate.

(iv) The Ge block is placed on a moveable stainless steel plate in a vacuum evaporator. A heater near the stainless steel plate is heated to 450°C. The vacuum is pumped down and lithium is evaporated

down onto the face of the germanium block. The stainless steel plate holding the germanium block is then moved over onto the heater and dry nitrogen is admitted to the vacuum belljar to give heat conduction between the heater and the steel plate. Under these circumstances the germanium requires about 2 minutes to reach 450°C. It is left on the heater for another 5 minutes (this gives about a 0.5 mm thick diffused region). The stainless steel plate with the germanium block on it is then moved onto a water cooled plate; in 2 minutes the germanium is cooled and can be removed from the belljar.

(v) The excess lithium is washed off in distilled water. The sides of the germanium block are now cut off on the diamond saw to give a rectangular germanium block 2 cm x 3 cm x 1 cm (typical).

(vi) The edges of the block are lapped and washed and the whole germanium block is etched for 1-1/2 minutes in standard 3:1 HNO_3:HF with 6% (by volume) of red fuming nitric acid added to the etch to speed up the start of the etching process.

(vii) Side surfaces are now treated chemically to reduce leakage currents which will flow in the device during the drift step which follows. The best treatment we have found consists of a 1 minute etch in 3:1 HNO_3:HF plus red fuming HNO_3 as in (vi); quench with CH_3OH; 30 seconds in 30% aqueous NH_3; a brief quench in CH_3OH; 20 seconds in 30% H_2O_2. During these-treatments the front and back faces of the device are protected by an etch-resistant adhesive tape.

(viii) The tape is removed and the device is inserted in the drifting unit. In this unit, illustrated in Fig. 2.13, the detector is clamped between a pair of thermo-electric coolers with an indium-

gallium eutectic alloy between the faces of the detector and cooling plates. The coolers are insulated electrically from the actual cooling plates holding the device so that reverse bias can be applied to the detector via these plates. Power to the coolers is controlled by a circuit in such a way that the thermo-elements either heat or cool the detector to maintain its leakage current at a preselected value. The drift voltage is approximately 500 volts and the current through the detector is selected to give a temperature in the range 30-60°C. Initially, this means that the preset demand-current might be 10 mA and the thermo-elements are operating mainly in a heating mode to maintain the leakage at the 10 mA value. The detector temperature might be 60°C. Later, as the drifted region becomes thicker and the thermal generation current increases, the preset demand-current will be increased to ~ 60 mA to keep the temperature up to about 35°C and the thermo-elements will now be operationg mainly in the cooling mode to pump out the 30 watts of heat being generated by the leakage in the detector.

(ix) When calculations indicate that drifting has reached the desired depth (usually 8 mm), the device is removed from the drifter and the drifted region is revealed by a staining technique. This consists of immersing the device in a solution of about 20 g/litre of $CuSo_4$ in water at 25°C with a reverse bias applied to the junction such that up to 50 mA flows in the detector. This immediately reveals the periphery of the depleted region.

(x) If the desired drift depth has been achieved the device is given a 30 sec etch all over. The front and back faces are now taped with etch resistant tape and the 1 minute etch and chemical surface treatment described in (vi) is repeated.

(xi) The tapes are removed and the detector is mounted in its holder. The thermal contact is improved by using a thin indium foil between the detector and the cold plate with a thin smear of indium-gallium eutectic between the detector and the indium foil. The eutectic is also used between the opposite face of the detector and its contact point to give good electrical contact. We often find it necessary to thoroughly clean the holder with organic solvents and dry it thoroughly immediately before mounting the detector. A diagram of the type of holder and cryostat used at Berkeley is shown in Fig. 2.14. After mounting the detector the vacuum is pumped down to 10^{-5} mm of Hg, and the system is then cooled down to liquid nitrogen temperature. After a few minutes the vacuum ion-pump is switched on and the unit can be used. The preamplifier mounts directly on the side of the holder with a connection to the detector which has very low shunt capacity to ground.

2.5 DETECTORS NOT EMPLOYING JUNCTIONS

In our first discussion of semiconductor detectors we assumed that the device might consist of a block of semiconductor with metallic contacts at either side. The reader may wonder why we became involved in p-n junctions and departed from the simple concept. In fact the earliest semiconductor detectors used diamonds and the simple metallic contact approach was employed.

Later gold-doped silicon, which behaves much like intrinsic silicon at liquid nitrogen temperature, was used. Both these approaches have now been displaced by the p-n junction devices we have discussed.

A major reason for this is that metallic contacts, if they behave in an ohmic fashion (i.e., not rectifying) allow free passage of holes or electrons from semiconductor to metal and vice versa. Thus if an ionizing event produces a hole-electron track in a detector of this type made of very lightly doped n-type material, the electrons may be quickly swept out of the material by the electric field while the holes move more slowly.* Thus while the holes are being collected a localized positive charge exists in the material. To compensate this positive charge, electrons will be injected from the more negative contact of the device. These electrons travel rapidly across the material and still more electrons are required to correct the charge unbalance. Thus a rather unpredictable charge multiplication effect occurs and a large spread in signal amplitude may result, If the more negative contact were a p^+ contact almost no electrons could be injected into the material in the manner described. This is the basic reason for using the p-n junction device.

We have used a grossly oversimplified model in this explanation. In fact, the existence of a localized positive charge will only cause injection of electrons after a time of the order of the dielectric relaxation time of the material, (i.e., $1.1 \frac{\cdot K}{4} \times 10^{-12}$ sec) and, if the collection time is short compared with this, no multiplication will occur. One must attribute the success of the early detectors to this. On the other hand, it is difficult to make ohmic contacts to high resistivity material and it is possible that the devices behaved as surface barrier detectors. The

*If traps which selectively trap one carrier are present in the material, the effect described here is enhanced.

behaviour of the p-n junction is more predictable and this is the reason for its general superiority for nuclear spectrometry.

2.6 MAKING THE CHOICE BETWEEN DETECTOR TYPES

In planning an experiment which might use semiconductor detectors the choice between the various types of detector might not be obvious to the physicist since the lithium-drifted silicon detector's areas of applications overlap those of both lithium-drifted germanium and diffused silicon. We will therefore attempt here to indicate the specific advantages and limitations of each type.

Oxide-passivated diffused detectors possess the paramount advantage of long-term reliability due to the complete surface protection offered by the oxide. They can be made in a totally depleted form and, in this case, the dead layers at front and back are very thin ($\sim 0.5\ \mu$). This is an important feature if a detector is to be used as a DE detector in a particle identifier system. Conversely, if the detector is not totally depleted, the thickness of the sensitive region can be varied by changing the applied voltage. This can be useful in discriminating between long-range and short-range particles. A further advantage of the diffused detector as compared with the other types is its relative insensitivity to radiation damage. This results from the high acceptor or donor concentration in a diffused detector compared with lithium drifted detectors. Against these advantages must be set the limited thickness of the sensitive region which reduces the range of particles which can be stopped and also gives a high detector (electrical) capacity with consequent relatively poor resolution due to electronic noise.

Diffused detectors are used primarily for natural and low-energy machine-produced particles (resolution $\approx$ 15 keV FWHM on natural alphas),

-particles (resolution ≈ 8 keV FWHM at 300 keV), fission fragments and heavy ions. The majority of our diffused detectors are used for fission fragments and heavy ions as radiation damage is a serious problem in this work. Good diffused detectors made of 400 ohm cm silicon can withstand up to 10^8 - 10^9 fission fragments for sq. cm. before becoming unusable. In nearly all these applications the detectors are used at room temperature although recent tests have indicated good operation and improved radiation life when irradiated with fission fragments at liquid nitrogen temperature.

Lithium-drifted silicon detectors find the widest range of uses. The ability to make fairly thick sensitive regions which give low capacity and allow the detector to totally absorb particles of a wide range of energies contribute to their versatility. Cyclotron produced particles (for example alphas in the energy range 10 to 120 MeV) are commonly measured with these detectors. In this case, the detectors are generally used at room temperature as the electrical noise due to the detector leakage current produces a small signal spread compared with other sources. On the other hand, by cooling the detectors,* high resolution -particle spectroscopy becomes possible. Resolution (FWHM) figures of 3 to 5 keV are obtained. These detectors also find application in low energy gamma-ray spectroscopy (up to 50 keV) where the thin dead layers on both faces of the wafer absorb fewer gamma-rays than do the much thicker dead layers on germanium detectors. Cooled lithium-drifted silicon detectors may also be used for natural alpha-particle spectroscopy but the dead layers on these detectors are not as well controlled as those on diffused detectors and this can be a source of trouble.

---

*Some silicon detectors show polarization effects due to deep lying traps at liquid N_2 temperature. We usually cool silicon detectors at -50°C to -100°C.

Lithium-drifted germanium detectors must always be used at low temperatures (77°K is convenient and is generally used) in order to reduce the leakage current and its noise. However, the higher atomic number of germanium compared vith silicon, the ease of drifting very thick (1 cm) devices, and the lower energy required per hole electron pair all favour germanium as compared with silicon for most gamma-ray spectroscopy. At low energies the dead layers* at either side of the sensitive region absorb a large fraction of the gamma-rays -- a factor which favours silicon at the present time.

In conclusion we might say that the choice of detector is usually fairly obvious and, in cases where it is not, the choice is usually a compromise between a number of factors which can only be evaluated in terms of the specific experiment.

*In general the dead layers have been at least 25 x 10^{-3} cm thick. Recently we have demonstrated that a gold back can be made to the intrinsic region yielding a very thin access window. It remains to be seen whether this process can be reproduced. Tavendale[15] has reported results for a thin window germanium detector made by drifting right up to an aluminum alloyed

LECTURE 2. FIGURE CAPTIONS

Fig. 2.1 Depletion Layer Thickness Curves for N end P-Type Silicon.

Fig. 2.2 Illustration of Charge Injection at Rear Contact.

Fig. 2.3 Models of Surface Layers at Junction Edge.

Fig. 2.4 Effect of Ambients on Leakage Current of a Junction (T.M. Buck).

Fig. 2.5 Guard-Ring Structure.

Fig. 2.6 Typical Leakage Curve for Guard-Ring Detector.

Fig. 2.7 Steps in Preparing a Planar Junction Device.

Fig. 2.8 Distribution of Lithium at States of Lithium Drift.

Fig. 2.9 Drifted Region Thickness - Time Relationship for Silicon.

Fig. 2.10 Drifted Region Thickness - Time Relationship for Germanium.

Fig. 2.11 Illustration of Silicon Wafer Prior to Drifting.

Fig. 2.12 Cutaway View of Lithium-Drifted Silicon Detector.

Fig. 2.13 Germanium-Lithium-Drift Unit.

Fig. 2.14 Diagram of Germanium Detector Holder and Cryostat.

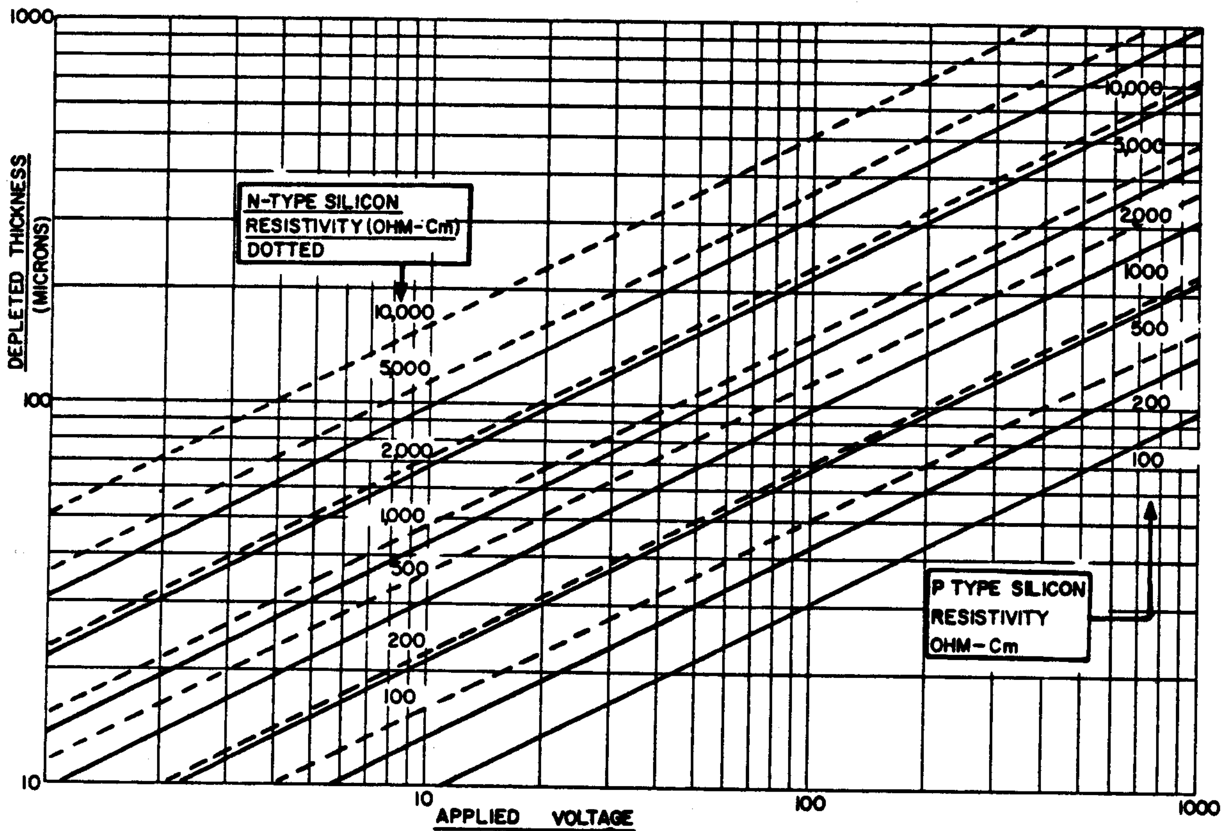

FIG 2.1 DEPLETION LAYER THICKNESS FOR P^+N AND N^+P SILICON JUNCTIONS

MUB-6969

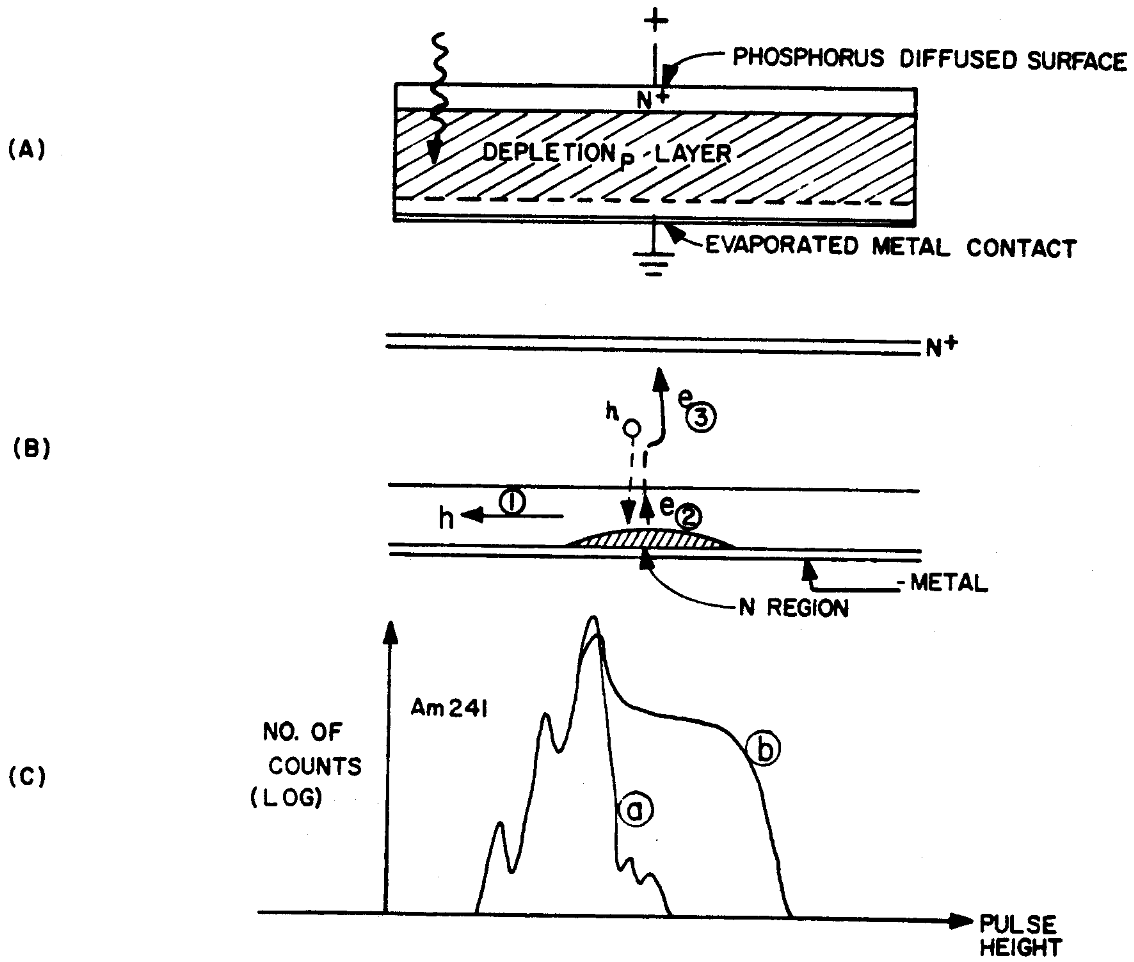

FIG 2.2
PEAK CONTACT CHARGE INJECTION IN DIFFUSED DETECTORS

MUB-6970

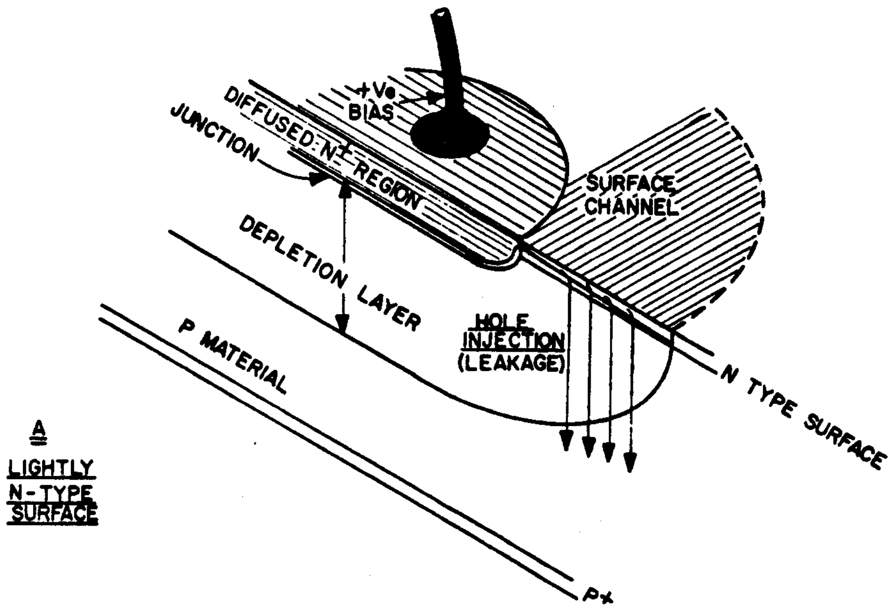

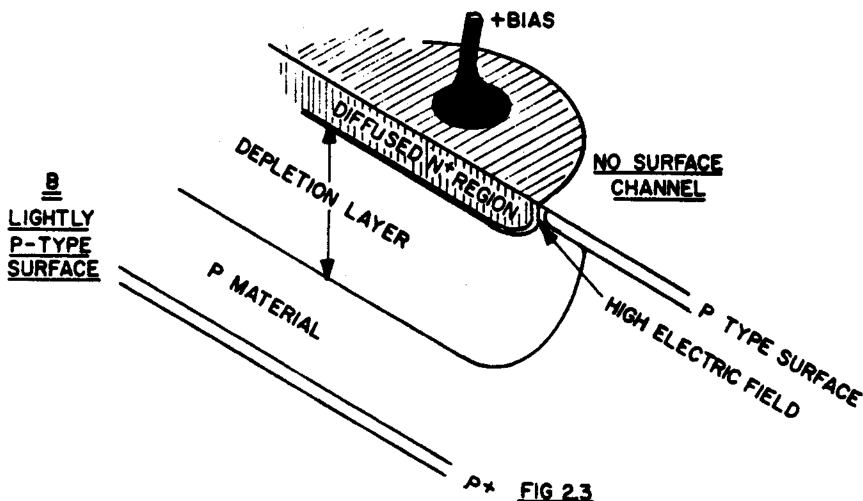

FIG 2.3
SURFACE PROPERTIES OF JUNCTION (SECTIONED VIEWS)

MUB-6971

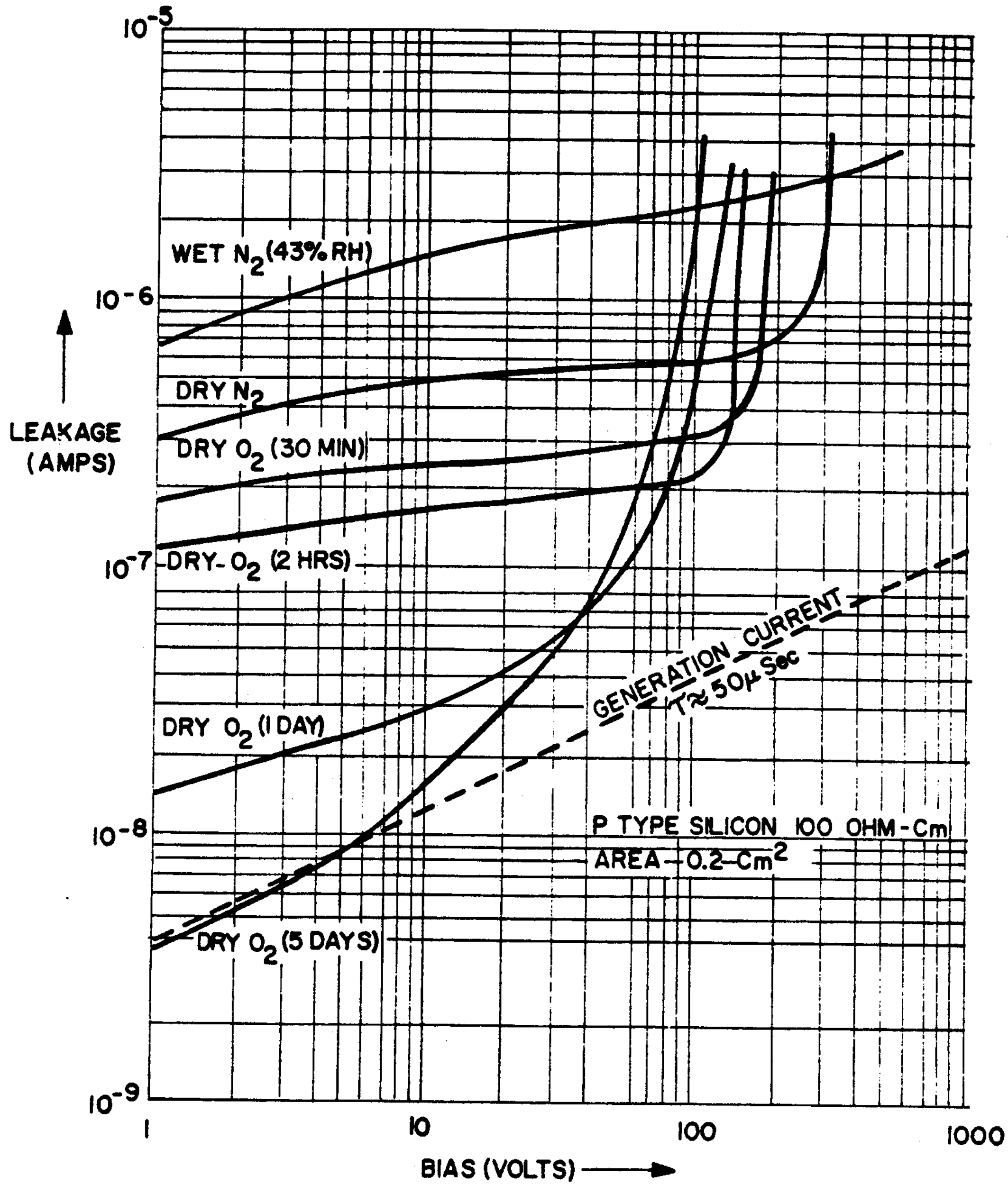

FIG 2.4
EFFECTS OF ATMOSPHERE ON BARE SILICON JUNCTION
(T.M. BUCK 1960)

MUB-6972

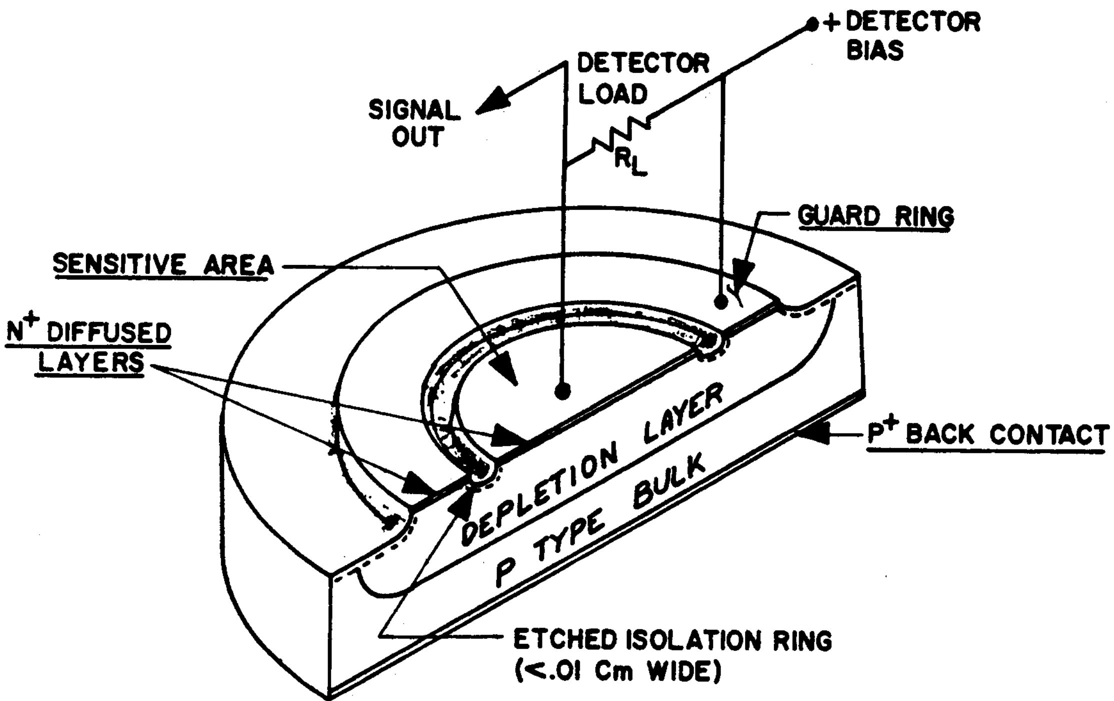

FIG 25
A GUARD RING DETECTOR(SECTIONED VIEW)

MUB-6973

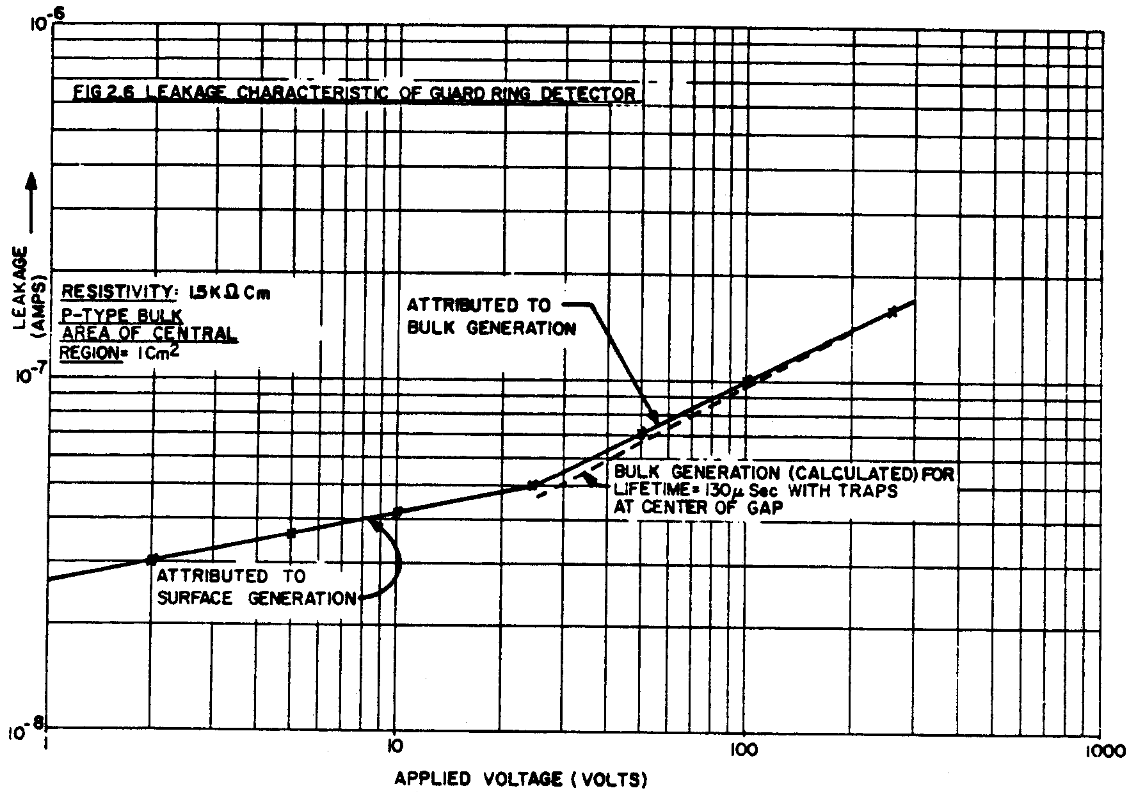

MUB-6974

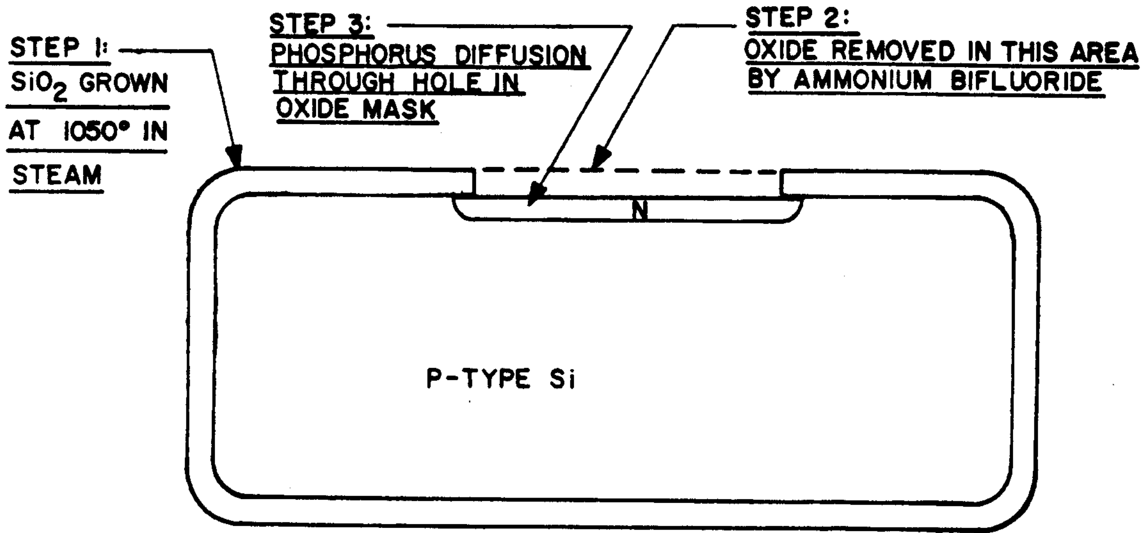

FIG 2.7
ILLUSTRATING OXIDE PASSIVATION TECHNIQUE

MUB-6975

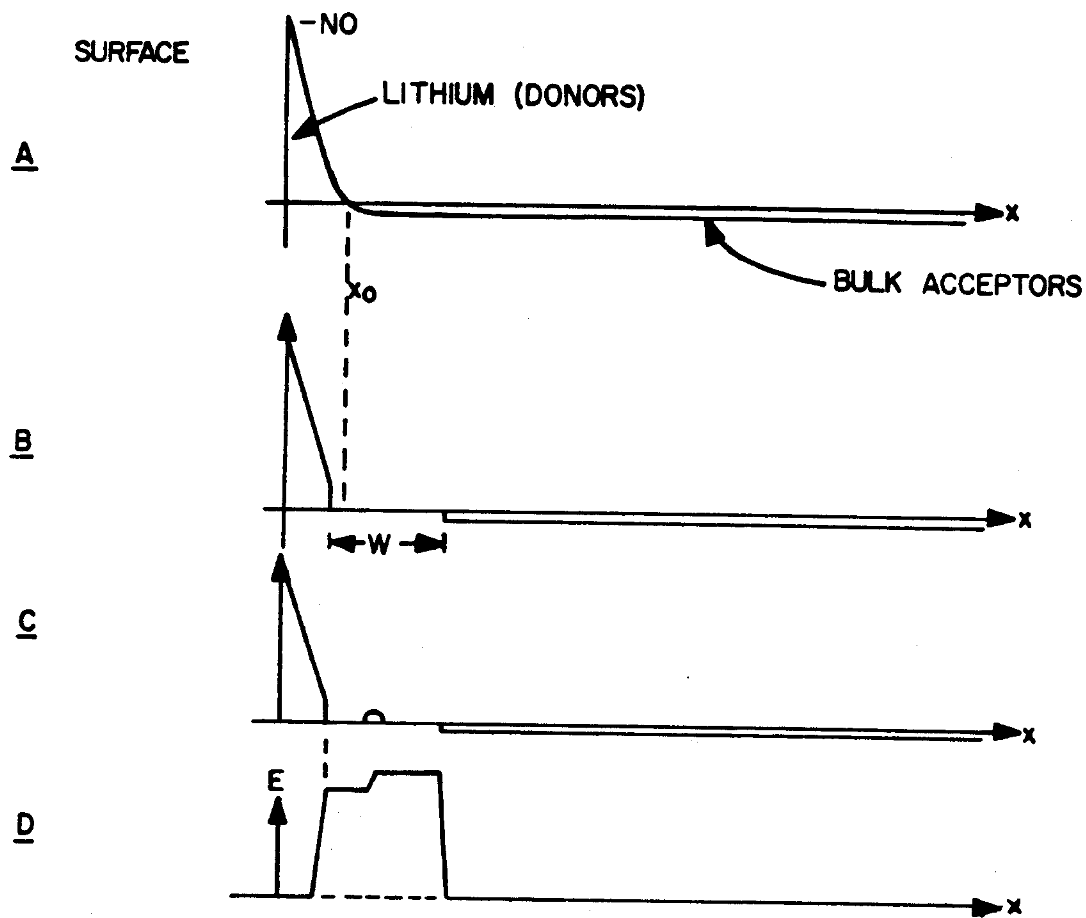

FIG 2.8 ILLUSTRATING THE LITHIUM DRIFTING OPERATION

MUB-6976

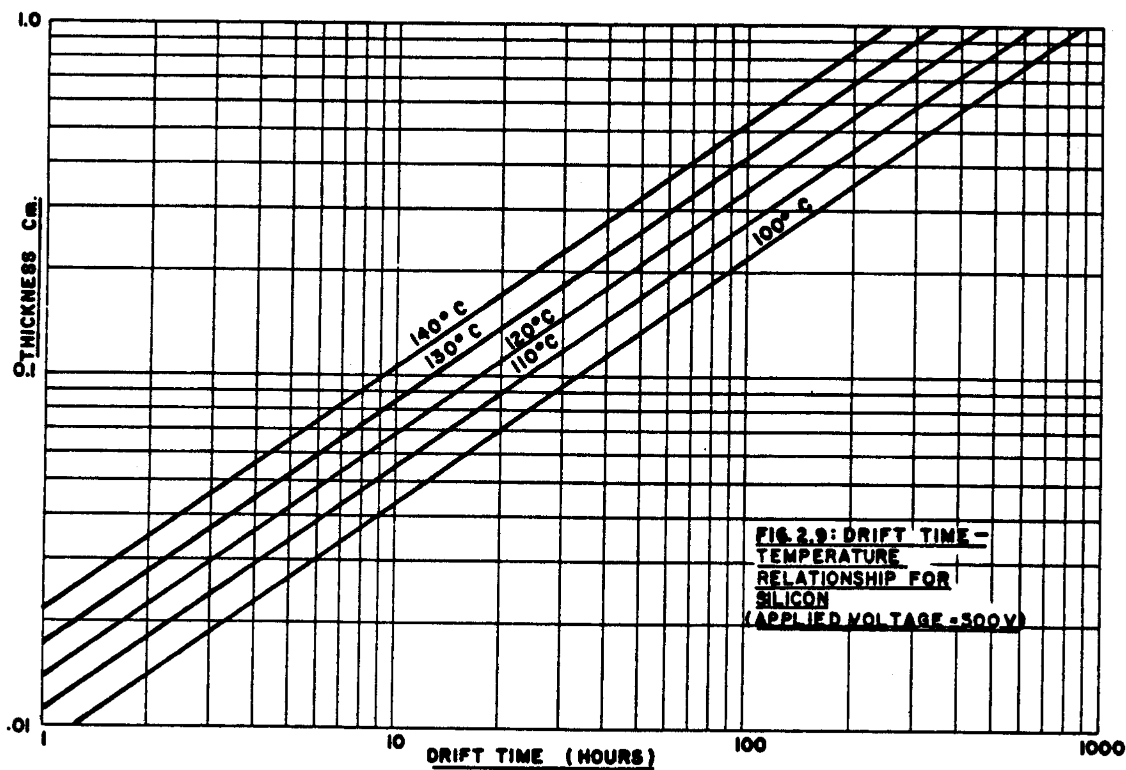

MUB-6977

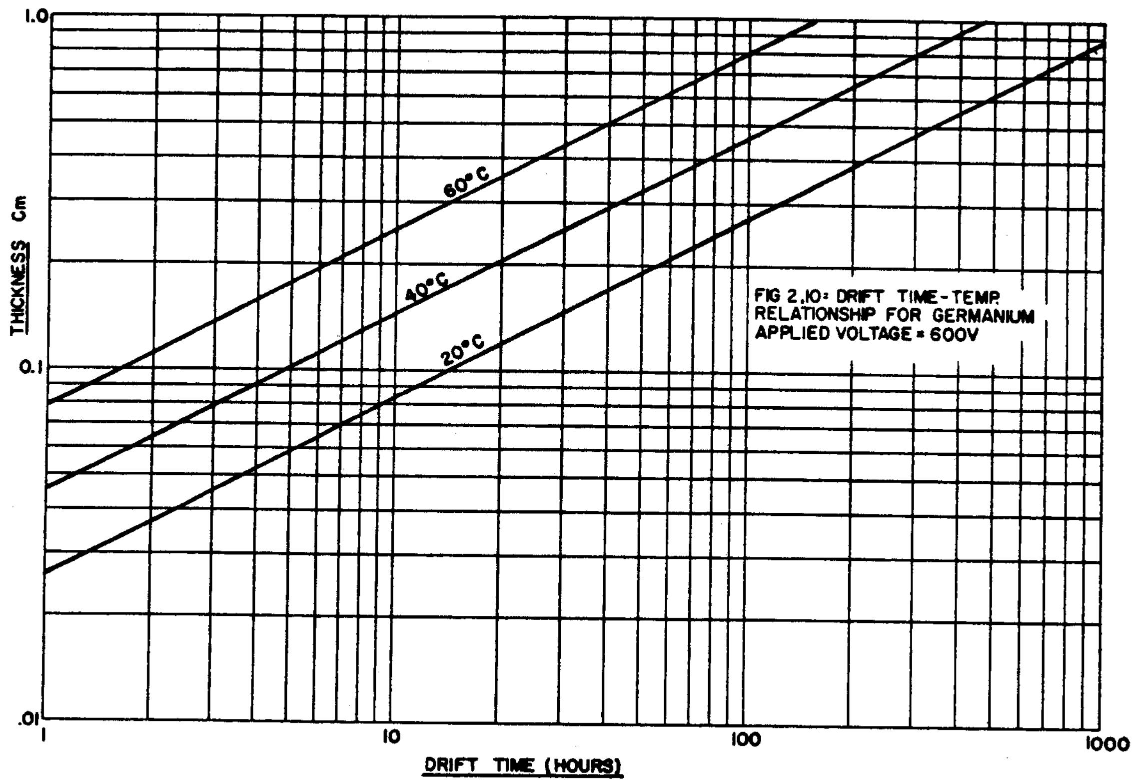

MUB-6978

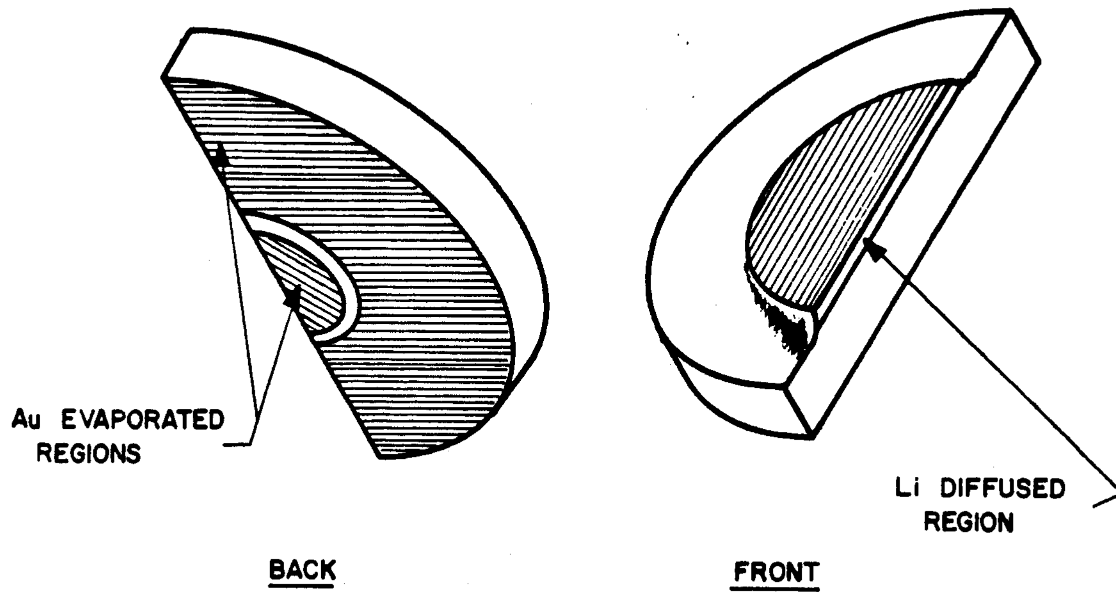

FIG 2.11

ILLUSTRATION OF SILICON WAFER PRIOR TO DRIFTING

MUB-6979

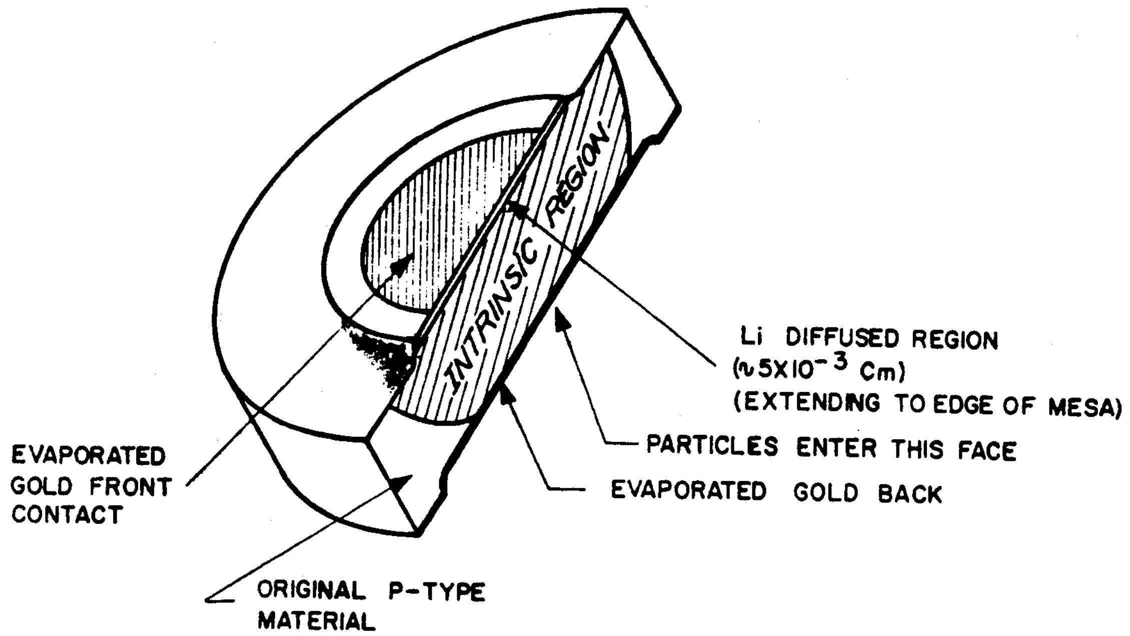

FIG 2.12
CUTAWAY VIEW OF LITHIUM-DRIFTED SILICON DETECTOR

MUB-6981

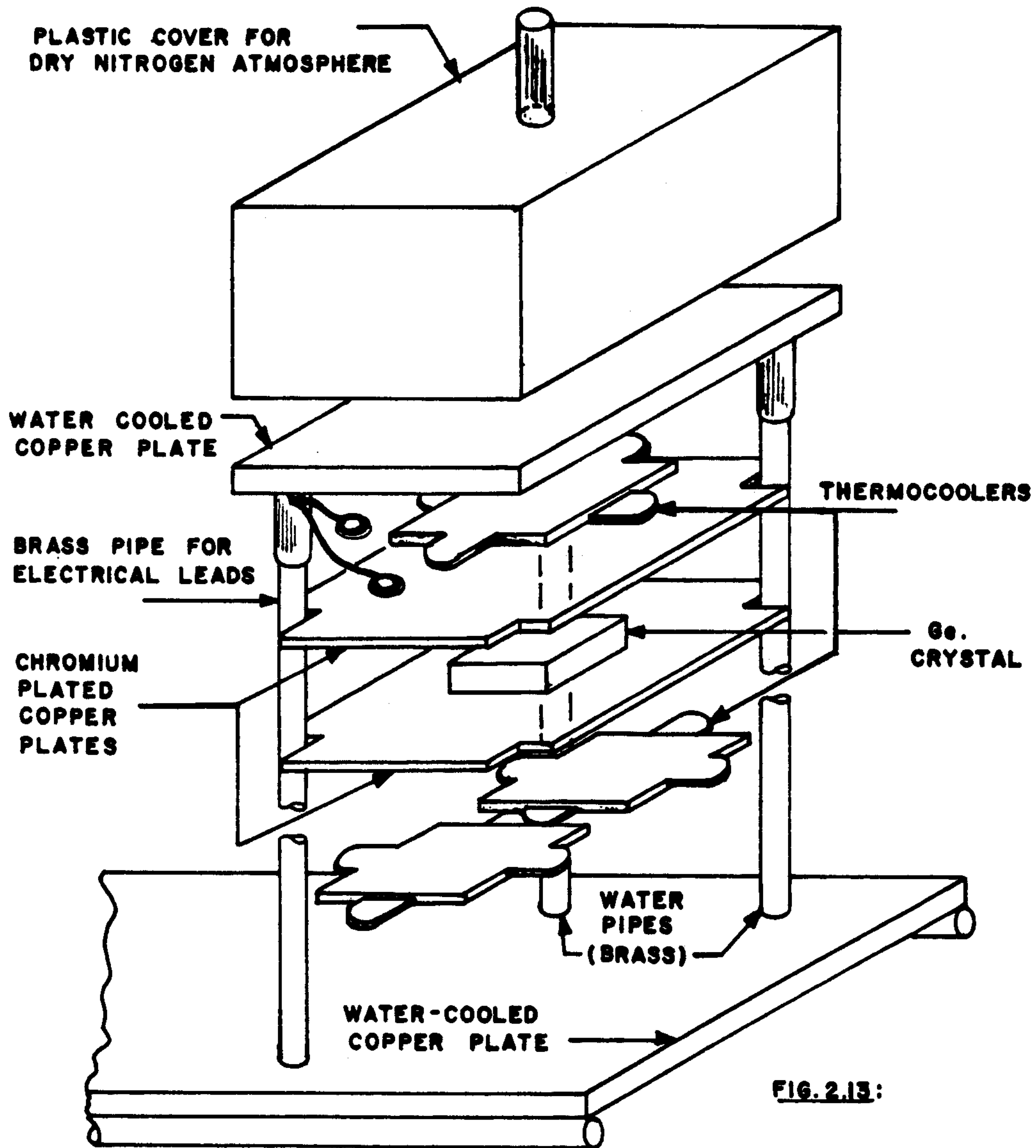

FIG. 2.13:

GERMANIUM - LITHIUM - DRIFT UNIT

(THE THERMOCOOLERS ARE ELECTRICALLY INSULATED BY MICA-SHEETS COVERED BY SILICON-GREASE FOR THERMAL CONTACT)

MUB-6982

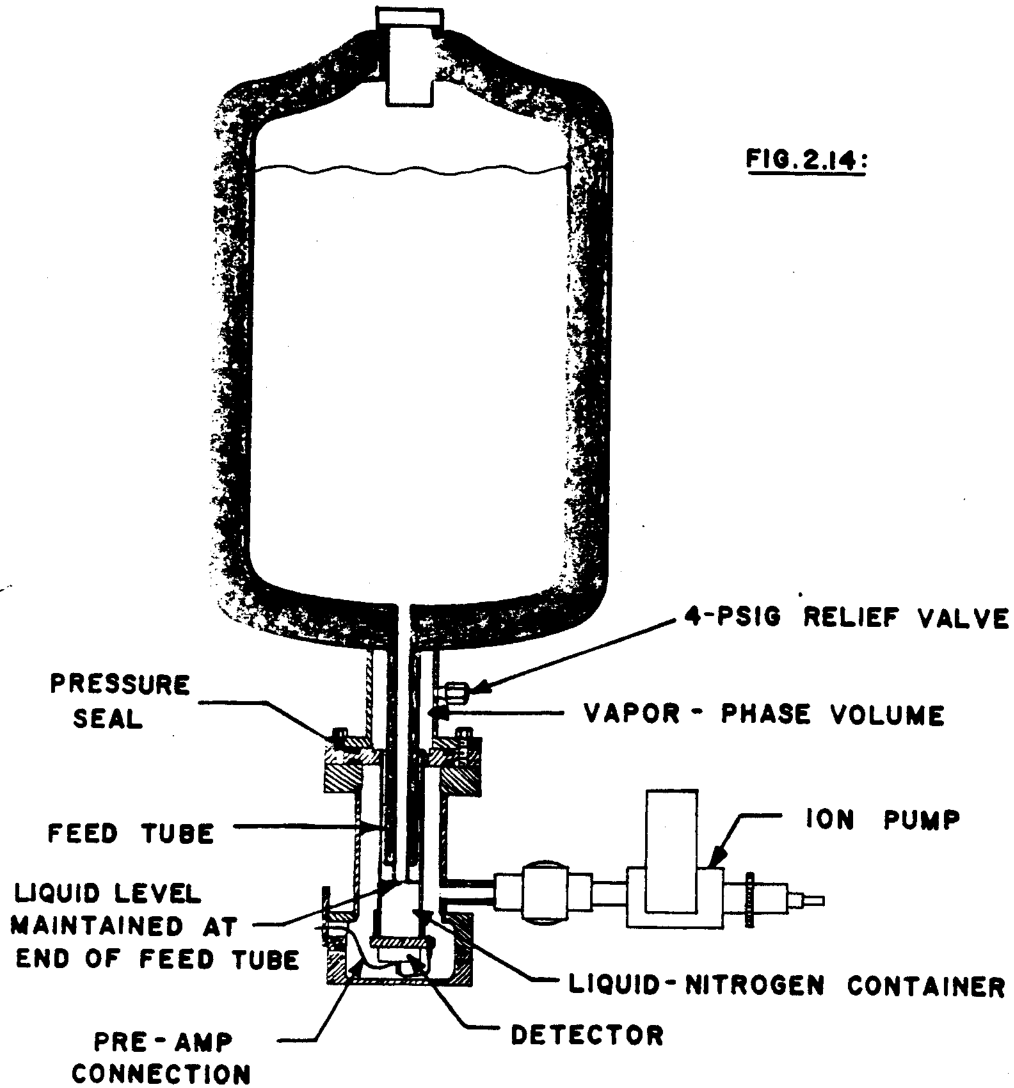
SECTIONAL VIEW OF CRYOSTAT AND DETECTOR HOLDER
FOR LITHIUM-DRIFTED GERMANIUM DETECTOR
FIG. 2.14:
4-PSIG RELIEF VALVE
PRESSURE SEAL
VAPOR - PHASE VOLUME
ION PUMP
FEED TUBE
LIQUID LEVEL MAINTAINED AT END OF FEED TUBE
LIQUID-NITROGEN CONTAINER
PRE-AMP CONNECTION
DETECTOR
MUB-6980

LECTURE 3. FACTORS DETERMINING THE ENERGY RESOLUTION IN MEASUREMENTS WITH SEMICONDUCTOR DETECTORS

Fred S. Goulding

Lawrence Radiation Laboratory
University of California
Berkeley, California

July 30, 1965

3.1 INTRODUCTION

It is difficult to give a general account of the problems of achieving high-resolution in semiconductor detector measurements as several inter-related factors are involved in the final result. In some applications one set of factors is dominant while an entirely different set may be of crucial importance in another case. Some of the factors are under the control of the experimenter (such as counting rate, optimazation of amplifier time constants, etc.), others are of a semi-fundamental nature (such as vacuum tube noise) while yet others are truly fundamental in nature (e.g., statistics of charge production in the detector). In each experiment it is necessary to appreciate which factors are important and to optimize the parameters accordingly. In this paper we will deal in some detail with the fundamental and semi-fundamental limitations and in less detail with other factors which may be encountered. Finally, an effort will be made to indicate types of experiments in which different factors are likely to be important.

In discussing the energy resolution capability of detector systems we must choose a standard of comparison between them. The standard is always based upon the equivalent spread in signals at the input to the system but the particular one employed by a writer often depends whether he is primarily concerned with designing electronic systems or is concerned with the physical aspects experiments. In the former case, the signal spread is usually quoted

in terms of the equivalent number of ion pairs corresponding to the signal spread at the input to the amplifier. To translate this into energy absorbtion in the detector, the physicist allows for the value of the average energy required to produce an ion pair in his particular detector. Most of the results on preamplifier noise are expressed here in terms of the equivalent RMS input quoted in ion (or hole-electron) pairs. On the other hand, the experimental results will be expressed as the full width at half-maximum of a peak in an energy spectrum (E_{FWHM}). For peaks with a Gaussian shape this corresponds to about 2.3 times the RMS energy spread. If two or more sources of uncorelated spread are present their effects must be added in quadrature (i.e., $\overline{E^2_{TOTAL}} = \overline{E^2_1} + \overline{E^2_2} + \ldots\ldots$).

3.2 STATISTICAL SPREAD IN THE DETECTOR SIGNAL

If all the energy lost by ionizing particles (or gamma-rays) in a detector were converted into ionization, signals produced by monochromatic radiation quanta or particles would show no fluctuations.* On the other hand, if the energy was mainly dissipated in thermal heating of the lattice and the probability of an ionizing event was very low compared with that of thermal processes, we would expect normal statistical fluctuations in the number of hole-electron pairs produced. In this case, the RMS fluctuation $< n >$ in the number of pairs produced would be given by:

$$< n > = \sqrt{\frac{E}{\varepsilon}} \tag{3.1}$$

where E = energy absorbed by the detector,

ε = average energy required to produce a hole-electron pair.

In semiconductor detectors the situation lies between these two extremes. In silicon, for example, the yield (i.e., the ratio of the energy used in ionizing events to the total energy absorbed) is about 1.1:3.6 or about 30%. Fano

*We assume here that the entire particle energy is absorbed in the detector so that such effects as the Landau collision processes can be neglected.

studied the equivalent situation in gaseous detectors[1,2] and the signal spread is now usually expressed in terms of the Fano factor F. If no is the observed RMS spread we have:

$$\overline{n_o^2} = F < n >^2 \tag{3.2}$$

In our case, it will be clear from the preceeding discussion that F must be smaller than unity. Van Roosbroeck has recently performed an elaborate statistical analysis of the situation. His methods and results are outlined in the following paragraphs.

A high energy ionizing particle (or the electron produced by a gamma-ray) produces secondary electrons of lower energy, which produce further lower energy electrons and so on. Energy losses in this shower process are of three types:

(a) An electron may impart sufficient energy to an electron in the lattice to raise it into the conduction band and produce a hole in the lattice. In this case the original energy is reduced by a small amount equal to the band-gap of the material and the remainder of the energy is shared between the degraded incident electron, the secondary electron and secondary hole. It is usual to assume that the secondary electron and hole are given equal amounts of energy although this is dependant upon details of the band structure of the material. The sharing of energy between the degraded incident electron and the hole-electron pair can be considered to be random in nature.

(b) An electron travelling through the lattice may lose energy by interactions with the lattice itself. Most of these interactions excite the lattice in an optical mode of vibration. The energy exchange in these interactions is quantized and the quanta are characterized by

the Raman frequency of the lattice. For silicon and germanium the Raman phonon energy is ~ 50 x 10^{-3} eV and the fact that the ionization yield is only ~ 30% indicates that many optical phonon collisions take place for each ionizing collision.

(c) The large numbers of very low-energy electrons produced at the end of the shower process, not having sufficient energy to produce secondary ionization, must lose the remainder of their energy by thermal losses to the lattice.

The overall process is shown diagramatically in Fig. 3.1. Using this model Van Rocsbroeck24 has calculated the curves shown in Fig. 3.2. As the average energy expended per hole-electron pair finally released is determined by the same processes as the fluctuations in the number of hole electron pairs, he has expressed both the yield (i.e., $\frac{\text{Energy Gap } (E_g)}{\text{Average energy per hole electron pair ( )}}$) and the Fano factor as functions of the average number of phonon collisions per ionizing collision (i.e., r/l-r). If we use the measured values of the average energy absorbed per hole electron pair we can, by applying Van Roosbroeck's data, derive a value for the number of phonon collisions per ionizing collision (~50 for Si, ~90 for Ge) and thence obtain probable values for the Fano factor (0.28 for Si, 0.36 for Ge).

Unfortunately accurate experimental determination of the Fano factor for silicon and germanium proves difficult due to several factors. At low energies, the statistical spread clue to the basic charge production mechanism is usually small compared with the amplifier noise. This leads to large possible errors in the determination at low energies. At high energies, many germanium detectors show poor energy resolution due, we believe, to material non-uniformity. Gamma-ray measurements at high energies in silicon are difficult due to the very low efficiency in the photo-peak which makes the measurement doubtful if done with

large activities due to the high counting rate of Compton events and, if done with small activities, due to amplifier drift, p-particle measurements, on the other hand, suffer energy loss in the entry window into the detector. Other complicating factors arise which will not be detailed here. Despite these difficulties some measurements have been carried out in both silicon and germanium and the results are consistent with Van Roosbroeck's theory. A recent set of measurements by Sven Antman and Don Landis in our laboratory is shown in Fig. 3.3. This shows a plot of the energy resolution (squared) of a 2 x 1 x 0.8 cm germanium detector as a function of gamma-ray energy. Great care was taken to eliminate amplifier drift, etc. and the fact that the points fit well on a straight line indicates that we were dealing with a purely statistical process. The Fano factor established by these measurements is 0.30 ± 0.03 which is entirely consistent with the approximate value of 0.32 derived from Van Roosbroeck's curves.

3.3 ELECTRICAL NOISE SOURCES

For practical purposes we can assume that all the charge produced in the detector is collected (i.e., it flows as current in the external circuit). Therefore, the statistical fluctuations discussed in the previous paragraph represent the only truly fundamental limits to the energy resolution. However, several factors prevent our realizing the ultimate resolution in existing systems. Before outlining these factors it will be useful to discuss a typical electronic system associated with a semiconductor detector.

Fig. 3.4(A) shows a block diagram of a typical system. The detector supply voltage is applied through a load resistor, always large in value, so that the small pulse of charge which flows in the detector in response to the passage of an ionizing particle will flow into the input of the preamplifier via the coupling capacitor C_c. After amplification the signal is passed through a

frequency selective filter (often called a pulse shaper) which, in essence, rejects as much noise while retaining as much signal as possible. A charge sensitive configuration of the preamplifier as shown in Fig. 3.4(B) is usually employed as this type of circuit gives an output signal size which, to a first approximation, is independant of the value of the detector and stray capacities which appear from its input to ground. This is purely a matter of convenience and the tradition has grown due to the fact that the capacity of a junction detector varies as the applied voltage is changed. The charge sensitive configuration is a little poorer than the conventional voltage amplifier from the point of view of resolution due to the feedback capacitor C_F behaving as an additional capacity to ground in the equivalent noise circuit (i.e., a part of CIN in Fig. 3.4(C)).

The equivalent input circuit for studying the energy resolution capabilities of the system is shown in Fig. 3.4(C). The various noise and signal elements are as follows:

(a) The input signal Q, usually assumed to be a pulse of current of very short duration compared with the time constants involved in the system. We will see later that this approximation is not always valid but will neglect these cases for the moment.

(b) The detector leakage current noise $(i_N)_D$. This is assumed to be pure shot noise which implies that it consists of individual electrons and holes crossing the depletion layer with no interaction (e.g., space charge effects) occurring between the individual carriers. It arises due to thermal generation of electron-hole pairs in the depletion layer as expressed in equations 1.13 to 1.15. The mean square value of the current fluctuations in a leakage current of

this nature is given by:

$$\overline{i^2} = 2\ q \cdot i\ \ f. \qquad (3.3)$$

where f is the frequency interval in which the noise is measured.

(c) The detector series resistance noise $(e_n)_{R_S}$ is due to resistance in the connections to the sensitive volume of the detector. If the sheet resistance of the n-type diffusion or the resistance of the bulk material at the rear of the depletion layer is high this might be an important source of noise but in well designed detectors it can be made negligible. We will assume that it is unimportant in the following discussion. This allows us to simplify the equivalent circuit by regarding the detector capacity C_D and the amplifier input capacity C_{IN} as being in parallel. We will replace $C_D + C_{IN}$ by C_T in the following discussion.

(d) The input current noise $(i_N)_G$ is due to fluctuations in the input current to the first amplifying device in the system. If this is a vacuum tube,it is the sum of the positive and negative grid currents, assuming that both are present simultaneously. The fluctuations in this current behave like those in detector leakage current and, since the two sources in the simplified circuit are in parallel, we can use equation 3.3 to represent their sum if $i = i_D + i_G$.

(e) The parallel resistance noise $(e_n)_{R_L}$ arises from any resistors shunting the input circuit. This includes the detector load, any input biasing resistor in the first stage and any resistor included across C_F in a charge sensitive preamplifier. In practice, very large values are used for these resistors* and we can regard the

*If R_L is the total effective parallel resistance the criterion of interest here is that the value of the product R_L. C_T shall be much larger than the time constants used for pulse shaping in the amplifier.

voltage source $(e_n)_{R_L}$ in series with the large resistor R_L as a current source which must also be included in the value of the current generator $\overline{i^2}$ in the previous paragraphs. The increase in $\overline{i^2}$ due to this $4 \frac{kT}{R_L}$ f. For this to be negligible we should make:

$$R_L \gg \frac{2\ kT}{q\ i} \qquad (3.4A)$$

For example, if $i = 10^{-7}$ A; $R_L \gg 5 \times 10^5$ ohm meets the requirement. We will assume now that this requirement is satisfied.

(f) The noise developed in the first amplifying device produces a voltage noise source $(e_n)_{R_{eq}}$. If this device has adequate gain the noise due to later amplifier stages is negligible. This source of noise can be represented by Johnson noise in a resistor and has the value:

$$\overline{e_n^2} = 4\ kT\ R_{eq}\ \ f \qquad (3.4B)$$

Where R_{eq} is an equivalent input noise resistance in the amplifying device. In the case of a vacuum tube it is due to fluctuations in the anode current partially smoothed by the space charge in the grid-cathode region. Its value is about $\frac{2.5}{g_m}$ for a triode having a mutual conductance g_m.

Two sources of noise are not shown in Fig. 3.4(C) but must receive some attention:

(g) Surface leakage currents arising at the periphery of the junction produce severe low frequency noise in many detectors. The guard-ring structure and correct surface passivation as described in the section on diffused detectors in Lecture #2 largely eliminate this source of noise in many applications. As no adequate theory exists

to explain the details of the behavior of this noise we will neglect it here.

(h) The plate current of a vacuum tube or other amplifying device shows fluctuations of a similar nature to those occurring at the surface of a junction detector. These fluctuations are believed to arise in processes occurring in the cathode and are dominantly in the low frequency part of the spectrum.

This source of noise, commonly called "flicker effect" is usually represented by a noise voltage generator in the input lead having the value:

$$\overline{e_F^2} = \frac{A}{f} \Delta f \qquad (3.4C)$$

where f is the frequency at which the frequency increment f is centered and A is a constant (commonly said to be about 10^{-13}).

We can therefore simplify the input circuit for practical purposes to the one given in Fig. 3.5(A). This can be further simplified to contain only voltage generators as shown in Fig. 3.5(B). We must now examine the effect of the amplifier frequency response upon the relative values of signal and noise at the amplifier output.

3.4 EFFECT OF AMPLIFIER SHAPING NETWORKS

One purpose of the amplifier is the trivial but important one of amplifying the signal to a level at which it can be used to operate logic circuits. However, both noise and signal are amplified and frequency dependant networks must be used to selectively amplify the signals more than the noise. It will be immediately obvious that a shaping network which results in the amplifier passing only a narrow range of frequencies will minimize the noise output power but, unfortunately, it will also reduce the output signal. Therefore it is reasonable to suppose that the frequency selective network has to be

optimized and the optimum network will depend upon the relative values of the voltage noise components shown in Fig. 3.5(B). Examination the noise generators indicates immediately that the noise due to input current is dominantly low frequency noise, while shot noise in the input element is more important at high frequencies and flicker noise falls between these extremes. To determine the actual contributions due to each of these terms we must evaluate their effect over the full frequency range of the amplifier.

Let F(f) represent the frequency response of the amplifier. The three contributions to output noise are then:

(a) Shot $$\overline{E_N^2} = 4\ kT\ R_{eq} \int_0^\infty \left(F(f)\right)^2 df \qquad (3.5)$$

(b) Flicker $$\overline{E_F^2} = A \int_0^\infty \frac{(F(f))^2}{f}\ df \qquad (3.6)$$

(c) Current $$\overline{E_I^2} = \frac{qi}{2\ \pi^2\ C_T^2} \int_0^\infty \frac{(F(f))^2}{f^2}\ df \qquad (3.7)$$

We must now examine typical frequency selective networks to permit evaluation of the three integrals in (3.5), (3.6) and (3.7). In general, the complete network will consist of at least one low-pass network (e.g., an RC integrator) to reduce the shot noise, which would otherwise increase rapidly at high frequencies, and at least one high-pass network (e.g., an RC differentiator) which serves to reduce low frequency noise due to input circuit currents. It will be convenient to express the parameters of the networks in terms of a normalized frequency f_o (and an equivalent time constant $t_o = \frac{1}{2\ \ f_o}$). Thus, a single RC integrator network of time constant , will be represented by a parameter n, where = n $_o$. The frequency f will be represented by the parameter m where $f = m\ f_o$. The gain-frequency function for the RC

integrator shown in Fig. 3.6(A) therefore becomes:

$$\text{Gain}^2 = \frac{1}{1 + 4\,\pi^2\, f^2\, R^2\, C^2} = \frac{1}{1 + (nm)^2}$$

The gain-frequency function for a number of elements used to build up shaping networks: expressed in this form, are shown in Fig. 3.6.

In terms of the parameters m and n the equations 3.5, 3.6 and 3.7 can be rewritten:

$$\overline{E_N^2} = 4\,kT\,R_{eq}\,f_o \int_0^\infty (F_1\,(m_1,n_1)\cdot F_2\,(m_1,n_2)\;....)\;dm \qquad (3.8)$$

$$\overline{E_F^2} = A \int_0^\infty \frac{(F_1\,(m_1,n_1)\cdot F_2\,(m_1,n_2)\;....)}{m}\;dm \qquad (3.9)$$

$$\overline{E_I^2} = \frac{qi}{2\,\pi^2\,C_T^2\,f_o} \int_0^\infty \frac{(F_1\,(m_1,n_1)\cdot F_2\,(m_1,n_2)\;...)}{m^2}\;dm \qquad (3.10)$$

where $F_1\,(m_1,n_1)$ represents the frequency response (squared) of the first element in the shaping network.

$F_2\,(m_1,n_2)$ represents the frequency response (squared) of the second element in the shaping network, etc.

We note now that once a network is chosen (and we assume here that it is built up of some of the elements shown in Fig. 3.6; elements may be repeated more than once) the integrals involved in equations (3.8), (3.9) and (3.10) can be evaluated. We then see that the time scale can be changed (i.e., f_o is changed but n_1, n_2, etc., remain the same) and only the constants before the integration signs are affected. Thus the shot noise^2 is always proportional to f_o (or inversely to $_o$), the flicker noise^2 is always

---

*These elements may require a few words of explanation. The RC integrator and RC differentiator require no elaboration. The delay line integrator is a little different from the shorted line frequently employed in amplifiers but, analytically, it amounts to the same thing. A delayed signal is subtracted from the input signal at the input to an operational amplifier stage. The fedback integrator and differentiator are standard operational amplifier configurations and, for the purpose of analysis, the open-loop gain of the amplifier is assumed to be infinite.

independant of f_o and the input current noise^2 is always inversely proportional to f_o (or proportional to $_o$). This is independant of the specific types of element used in the shaping network.

To illustrate a specific case of equations (3.8), (3.9), and (3.10) we will look at the shaping network containing a single RC integrator of time constant $_o$ and a single RC differentiator of time constant to isolated by a suitable stage $_o$ prevent interaction between the two elements. In this case equations (3.8), (3.9), and (3.10) become:

$$\overline{E_N^2} = 4\ kT\ R_{eq}\ f_o \int_0^\infty \frac{m^2}{(1 + m^2)^2}\ dm \tag{3.11}$$

$$\overline{E_F^2} = A \int_0^\infty \frac{m}{(1 + m^2)^2}\ dm \tag{3.12}$$

$$\overline{E_I^2} = \frac{qi}{2\ \pi^2\ C_T^2\ f_o} \int_0^\infty \frac{1}{(1 + m^2)^2}\ dm \tag{3.13}$$

These integrals can easily be evaluated analytically and, for this reason, this case is dealt with in all textbooks. More complex networks containing several RC integrators, delay line shapers, etc., are analytically quite unmanageable but the author has recently dealt with a number of such complex networks by a numerical integration procedure using a computer (see Table 3.1). The results will be presented shortly.

Hitherto we have concerned ourselves primarily with the effect of these shaping networks on noise. We must now see what effect they have in the signal. We mainly interested in the peak height of the output signal as this is the quantity measured by a pulse-height analyzer. The input signal, as shown in Fig. 3.5(B), consists, to a first approximation, of a step function of amplitude $\frac{Q}{C_T}$. The response of a number of typical networks to a unit step function has

been calculated using a digital computer (see Table 3.1) and, for the moment, we will assume that the output peak pulse height (for unity amplitude input) is P. Since we are dealing with a linear network the output pulse amplitude due to the detector signal is then $\frac{PQ}{C_T}$. In comparing this with the noise we must either square the signal or take the square root of the $\overline{\text{noise}^2}$. We will choose to use the signal squared:

$$S^2 = \frac{(PQ)^2}{(C_T^2)} \quad .$$

The general equations (3.8), (3.9), and (3.10) can be rewritten:

$$\frac{\overline{E_N^2}}{S^2} = \frac{4\ kT\ R_{eq}\ C_T^2}{P^2\ Q^2}\ f_o \int_0^\infty (F_1\ (m_1,n_1)\ \cdot\ F_2\ (m_1,n_2)\ \ldots)\ dm \qquad (3.14)$$

$$\frac{\overline{E_F^2}}{S^2} = \frac{A\ C_T^2}{P^2\ Q^2} \int_0^\infty \frac{(F_1\ (m_1,n_1)\ \cdot\ F_2\ (m_1,n_2)\ \ldots)}{m}\ dm \qquad (3.15)$$

$$\frac{\overline{E_I^2}}{S^2} = \frac{qi}{2\ \ {}^2\ P^2\ Q^2\ f_o} \int_0^\infty \frac{(F_1\ (m_1,n_1)\ \cdot\ F_2\ (m_1,n_2)\ \ldots)}{m^2}\ dm \qquad (3.16)$$

It is common to express the noise as the equivalent input noise signal quoted in ion (or hole-electron) pairs. This implies rewriting equations (3.14), (3.15) and (3.16) with 1.6×10^{-19} coulombs inserted for Q. To simplify the presentation we will also substitute I_1, I_2, and I_3 for the three integrals and will assign values to some of the constants:

$$\overline{E_N^2} = 2.08\ T\ (R_{eq}\ C_T^2).\ \ f_0 \left[\frac{I_1}{P^2}\right] \times 10^{15}\ (\text{ion pairs}^2) \qquad (3.17)$$

$$\overline{E_F^2} = 3.9\ (A\ C_T^2).\ \left[\frac{I_2}{P^2}\right] \times 10^{37}\ (\text{ion pairs}^2) \qquad (3.18)$$

$$\overline{E_I^2} = 3.15\ (i).\ \frac{1}{f_0}\ \cdot\ \left[\frac{I_3}{P^2}\right] \times 10^{17}\ (\text{ion pairs}^2) \qquad (3.19)$$

We note that the dependance of the three types of noise on the shaping network is contained in the second terms in parenthesis. The inverse of these ratios, calculated by a computer for a number of types of netvork, are shown in Table 3.1. The dependance of noise on the input circuit and on the input amplifying element is contained in the first terms in parenthesis. The equivalent shot and flicker noise squared are each proportional to the total input capacity squared. On the other hand, the equivalent input current noise squared is independent of the capacity. The overall frequency dependance of the three types of noise is shown in the terms containing f_o.

In Table 3.1 the first four cases involve only RC shaping elements while the remaining cases use delay-line feedback integrators and simple RC shaping elements. Comparison of cases #9 and 10 illustrates the worsening of noise due to double delay-line differentiation. Case #8 is a special one which was studied mainly from the point of viev of the rather ideal pulse shape it produces. In all cases, the value in the $\frac{P^2}{I}$ column can be regarded as a figure of merit of the network for that particular type of noise. Comparing case #5 with case #1 we see that the single delay line with RC integrator is superior in shot noise ($\frac{P^2}{I_1} \approx 0.200$ as compared with 0.172), flicker noise (0.376 compared with 0.270) and input current noise (0.34 compared with 0.172.). The use of two RC integrators ($\frac{{}_o}{2}$) with the delay line (${}_o$) improves shot noise at a small cost in flicker and input current noise.

However, comparison between networks is not as simple as indicated in Table 3.1. In many experiments an important factor involved in the choice of network is the speed of recovery of the shaped waveform to the baseline. This parameter determines the degree to which pulse pile-up will be a factor at high counting rates. Fig. 3.7 shows the pulse shapes produced by several of the networks listed in Table 3.1. We see that, of the cases shown here, the long

tail associated with the RC integrator-differentiator case (#1) is considerably worse than that in the RC integrator-DL differentiator case (#5). The network #8 is unique among the networks considered here in tha its tail has completely ended 2.0 μsec after the start of the pulse. Among the more conventional networks, the double delay line differentiator networks possess notable advantages at high counting rates. Not only is the tail on the double delay-line pulse comparatively short but the complete area balance between positive and negative components of the pulse means that base-line fluctuations at high rates are small. As seen in cases #9 and #10 of Table 3.1, however, the price paid for using a double as compared with a single delay line is an increase in noise.

Another factor influencing the choice between shaping networks is their sensitivity to input pulse rise-time variations. As will be seen in Lecture 4, the pulse shape from a practical detector does not have an infinitely short rise-time and the rise-time depends upon the initial location of the ionization in the detector. If the maximum collection time is an order of magnitude smaller than the time constants involved in the shaping network, the effect of detector rise time variations is negligible but this is not the situation when using thick silicon and germanium detectors. We have experienced difficulties in using 3 mm thick silicon detectors for alpha-particles in the energy range 20 - 120 MeV due to the variation of rise-time in the detectors which ranges from about 100 nsec to 300 nsec depending upon particle energy.* This is in the same general range as the time constants used in the shaping networks so that the output amplitude departs from being a linear function of input particle energy. Moreover, since the particle range is subject to statistical variations, another source of spread in the amplitude of output signal becomes evident. In cases where this might happen, the choice of shaping network is influenced by its sensitivity to input pulse rise-time in addition to the signal to noise

* The particles are incident normal to the detector window and therefore the particle track extends along the lines of electric force.

and counting rate factors discussed earlier. As a general rule, networks whose output pulse shape has a rounded top (i.e., $\frac{d^2V}{dt^2} = 0$ at V_{max}) exhibit less input pulse shape dependance than networks having a peaked top. It will be evident from Fig. 3.7 that the single RC integrator delay-line differentiator #5 (with the delay line length equal to the RC integrator time constant) is poor in this respect. Using a numerical method the behavior of several typical networks with regard to input pulse shape sensitivity has been calculated and the results are given in Table 3.2. This table shows the percentage loss in pulse height at the output when 40 and 85 MeV alpha-particles enter a 3 mm silicon detector (at 25°C with 350 V applied to it) as compared with the pulse height if the detector exhibited an infinitely short rise time. We note that similar results would be obtained if gamma-rays interacted at various points in the detector.

Examination of Table 3.2 shows, as expected, that the networks which provide flat-topped pulses perform better with regard to pulse shape sensitivity. The Table also shows that increasing the time constants of a network to seperate them further from the input pulse rise time produces a considerable improvement. However, this increases the input current noise and counting-rate dependance. The network #9 (which is the same as #8 in Fig. 3.7 and also #8 in Table 3.1) was designed to produce good input pulse shape dependance at the same time as good noise and counting rate characteristics. This result is achieved but the complexity of the arrangement prohibits its general use. Finally we must note that the fact that the percentage loss figures in Table 3.2 differ for the 40 and 85 MeV particle results in a non-linearity in the energy calibration of the system. In case #5 this non-linearity amounts to about 2.1% and had been observed experimentally prior to these computations. A gross worsening of energy resolution had been observed at the higher energies in these experiments and both the linearity and resolution effects were largely corrected by changing to the conditions in Case #8.

3.5 VACUUM TUBES AS THE INPUT AMPLIFYING DEVICE

The optimum choice of vacuum tubes for use as input amplifiers depends upon the type and properties of the detector being employed. For the purpose of analysis it is usual to assume that the sources of noise associated with a vacuum tube are grid current noise (which contributes to the input circuit noise of equation (3.19)) flicker noise (which contributes to E_F in equation (3.18)) and shot noise (which is responsible for the R_{eq} of equation (3.17)). The grid current and shot noise in a modern vacuum tube are believed to be well understood theoretically but the flicker effect can differ greatly between different types of tube and even between individual tubes of one type. Therefore choice of tube type is made first on the basis of the two best understood parameters and final selection is usually made by carrying out noise measurements on many samples of the selected types of tubes to determine the amount of flicker and unexplained noise contributions.

According to Fairstein, the grid current of a triode operated in the normal mode* is caused primarily by photoelectric emission from the grid due to soft x-rays produced at the anode by electron bombardment. The grid current is given approximately by:

$$I_g = E_{g-p}^{\frac{3}{2}} I_K \times 10^{-10}$$

where I_g = grid current in amperes,

E_{g-p} = grid to anode voltage in volts,

I_K = cathode current in amperes.

For example, if I_K = 12 mA and E_{g-p} = 100 V; $I_g \approx 1.2 \times 10^{-9}$ A. The grid current of a typical EC-1000 (Phillips) tube operationg under these conditions is about 2×10^{-9} A which is in satisfactory agreement with Fairstein's theory.

*It is assumed that the grid bias is large enough to prevent electron collection at the grid.

It is well known that the equivalent noise resistance of a vacuum tube triode is approximately equal to $2.5/g_m$* where g_m is them utual conductance expressed in mhos. However, to prevent very high frequency oscillations in a vacuum tube it is necessary to insert a grid "stopper" resistance in the grid lead. This must be added to the tube noise resistance to obtain R_{eq} in equation (3.17). For the EC-1000 tube operated under the conditions of the previous paragraph and with a 22 ohm grid stopper $g_m \approx 16$ mA/V and $R_{eq} = 180$ ohms.

It will be clear from the previous two paragraphs that a tube which operates at a low plate voltage and current will produce a small grid current. However, this will result in a rather low value of mutual conductance. From equations (3.17) to (3.19) we see that this means that the vacuum tube will contribute little noise if long time constants are used in the shaping network (i.e., f_o small) and considerable noise for short time constants. If a detector (such as lithium-drifted germanium at liquid nitrogen temperature) has very little leakage current and low capacity, use of an input tube having these characteristics might make good sense. However, the optimum shaping network would have a long time constant (~5 μsec) and the performance at even moderately high counting rates performance would be very poor. Moreover, many extraneous sources of noise such as detector surface noise, microphony in the tube, etc., tend to increase at low frequencies. In practice it is usually more satisfactory to try to work with short time constants in the shaping network and to choose the tube accordingly.

A high-capacity high-leakage detector calls for a tube having the highest possible mutual conductance. Its high grid current is of little consequence since it is swamped by the detector leakage current. In this case the optimum time constant in the shaping network will be in the 0.5 to 1 μsec region. We use a 7788 for these purposes.

---

*If this value is to be put into equation (3.17) T must be assumed to be 300°K.

The preamplifer used in our laboratory for the great majority of high resolution experiments is shown in Fig. 3.8. As a large amount of data has been accumulated on this preamplifier we will examine its characteristics in some detail. The input tube's anode couples to the grounded base stage Q1, and the collector output of Q1 is emitter followed by Q2. The collector load of Q1 is bootstrapped from the emitter of Q2 via C1 so that the effective load presented to the collector of Q1 is almost purely capacitive in the frequency range of interest. The transistor type used for Q1 and Q2 has very low collector-base capacity to speed up the response at the collector of Q1 as much as possible. Feedback to make the input stage charge sensitive is taken from the emitter of Q2 via RF C_F to the grid of the input tube. A 0.5 pF test capacitor feeds a test signal to the input grid when required and the detector signal couples via C_c to the same point. The output signals from the charge sensitive loop feed the feedback amplifier stage containing Q3 and Q4 and their output feeds a similar stage containing Q5 and Q6. The total gain in these two stages is 8 but this can be reduced by a factor of 3 by switching S1 to the low gain position.

Fig. 3.9 shows the behavior of the equivalent noise (squared) for a typical preamplifier of this type used with equal RC integrator and differentiator in the shaping network. The plot shows the variation in the mean noise squared as a function of the shaping network time constant $_o$ ($_o = \frac{1}{2 \quad f_o}$) of equations (3.17) to (3.19)) and as a function of the capacity from input to ground. This simulates the effect on the resolution of detector capacity.

The full lines in Fig. 3.9 are experimentally measured curves while the dotted lines are calculated contributions (from equations (3.17) to (3.19)) from the three noise sources for a value of C_T = 14 pF. The constant A in the calculation of flicker effect has been chosen* to produce the best match of the

*The value of A which appears to be applicable to this case is about 7 times larger than the generally accepted 10^{-13}. All our experience indicates that the generally accepted value is too low.

sum of flicker, shot and grid current noise contributions to the experimentally measured curve for C_T = 14 pF. The match is almost perfect, and, if the noise contributions are calculated for the other values of CT, equally good agreement is obtained.

From Fig. 3.9 we note that the resolution of a germanium detector - preamplifier combination in which the detector has a capacity of 6 pF (i.e., C_T = 20 pF) and very low (< 10^{-9} A) leakage is best for a time constant of 1.0 µsec and corresponds to slightly over 2 keV FWHM. This is observed experimentally with good small area detectors. In Fig. 3.10, the effect of a slightly different shaping network is shown. If we add a second RC integrator equal in time constant to the first one (and to the differentiator), the energy resolution for the 6 pF detector becomes optimum at a time constant of 0.5 µsec and is about 1.85 keV. Also, shown at the right hand side of these curves are some results for delay-line shaping with two equal RC integrators. We see that the 6 pF detector case gives a little less than 1.8 keV. On the other hand, we note that, due to the short time constant (0.8 µsec) of the delay-line differentiator, the performance of the delay-line system is worse than the RC system (at its optimum point) when higher capacity detectors are used.

A convincing illustration of the validity of the theoretical model is shown in the comparison between Figs. 3.10 and 3.11. The only difference between the cases shown in these two figures is that the shunt input resistance (R_F in shunt with R_L) is 60 M ohm in Fig. 3.10 and 500 M ohm in Fig. 3.11. This should theoretically (see section 3.3(e)) change the effective value of the grid current by 0.8 nA. The improvement at long time constants in Fig. 3.11 is close to this value. The improvement in resolution for the 6 pF detector case is significant (now 1.7 keV).

For future reference in discussing some of the fast timing possibilities of detectors, the rise time behavior of this preamplifier is shown in Fig. 3.12. However, it should be remembered that, if a fast amplifier is used to amplify the signals from the preamplifier, the noise levels, instead of being those shown in Figs. 3.9 and 3.10, are determined by the time constants in the fast amplifier. If it contains a differentiator - integrator combination of 10 nsec time constant the energy resolution with a 12 pF detector will be in the region of 15 keV FWHM.

3.5 ALTERNATIVE LOW NOISE AMPLIFYING ELEMENTS

Particularly for low-energy gamma-ray measurements, the energy resolving capability of a semiconductor detector spectrometer is determined at the present time by the electrical noise properties of vacuum tubes. While minor improvements (e.g., higher gm and reduced igand capacity) in vacuum tube characteristics can be anticipated it seems unlikely that radical improvements will. arise in this area. It is natural, therefore, to inquire into the possibility of obtaining better performance by using techniques not based upon vacuum tubes. Ultimately we might hope that the energy resolution will be determined solely by the statistical process described in section 3.2 and, to accomplish this, we look for an improvement of about 5:1 in the electronic resolution of these systems.

A little work has been done on the use of a parametric amplifier system (Chase and Radeka) and some promising results have been obtained. However, parametric amplifiers are much more complex than our normal amplifiers in requiring the use of a very high frequency radio frequency carrier. As a consequence the behavior of such systems is difficult to analyze and, moreover, obtaining the ultimate performance depends upon critical aajustment of parameters. Probably for these reasons, no significant results have yet been published on systems of this type.

A more promising alternative at the present time seems to be the use of a bulk* field-effect transistor. The operation of this device is illustrated in Fig. 3.13 which shows a source and drain electrode connected by an n-type "channel" which is partially "pinched off" by the depletion layer produced by a reverse biased "p" region diffused into the side of the n-type channel. (Note that p-type channel devices are also available.) From our previous discussion it will be obvious that increasing the negative bias on the gate electrode of Fig. 3.13 causes the thickness of the conducting channel to be reduced thereby modulating its impedance. Moreover we note that the impedance seen looking into the gate electrode is very large - being that of a reverse biased diode. Due to the voltage drop along the length L of the channel the junction is reverse biased to a greater extent near the drain electrode and the voltage distribution along its length has the general form shown in Fig. 3.13. We will only discuss certain aspects of the theory of field-effect transistors here but the behavior of the device is well understood and has been thoroughly analyzed.

For some time we have been using field-effect transistors of this type in a general purpose preamplifier not used for very high resolution work. Fig. 3.14 shows the circuit of this unit and will be used to illustrate the mode of use of a field-effect transistor before we examine some of its noise characteristics, which are of major importance to us in high resolution spectrometry. Comparing this unit with the vacuum tube preamplifier we see that the basic configuration of the input charge sensitive stage containing Q1, Q2, Q3 and Q4 is similar to that of the stage containing input tube, Q1, and Q2 in Fig. 3.8. However, due to the low voltages required for the field effect transistor we are able to conveniently D.C. couple the complete loop. Also,

*We have delibertely used the word bulk to discriminate between this type of field effect transistor in which control of carriers takes place in the bulk material and the type (MOS) in which the conductivity of a surface layer under an oxide is modulated. Since conduction in a surface layer will most likely be noisy (this is confirmed by experiment) we will neglect the MOS type of transistor in this discussion.

owing to the rather low mutual conductance (4 mA/V) of the field-effect transistor, we have found it necessary to use a White emitter-follower Q3, Q4 within the feedback loop to raise its gain and thereby improve the rise time. Only a single gain stage is used at the output of this preamplifier; this is due to the particular area of use aimed for in the design. We should note two features concerning the input circuit of this preamplifier. The diode CR1 is provided to protect the transistor against high voltage surges introduced when switching detector voltage on or off. The adjustable feedback and test capacitor arrangements are used to align many preamplifiers to have the same energy calibration and, in fact, in the particular installation using these preamplifiers, a Helical potentiometer pulser dial is calibrated directly in MeV (100 MeV = 1 V into the test capacitor).

According to the analysis of Van der Ziel,[25,26] the noise introduced by a field-effect transistor is due simply to resistance noise occurring in segments of the conducting channel. A noise voltage developed in a small element of the channel modulates its width and thereby affects the channel conductance. Also, the noise modulation of the depletion layer width causes a noise current to flow in the gate electrode circuit. These effects can conveniently be expressed for all practical purposes in an equivalent noise resistance R_{eq} given by:

$$R_{eq} = \frac{0.7}{g_m} \left(1 + \frac{1}{3} \frac{C_{gs}}{C_T}\right) \qquad (3.20)$$

where C_T is the total input shunt capacity (as always).

C_{gs} is the gate-source capacitance of the FET.

Equations (3.17) to (3.19) are still valid for this case, where R_{eq} in equation (3.17) is assigned the value calculated from equation (3.20); constant A in equation (3.18) is the flicker noise constant (not known for FET's but probably quite variable from unit to unit due to surface effects at the edge of the junction); i is the gate junction leakage current.

In choosing a field-effect transistor for use as an input amplifying element the same considerations apply as in the vacuum tube case. Since, in most practical situations detector leakage current noise and surface noise cause noise at long time constants, the objective should be to design for an optimum shaping network with a time constant close to 1 μsec. This places emphasis on keeping R_{eq} small and, therefore, g_m large. Commercial units are available in the range 2 mA/V to 20 mA/V and these justify examination.* Assuming a slightly worse value of R_{eq} than equation (3.20) would indicate and a typical total capacity of 20 pF, Fig. 3.15 shows the noise behavior predicted for gate junction leakage current noise (assuming 10^{-9} A which is typical) and for channel noise for different values of g_m for room temperature operation. We have shown no flicker noise contribution in these curves but recognize that, in practice, such a contribution may be dominant. For a transistor having a g_m of 5 mA/V and $i_g = 10^{-9}$ A the FWHM resolution indicated by Fig. 3.15 is 1.6 keV with an optimum time constant of 2 μsec. If the mutual conductance is 10 mA/V the optimum moves to 1.3 μsec and the resolution becomes 1.3 keV.

While recognizing that practical devices rarely agree precisely with theory, it is extremely promising when theory predicts such attractive results. However the situation improves still further when we look at the theoretical behavior at liquid nitrogen temperature. At low temperatures one might expect flicker noise to disappear** and this removes an important unknown trom the theory. Moreover, in equation (3.17) we note that the absolute tempearture T

---

*We note that, if $C_T = C_{gs}$ (i.e., no added capacity) then $R_{eq} < 1/g_m$. This is to be compared with $2.5/g_m$ for a triode, a 2.5:1 improvement for the same g_m. On the other hand, a low g_m in the first amplifying element may cause noise in the second element to become important.

**One can argue that we see no flicker noise in very large area germanium detectors at 77°K and, therefore, can expect even less from the minute field-effect device gate junction.

appears and, unlike the vacuum tube case, we can use low temperatures to reduce this source of noise. Furthermore, the gate junction leakage current fails practically to zero and input current noise will be solely that due to generation of carriers in the bulk of the detector, Fig. 3.16 shows the predicted behavior of channel noise and input current noise at 77°K. We see that a g_m of 10 mA/V and detector leakage of 2×10^{-10} A gives optimum resolution of 0.6 keV at 1.5 μsec time constant.

It is interesting to note that it is, in principle, very simple to make high mutual conductance field-effect transistors for operation at liquid nitrogen temperature. Since, at this temperature, the donors (or acceptors except indium) are fully ionized, the behavior of the depletion layer as a function of gate voltage is unchanged as compared with room temperature operation. However, the channel conductivity in good material will be ~30 times larger at 77°K than at 300°K due to the increase in carrier mobility. Both the g_m and the device current will increase by this factor. If the power dissipated by the device can be removed while maintaining it close to 77°K a high value of g_m should be available. Alternatively, if the current is maintained constant while cooling the device, the depletion layer adjusts itself to thin down the channel and the gate-source capacitance is reduced -- another desirable result.

Measurements of commercial device parameters at low temperatures prove to be disappointing. Nearly all these devices are manufactured with a highly-doped poor quality epitaxial channel and impurity scattering limits the improvement in g_m to a factor of about 3 as compared with room temperature operation. Moreover, one suspects that the impurity scattering and trapping processes in the channel introduce aacitional noise sources. Due to this we are in the process of making our own FET using materials and techniques similar to those

employed in diffused detectors. However, with all their drawbacks, commercial field-effect transistors do perform as reasonably low-noise amplifiers and we present here some measurements on these devices.

The circuits used in these measurements are shown in Fig. 3.17. The upper circuit is used for testing n-channel devices while the lower one tests p-channel units. The designs are similar to that of Fig. 3.14 and employ the same output stage. Choice of resistor R in Fig. 3.17 permits adjustment of the current in the field-effect transistor over a wide range. In interpreting the results to be presented here, the fact that only a small number of samples were tested should be borne in mind. This may explain the apparently inferior results compared with those given in two published papers.[27,28] However, the results given here do represent nearly the best obtained from a lengthy investigation of several promising types of commercial field-effect transistors.

Fig. 3.18 shows performance curves for a p-channel unit (TIS-05) made by Texas Instruments. This transistor has an effective gate-source capacitance of about 10 pF and a mutual conductance at 25°C of 4 mA/V. In these tests it was operated with a source-drain voltage of 4.5 volts. Three samples were tested, all gave virtually the same results. Previous tests had shown that the conductance of the channel increased by a factor of three at the lower test temperature (about -160°C) as compared with room temperature. Consequently the low temperature test was carried out at a drain current of 15 mA while the room temperature test was at 5 mA.

For this type of transistor we note that a large flicker noise contribution is present at room temperature as indicated by the flatness of the curves. We also see that the value of $\overline{N^2}$ at low temperatures is almost an order of magnitude higher than would be predicted from Fig. 3.16. However, at time constants greater than 1 μsec the low temperature performance of this type of unit is better than the results obtained with the EC-1000 for the low capacity conditions.

Fig. 3.19 shows the results of a similar set of measurements on the Amelco 2N3458. We note again that the results for $\overline{N^2}$ are almost an order of magnitude larger than predicted despite the fact that these units are apparently largely free of flicker noise. The higher gate source capacity of these units partially accounts for the results on the Amelco device being worse than those on the TI unit.

In conclusion it might be said that commercial field-effect transistors made by the epitaxial process almost equal the best vacuum tube performance in low noise preamplifiers but unexplained sources of noise prevent them approaching their theoretical possibilities. The lack of understanding of these extra sources of noise is best illustrated by the fact that our tests on some samples of one type of transistor show that its noise level increases as the temperature is reduced. There is good evidence that a field-effect transistor made with good material will come close to theoretical predicted performance.

3.7 ADDITIONAL SOURCES OF SIGNAL AMPLITUDE SPREAD

The previous sections have been-concerned with rather fundamental sources of spread in the amplitude of signals. However, it is frequently the case that, due to the nature of the experiment or due to inadequate appreciation of the problems on the part of the experimenter, the forementioned sources of signal spread are swamped by other problems. We will briefly discuss a few of these problems here.

3.7.1 Noise Contribution of Main Amplifier.

Nearly all amplifier systems contain a signal attenuator to permit operation with large input signals as well as small ones. This usually appears between the preamplifier and the first amplifying stage of the main amplifier.

If large signals are produced at the input to the preamplifier, the attenuation must be increased to maintain the amplifier in its linear working range. This is always the case when dealing with high energy reactions using silicon detectors. In these cases one must be careful to avoid the noise in the first amplifying stage of the main amplifier becoming dominant. For this reason it is usually necessary to provide a further gain attenuator switch located later in the amplifying chain and this should be turned to its lowest gain position before attenuating at the input to the main amplifier.

3.7.2 Gain Drifts

In high resolution spectroscopy using semiconductor detectors one is frequently working with a spread in the amplitude of pulses equal to about 0.1% of their value. Gain drifts in amplifying systems over a period of a few hours may well be in the region of this same percentage. The experimenter must use either a very stable amplifier or one equipped with an overall gain stabilization servo system if he is to use the true potential resolution of semiconductor detector systems. This is particularly true when using silicon detectors for high energy nuclear reaction studies in the 10 to 100 MeV range and in the case of measurements of high energy gamma-rays (~ 1 MeV or greater) with germanium detectors.

3.7.3 High Counting Rates

At high counting rates pulse pile-up and baseline fluctuations may cause serious signal spread. It is a good rule to anticipate trouble from this source if the counting rate is higher than $p/\ _o$, where p is the fractional resolution in the detector amplifier system. Thus if p = 0.3% and $_o$ = 1 μsec, one begins to detect rate effects at about 3 kc/s. The counting rate at which these effects appear can be increased by an order of magnitude or more by using

double delay-line or double RC differentiation but use of this type of shaping network causes a loss of resolution at low counting rates (compare cases #9 and #10 of Table 3.1).

3.7.4 Finite Detector Pulse Rise Time

Since the detector pulse shape is a function of the position of formation of ionization in the detector, a spread in detector pulse shape results in many detector applications. If the detector pulse rise time is within a factor of 5 of the value of to used in the shaping networks, a spread in signal amplitude at the output of the amplifier can be anticipated. Table 3.2 gives some guidance toward choice of network in these cases and the section dealing with detector pulse shape in Lecture #4 also presents some information relevant to this situation.

Table 3.1. Noise Integral and Peak Response of Several Networks

	NETWORK DESCRIPTION	PEAK OUTPUT (P) (UNITY INPUT)	I_1	$\frac{P^2}{I_1}$	I_2	$\frac{P^2}{I_2}$	I_3	$\frac{P^2}{I_3}$
1.	RC INTEG (τ_o) +RC DIFF (τ_o)	.368	.784	.172	.500	.270	.785	.172
2.	TWO RC INTEG ($_o$) +RC DIFF ($_o$)	.271	.196	.372	.250	.292	.589	.124
3.	THREE RC INTEG ($_o$/2) +RC DIFF ($_o$)	.356	.407	.310	.421	.300	.771	.163
4.	RC INTEG ($_o$) TWO RC INTEG ($_o$/2) RC DIFF ($_o$)	.295	.233	.373	.290	.300	.640	.136
5.	RC INTEG ($_o$) D.L. DIFF ($_o$)	.628	1.98	.200	1.05	.376	1.16	.341
6.	TWO RC INTEG ($_o$/2) D.L. DIFF ($_o$)	.631	1.87	.214	1.20	.333	1.32	.303
7.	RC INTEG ($_o$) TWO RC INTEG ($_o$/2) D.L. DIFF	.388	.494	.303	.481	.312	.823	.182
8.	TWO F.B. INTEG ($_o$) TWO D.L. DIFF ($_o$) TWO D.L. DIFF (2 $_o$)	1.000	4.19	.239	3.61	.277	4.82	.208
9.	RC INTEG (0.4 $_o$) D.L. DIFF (1.6 $_o$)	0.981	7.70	.125	3.77	.254	3.79	.253
10.	RC INTEG (0.4 $_o$) TWO D.L. DIFF (1.6 $_o$)	0.981	23.0	.042	9.82	.098	6.37	.151

Table 3.2. Input Pulse Shape Dependance of Several Shaping Networks
(3 mm Li-drift Si detector at 350 V and 25°C)

		PERCENTAGE LOSS FOR 40 MeV ALPHAS	PERCENTAGE LOSS FOR 85 MeV Alphas
1.	RC INTEG (0.5 μsec) RC DIFF (0.5 μsec)	0.46	1.73
2.	RC INTEG (1.0 μsec) RC DIFF (1.0 μsec)	0.11	0.41
3.	THREE RC INTEG (0.2 μsec) RC DIFF (0.5 μsec)	0.54	1.96
4.	THREE RC INTEG (0.2 μsec) D.L. DIFF (0.8 μsec)	0.99	3.01
5.	RC INTEG (0.5 μsec) D.L. DIFF (0.8 μsec)	3.11	5.22
6.	RC INTEG (0.5 μsec) TWO D.L. DIFF (0.8 μsec)	3.59	5.74
7.	RC INTEG (0.2 μsec) D.L. DIFF (0.8 μsec)	0.89	1.63
8.	RC INTEG (0.5 μsec) D.L. DIFF (1.4 μsec)	0.95	1.51
9.	TWO F.B. INTEG (0.5 μsec) TWO D.L. DIFF (0.5 μsec) D.L. DIFF (1.0 μsec)	0.46	1.57

LECTURE 3. FIGURE CAPTIONS

Fig. 3.1 Diagramatic Representation of Energy Loss Process.

[e_r = Raman Phonon Energy for Lattice.
e_g = Band-Cap of Material
p Assumes a Random Value in the Range 0 to 1.]

Fig. 3.2 Calculated Yield and Fano Factor.

Fig. 3.3 Resolution-Energy Relationship Data for Germanium.

Fig. 3.4 Typical Electronics for Spectroscopy.

Fig. 3.5 Simplified Input Equivalent Circuits.

Fig. 3.6 Typical Shaping Networks and Their Frequency Response.

Fig. 3.7 Pulse Response of Several Networks (Unit Function Input).

Fig. 3.8 EC-1000 Preamplifier.

Fig. 3.9 Noise Performance Curves for EC-1000 Preamplifier.

Fig. 3.10 EC-1000 Preamplifier: Effect of Double Integrator.
(R_F = 60 M)

Fig. 3.11 EC-1000 Preamplifier. (Conditions as in Fig. 3.10 except
R_F = 500 M)

Fig. 3.12 EC-1000 Preamplifier Rise Time Curves.

Fig. 3.13 Bulk Field Effect Transistor (N-Channel Type Illustrated).

Fig. 3.14 General Purpose Field Effect Transistor Preamplifier.
(2N3458 at Room Temperature.)

Fig. 3.15 Predicted Noise Behavior of Field Effect Transistor at 300°K.
C_T = 20 pF; $R_{eq} = 1/g_m$ Assumed

Fig. 3.16 Predicted Noise Behavior of Field Effect Transistor at 77°K.
C_T = 20 pF; $R_{eq} = 1/g_m$ Assumed

Fig. 3.17 Circuit for Low Temperature Tests on Field Effect Transistors.

Fig. 3.18 Noise Performance of TIS-05 Field Effect Transistor.
Conditions: See Text; Dotted Lines: -170°C
Full Lines: + 25°C

Fig. 3.19 Noise Performance of Amelco 2N3458 Field Effect Transistor.
Conditions: Dotted lines: -170°C I_D = 12.5 mA
Full lines: + 25°C I_D = 5 mA

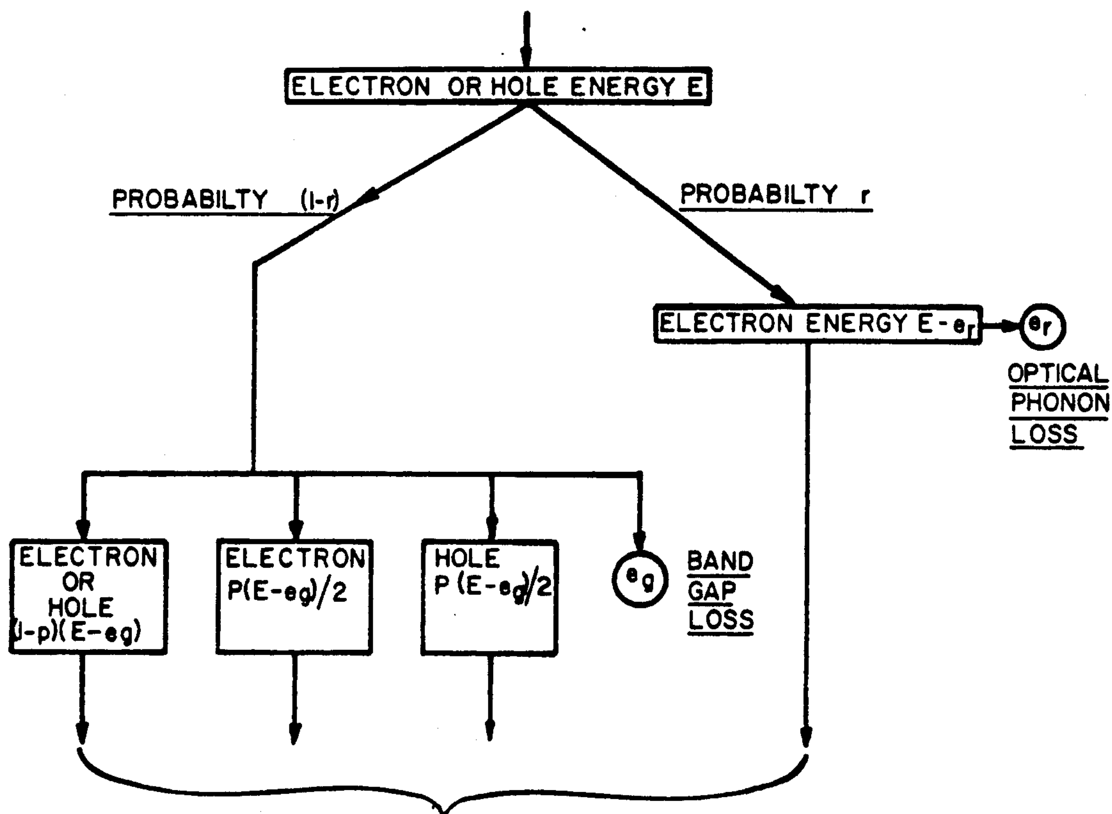

THESE NOW BECOME PARENTS FOR FUTURE GENERATION IF THEIR ENERGY IS ADEQUATE FOR PRODUCTION OF SECONDARIES

FIG 3.1

DIAGRAMATIC REPRESENTATION OF ENERGY LOSS PROCESS

e_r = RAMAN PHONON ENERGY FOR LATTICE

e_g = BAND– GAP OF MATERIAL

p ASSUMES A RANDOM VALUE IN THE RANGE 0 TO 1

MUB-6999

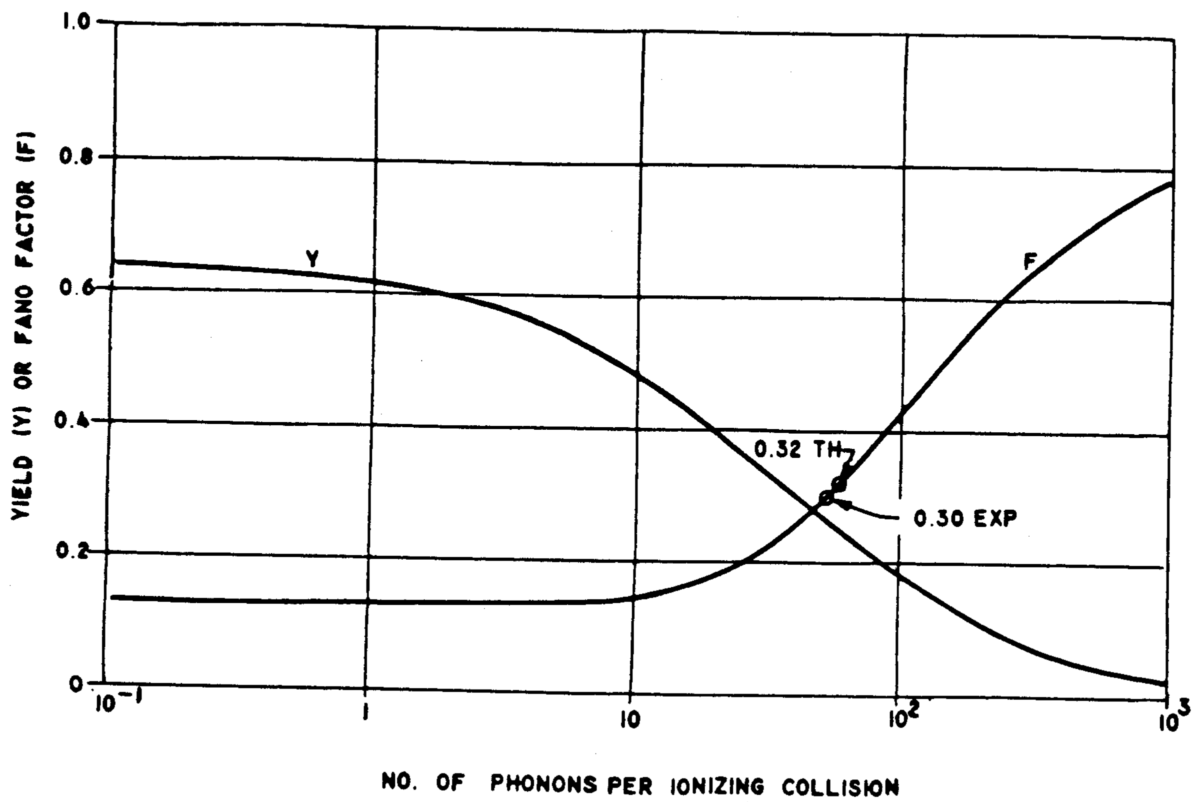

MUB 7362

Fig. 3.2 — Calculated yield and Fano Factor

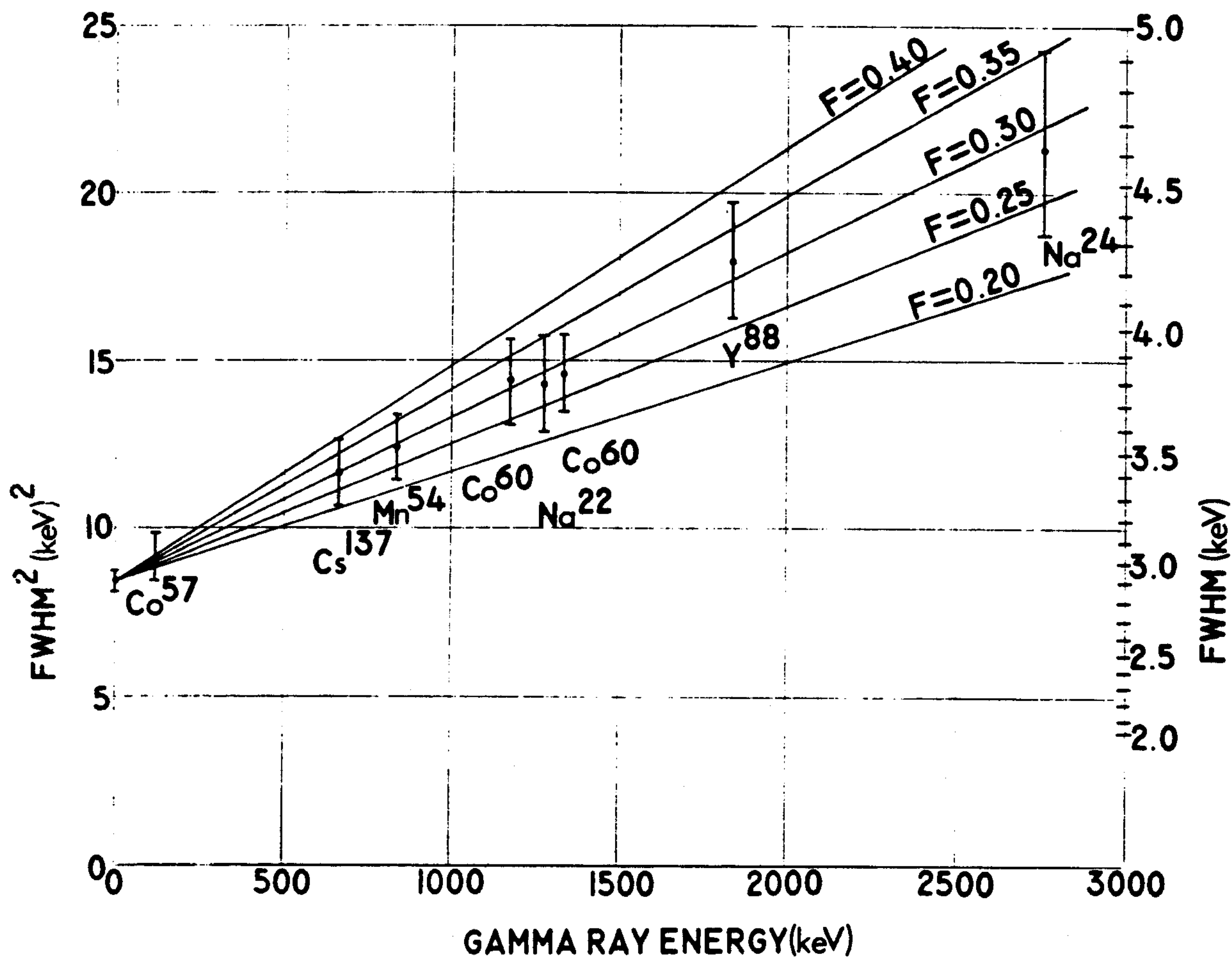

Fig. 3.3 – Resolution-energy relationship data for germanium.

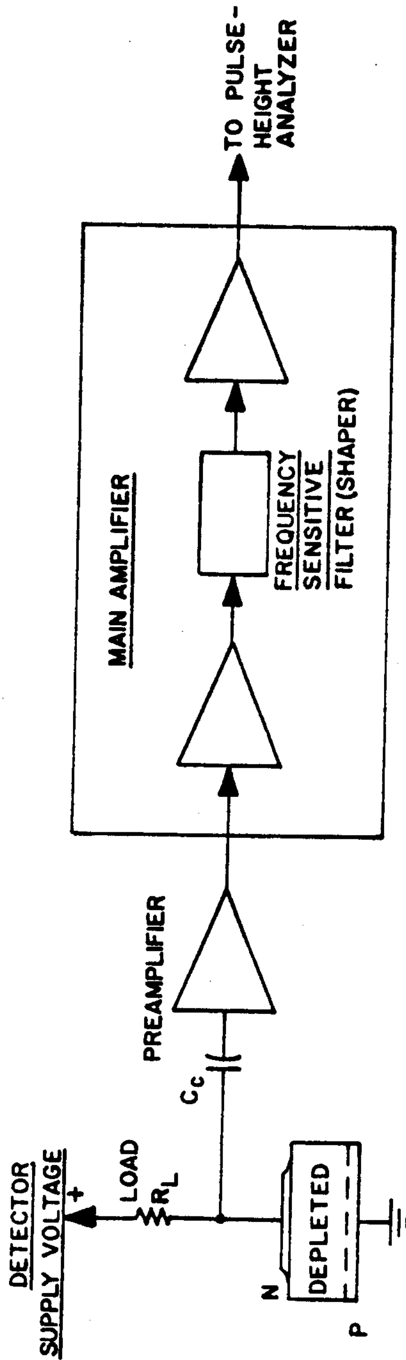

FIG 3.4A — BLOCK DIAGRAM

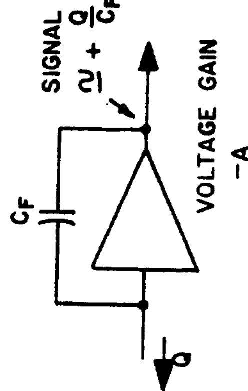

FIG 3.4B
CHARGE SENSITIVE
INPUT STAGE

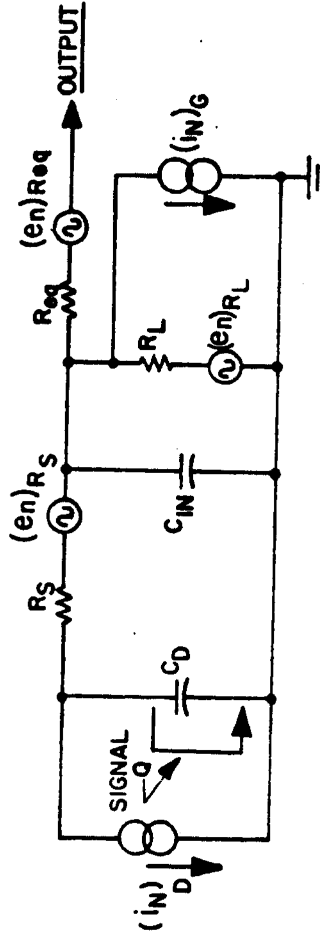

FIG 3.4C
EQUIVALENT INPUT CIRCUIT
SHOWING NOISE GENERATORS

FIG 3.4
TYPICAL ELECTRONICS FOR SPECTROSCOPY

MUB-7002

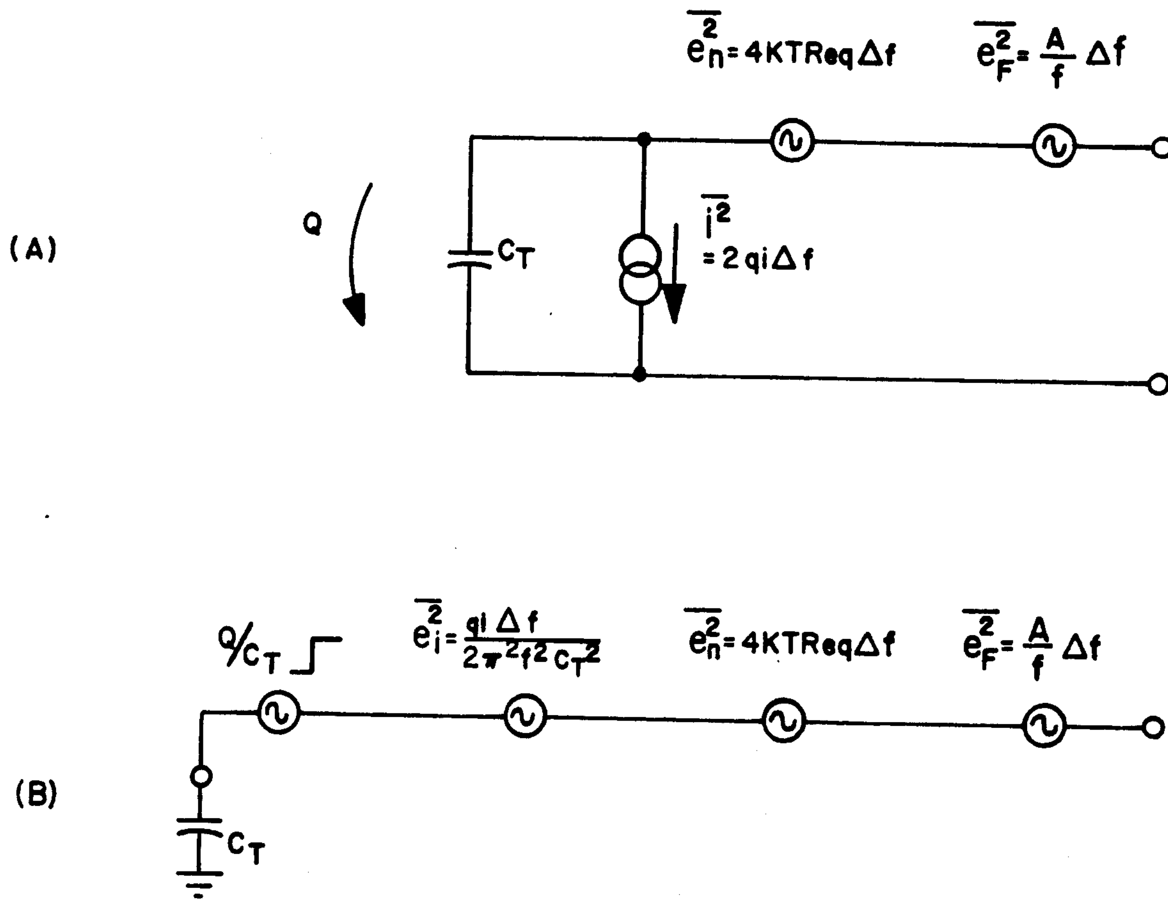

FIG 3.5

SIMPLIFIED INPUT EQUIVALENT CIRCUITS

MUB-7003

IN EACH CASE $RC = T = nT_0$; $f = mf_0$
WHERE $f_0 = \left(\frac{1}{2\pi T_0}\right)$ IS A REFERENCE FREQUENCY

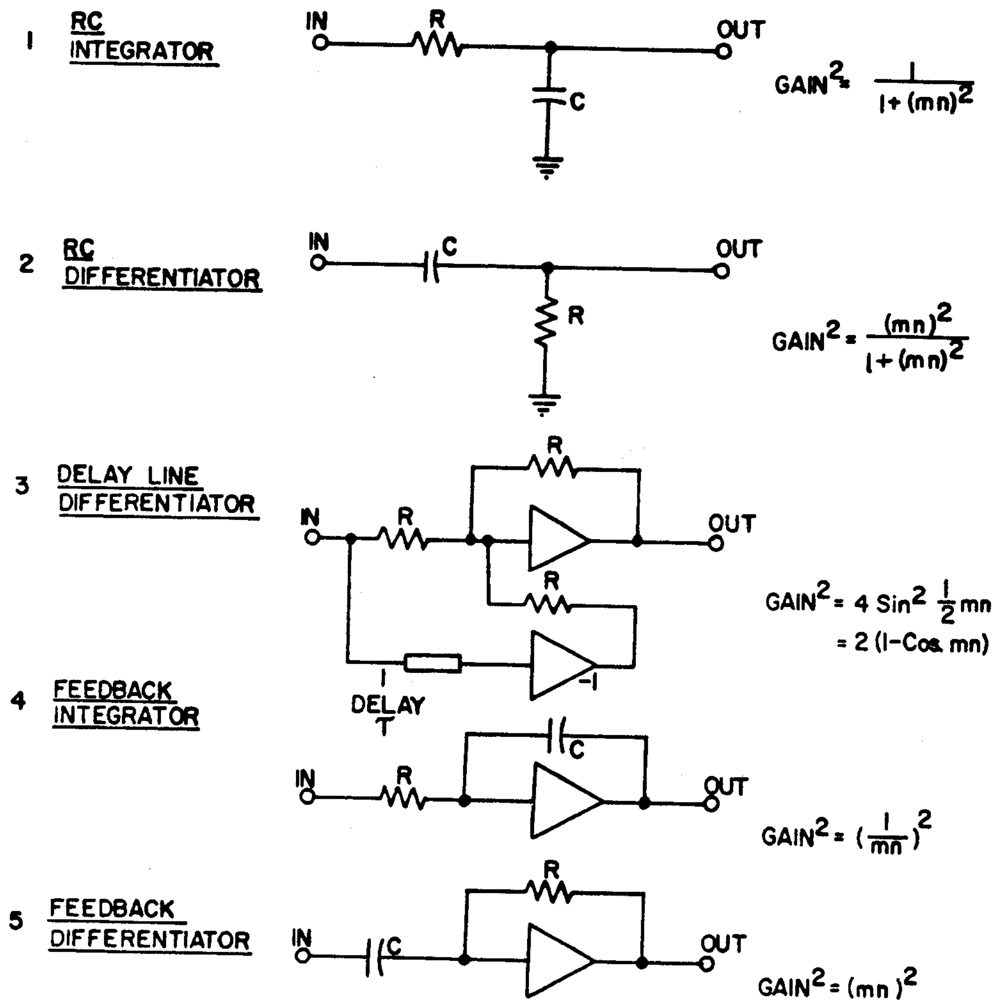

FIG 3.6

TYPICAL SHAPING NETWORKS AND THEIR FREQUENCY RESPONSE

MUB-7004

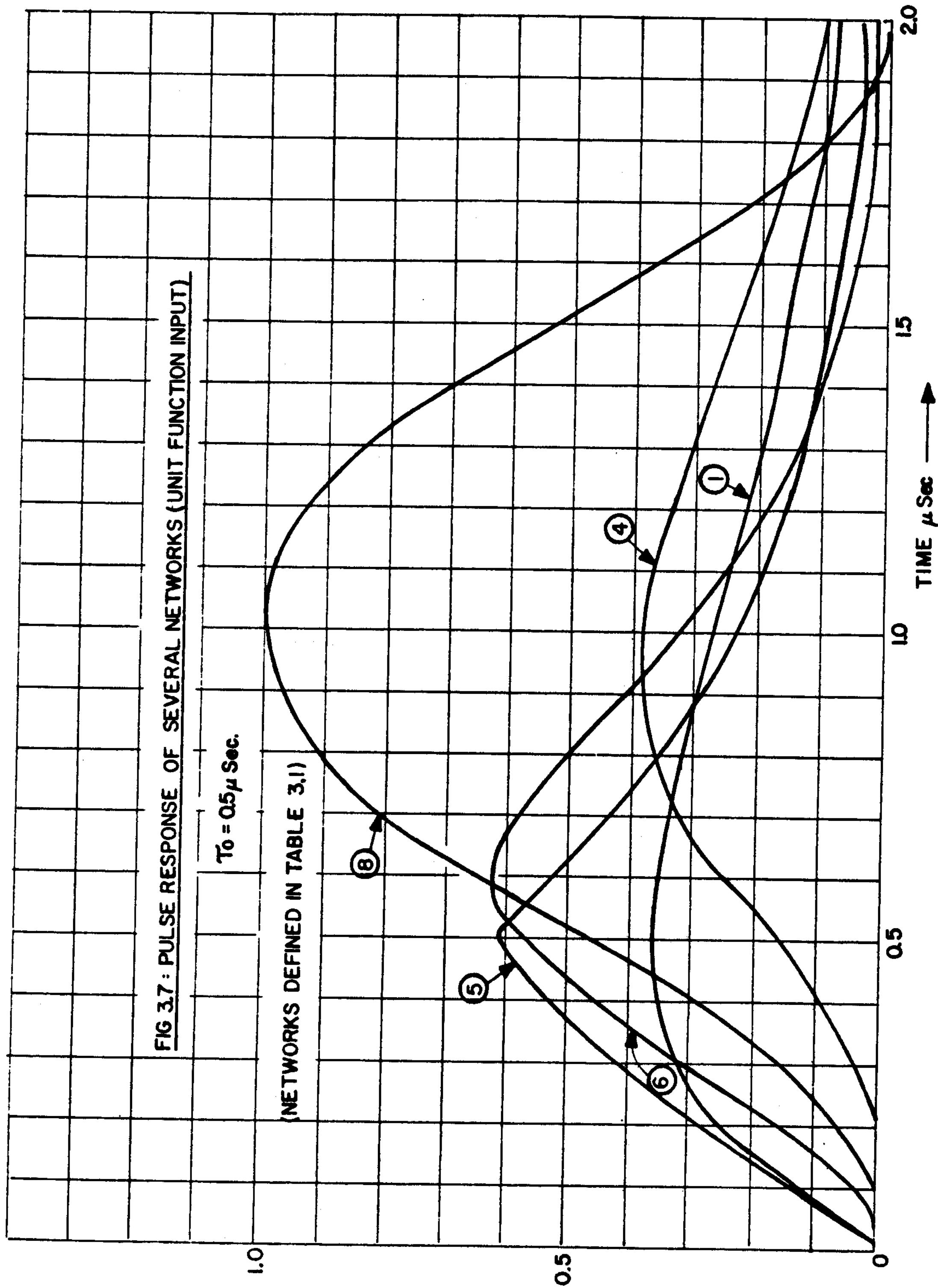

FIG 3.7 : PULSE RESPONSE OF SEVERAL NETWORKS (UNIT FUNCTION INPUT)

MUB-7005

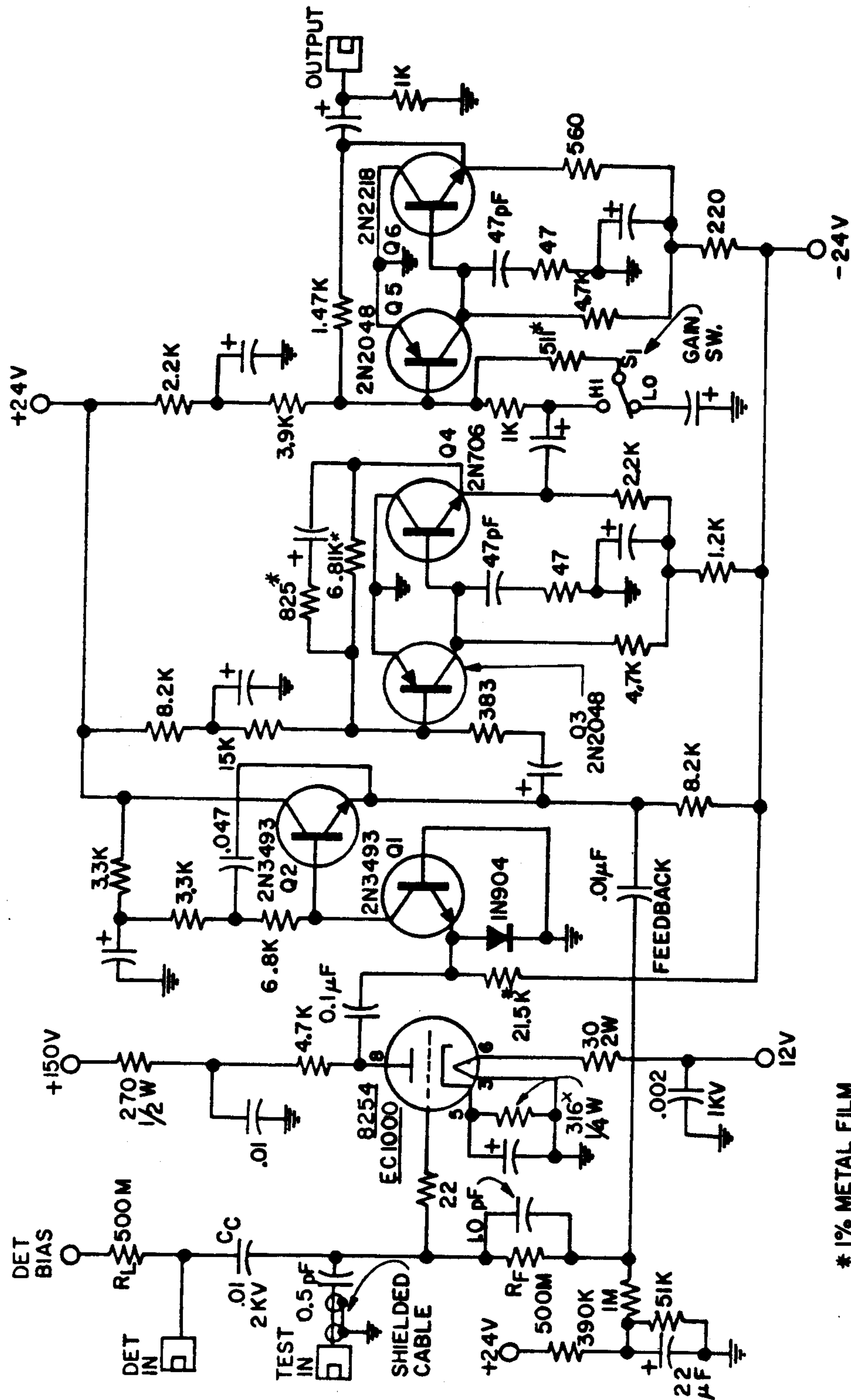

FIG 3.8
EC1000 PREAMPLIFIER

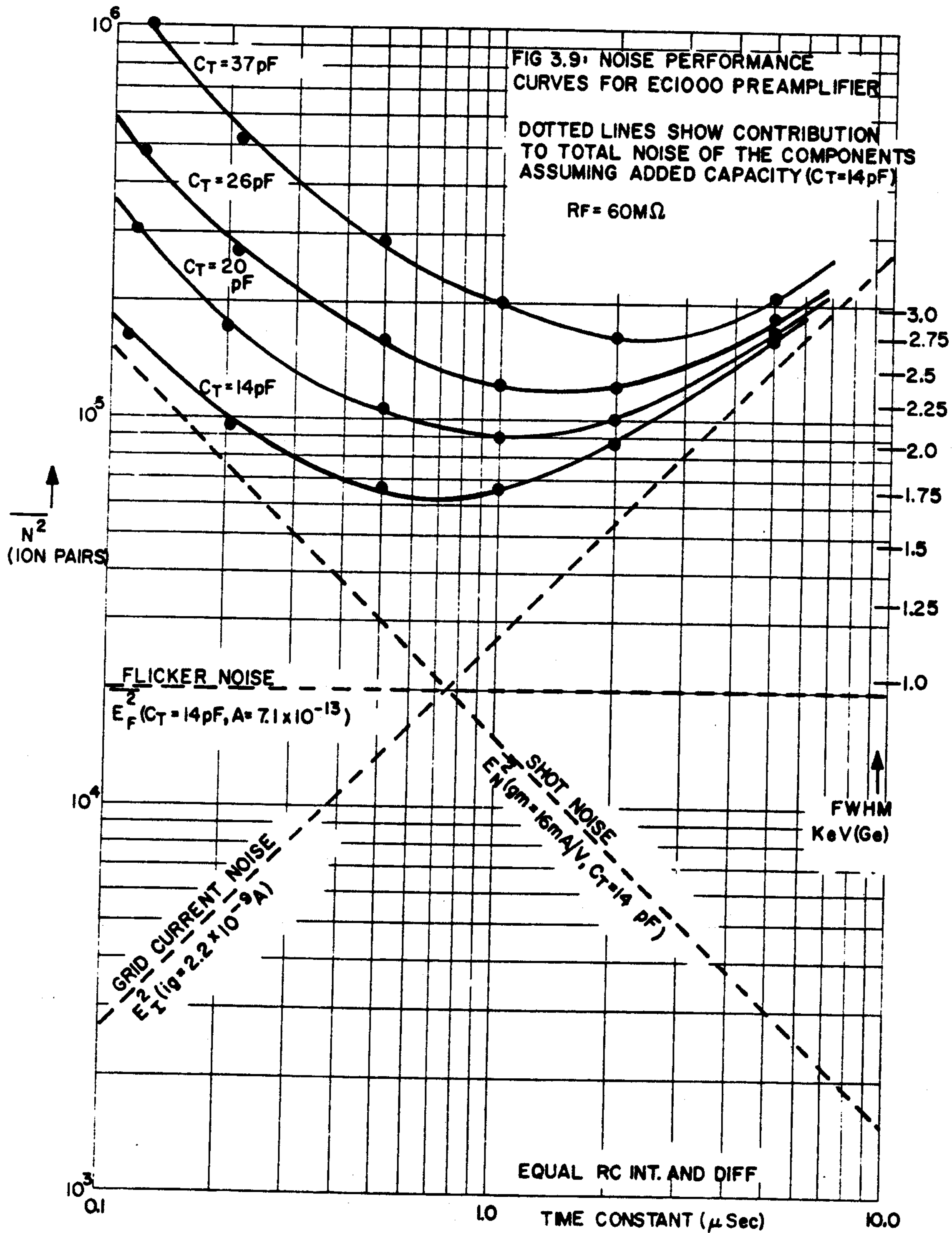

MUB-7007

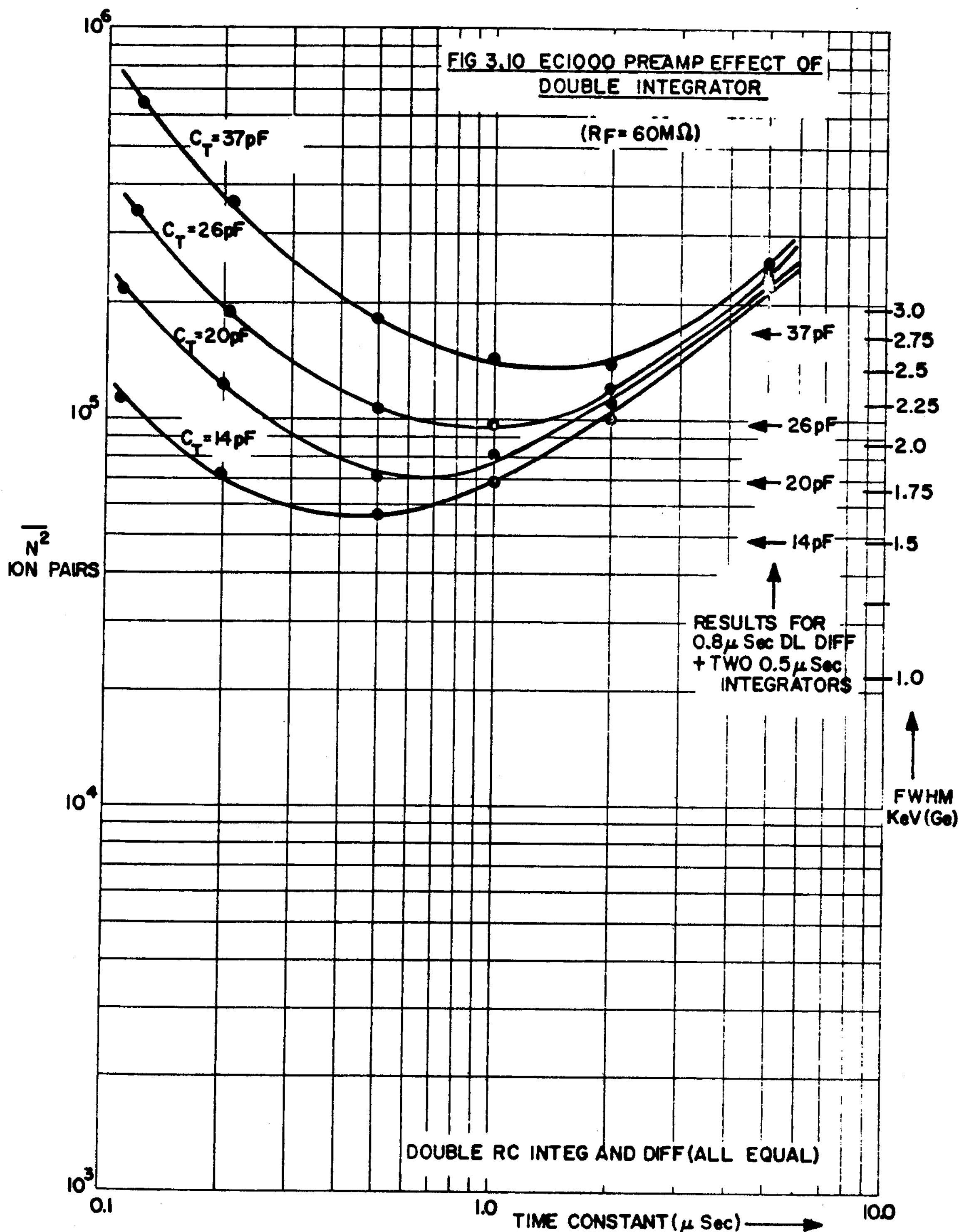

MUB-7008

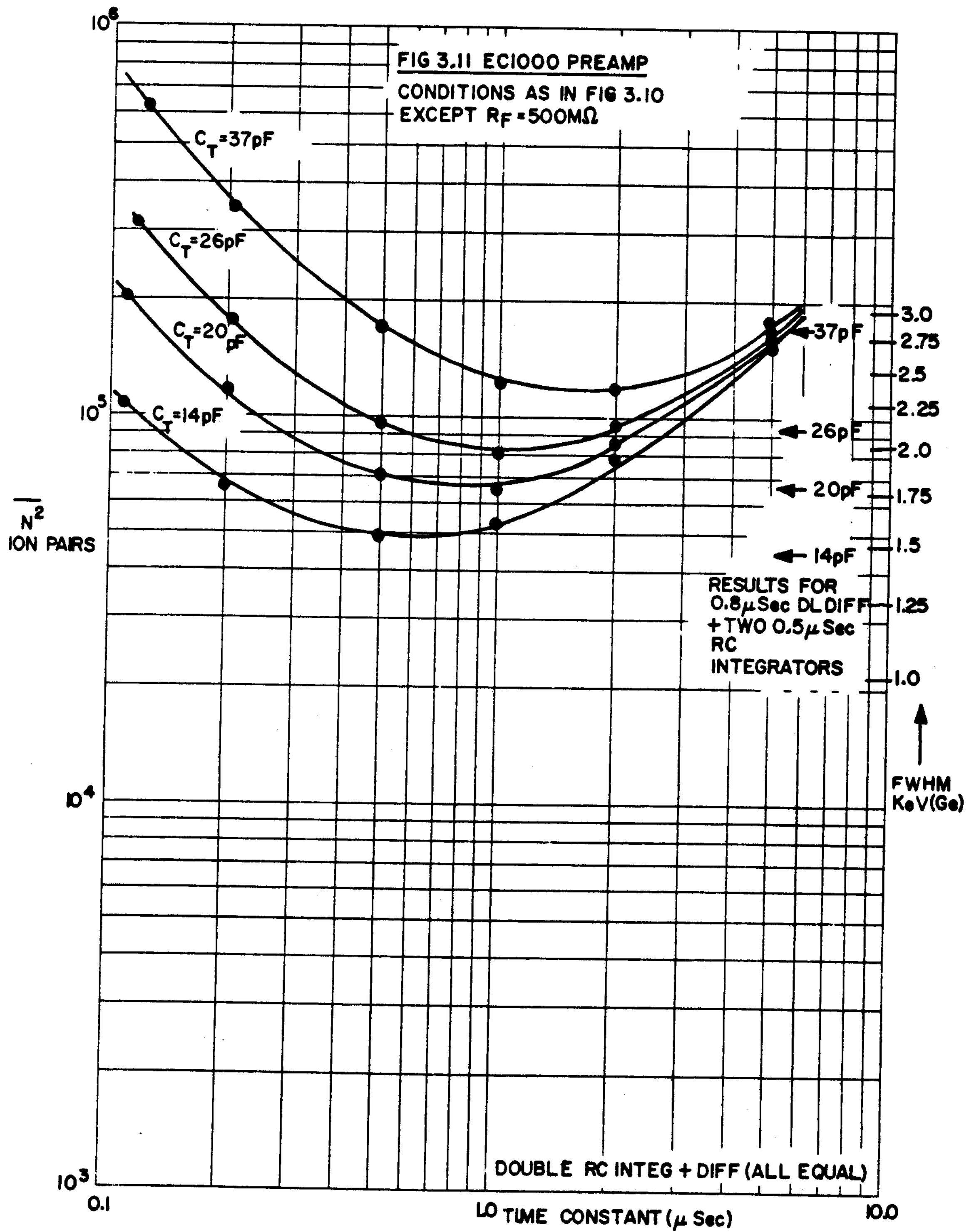

MUB-7009

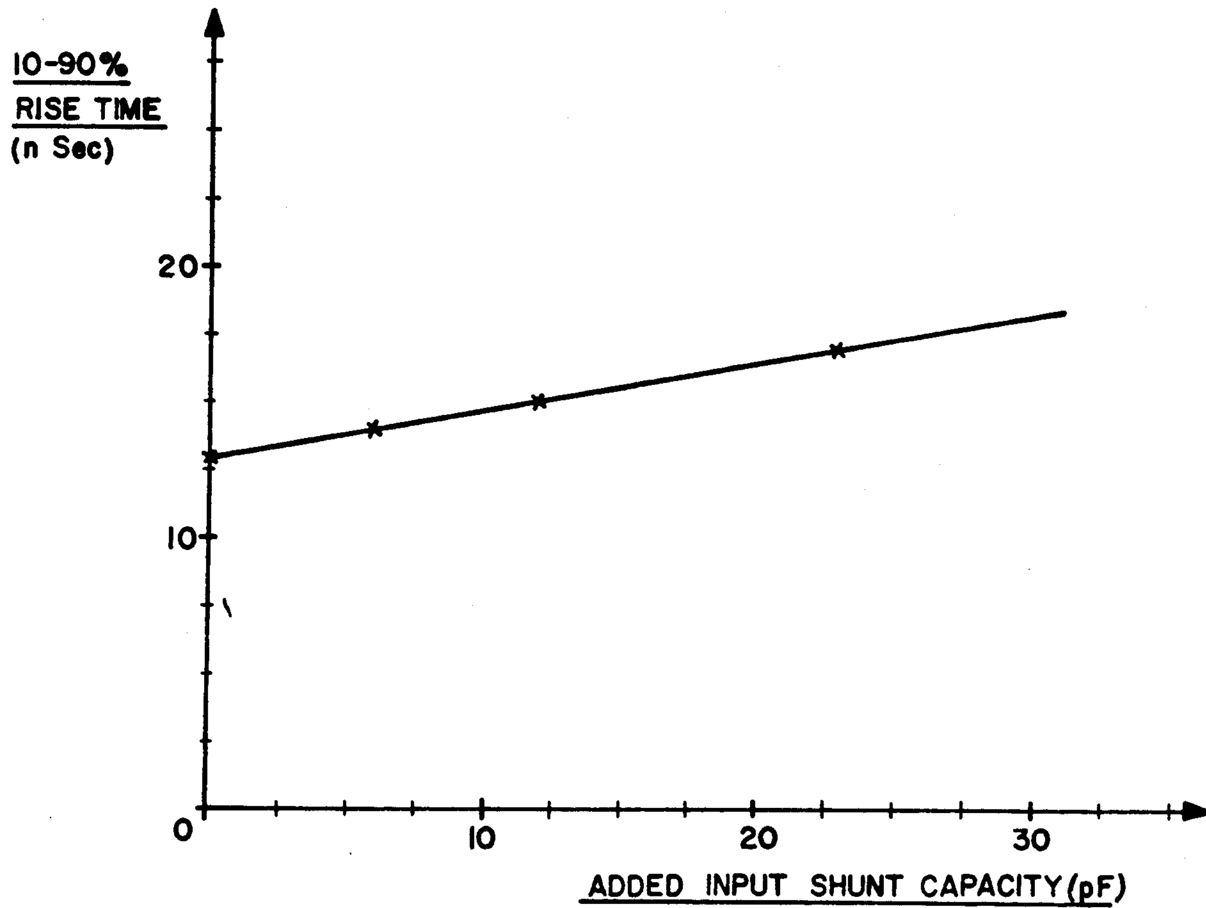

FIG 3.12
EC1000 PREAMP RISE TIME CURVES

MUB-7010

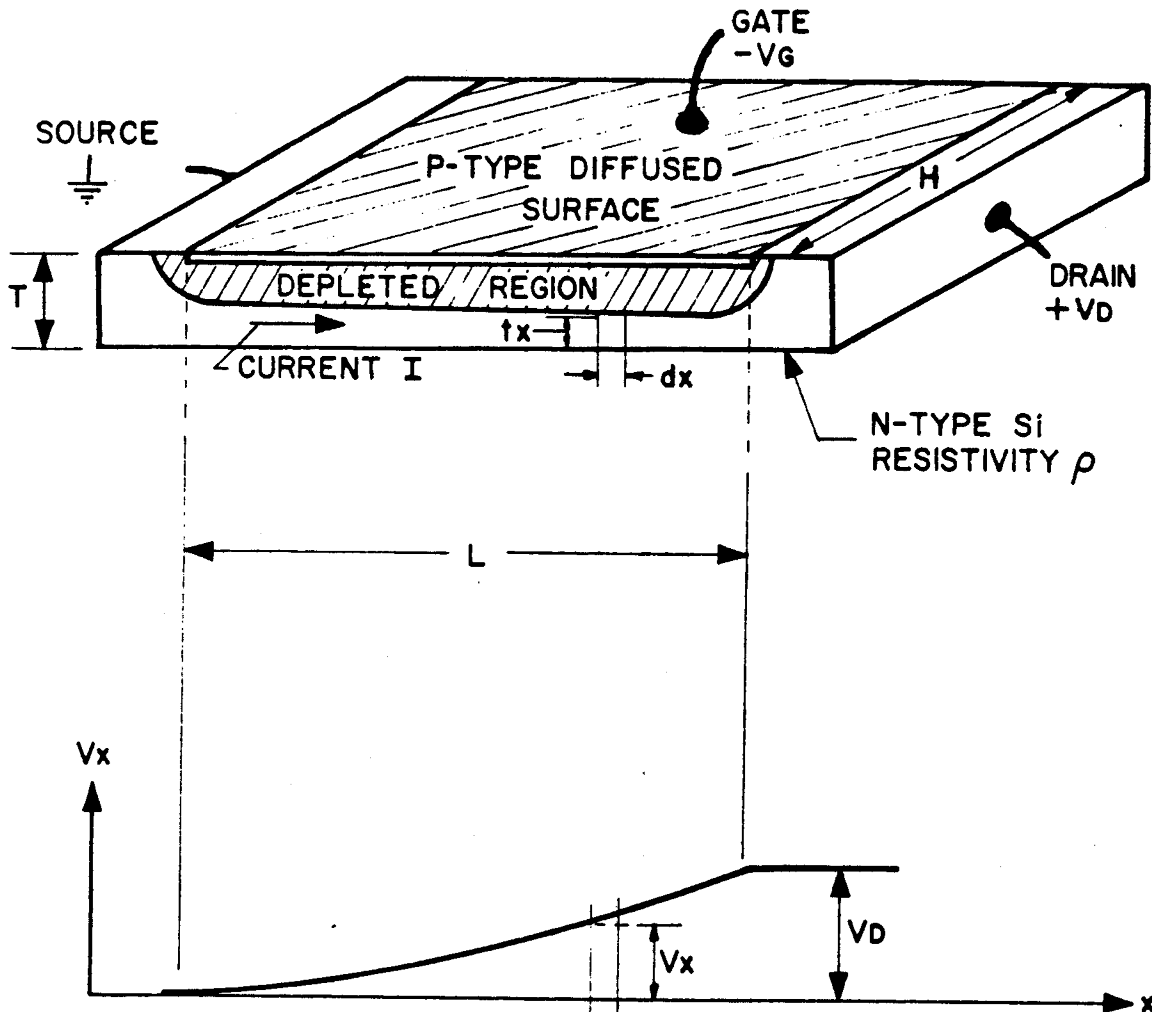

FIG 3.13
BULK FIELD EFFECT TRANSISTOR
(N-CHANNEL TYPE ILLUSTRATED)

MUB-7011

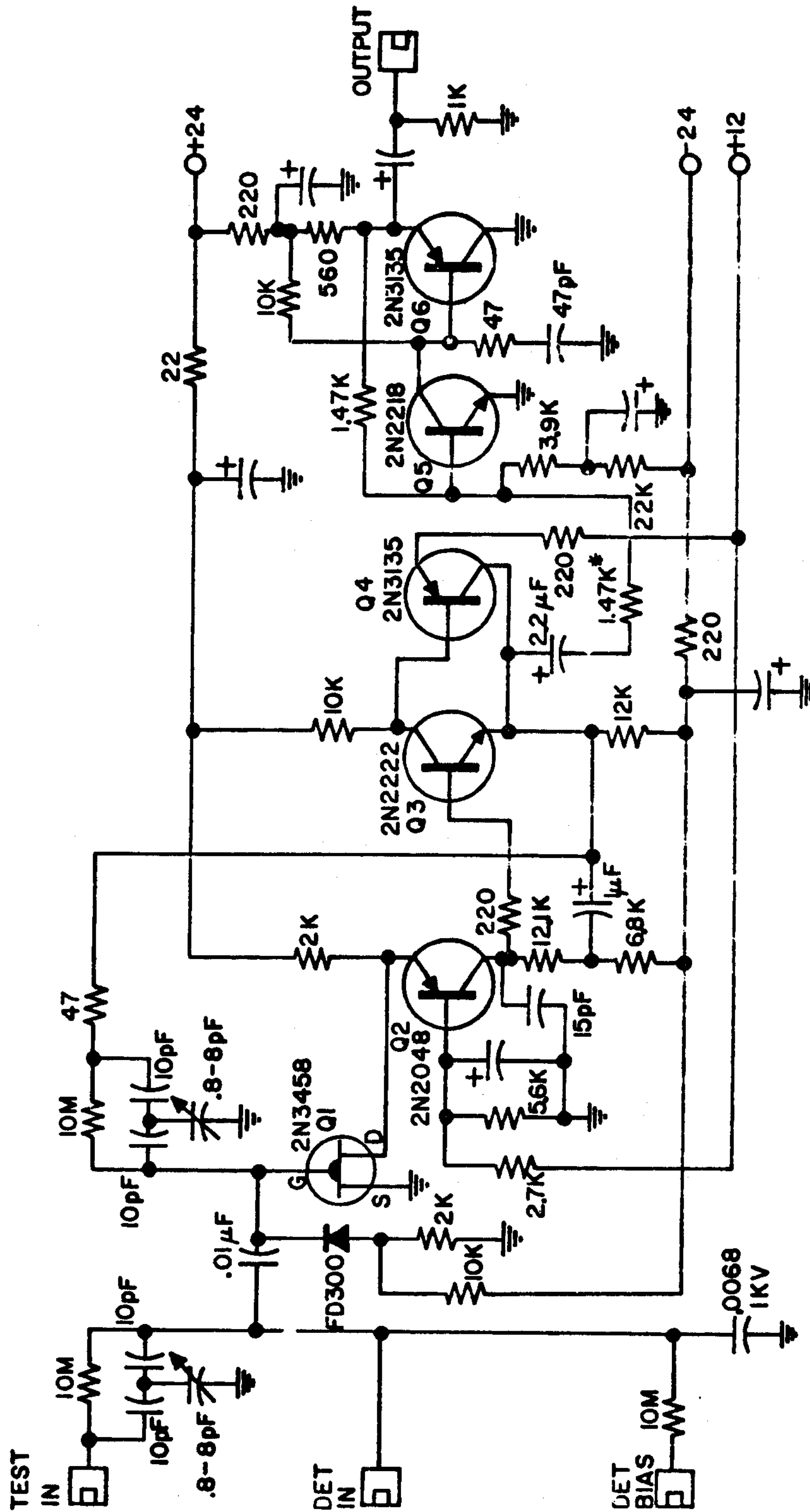

FIG 3.14
GENERAL PURPOSE FIELD EFFECT TRANSISTOR PREAMPLIFIER (2N3458 AT ROOM TEMP.)

MUB-7012

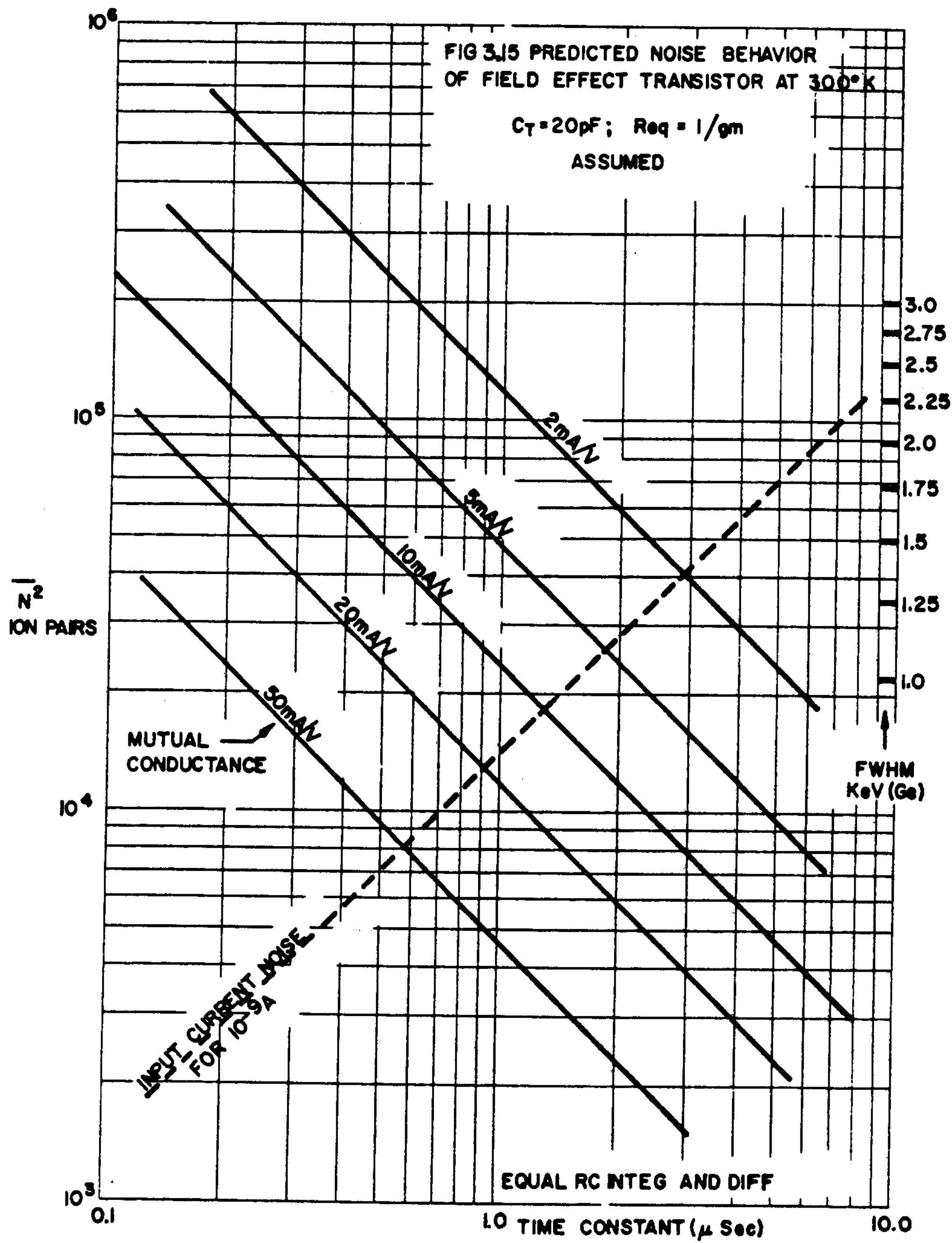

MUB-7013

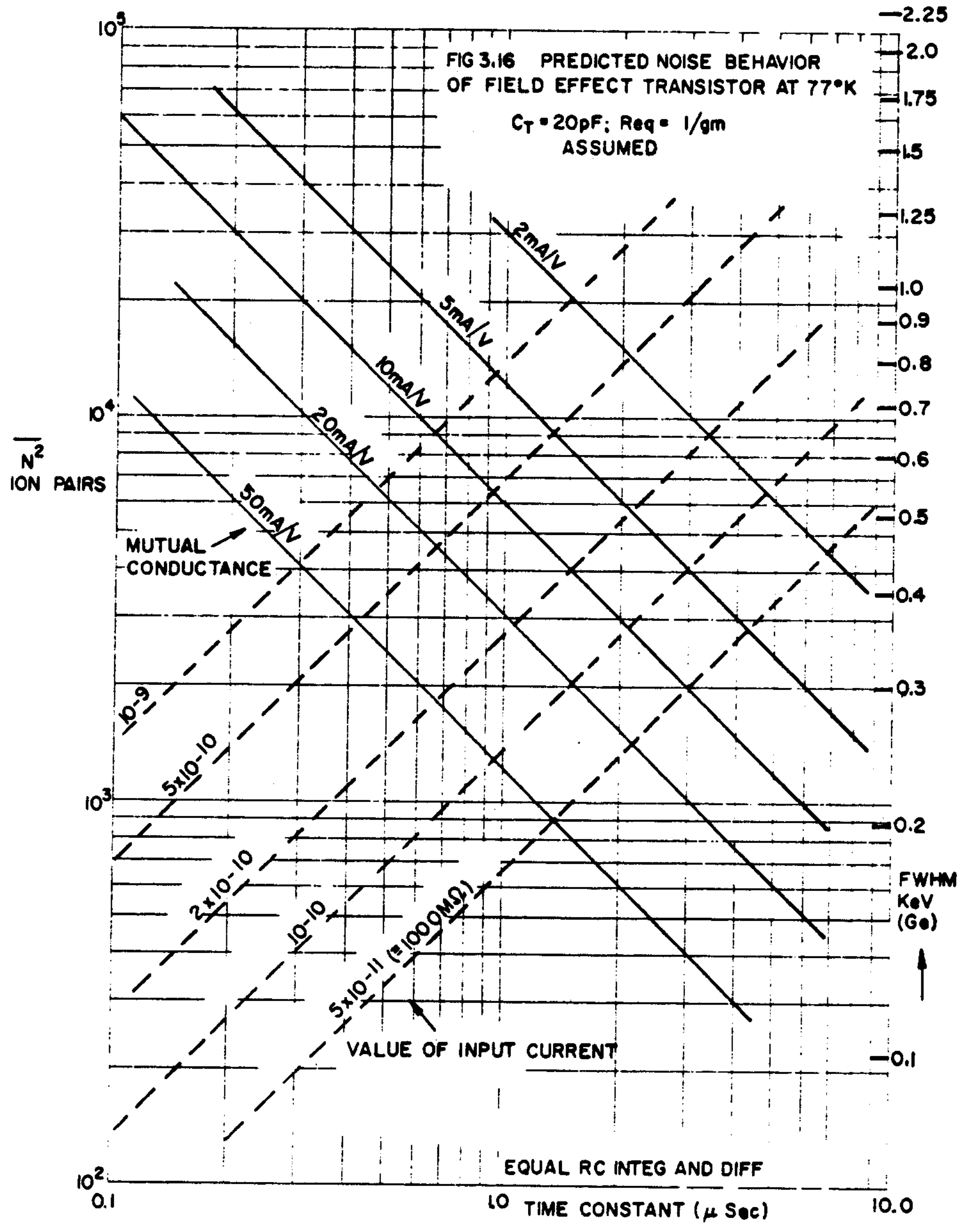

MUB-7014

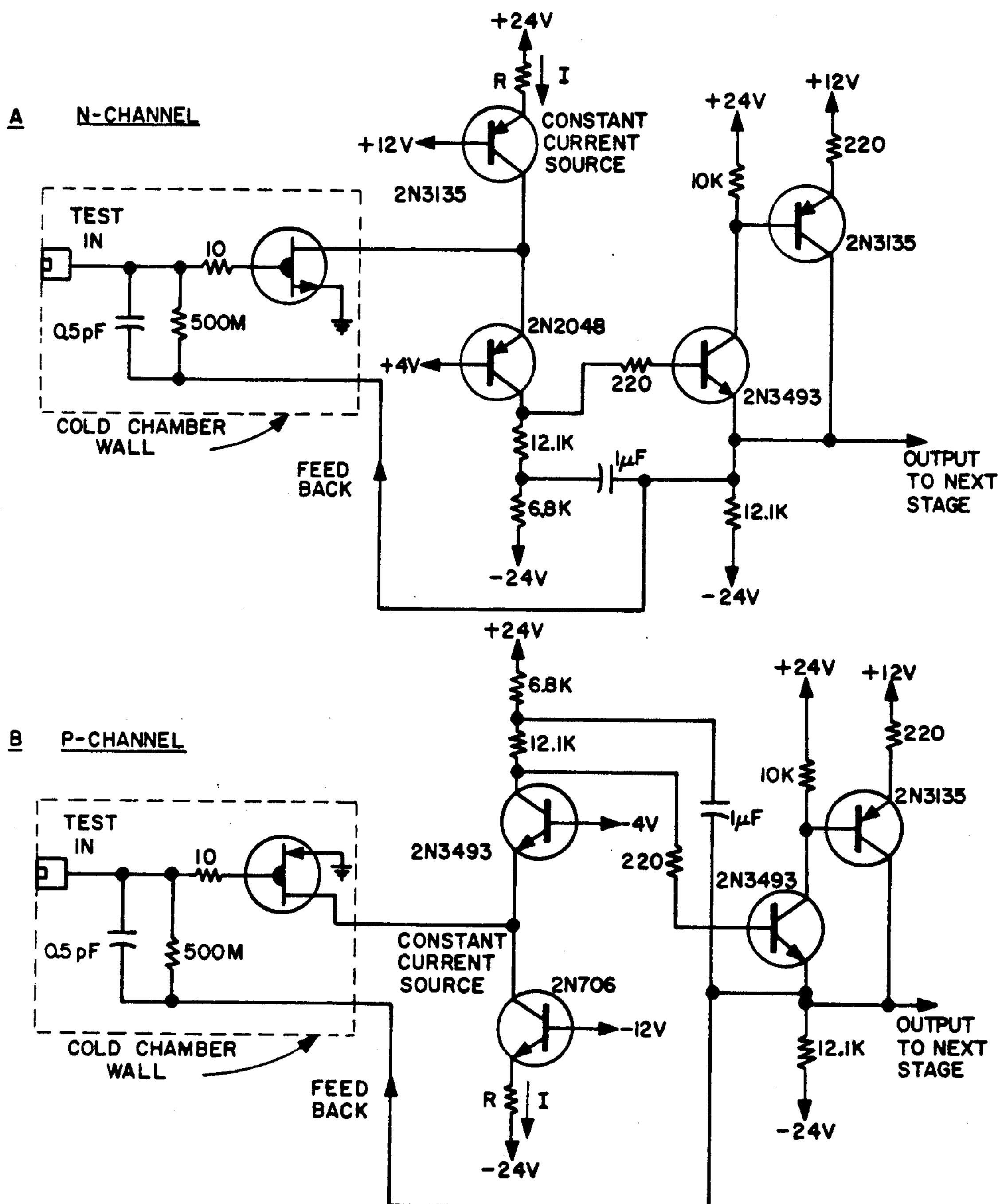

FIG 3.17
CIRCUIT FOR LOW TEMPERATURE TESTS ON
FIELD EFFECT TRANSISTORS

MUB-7015

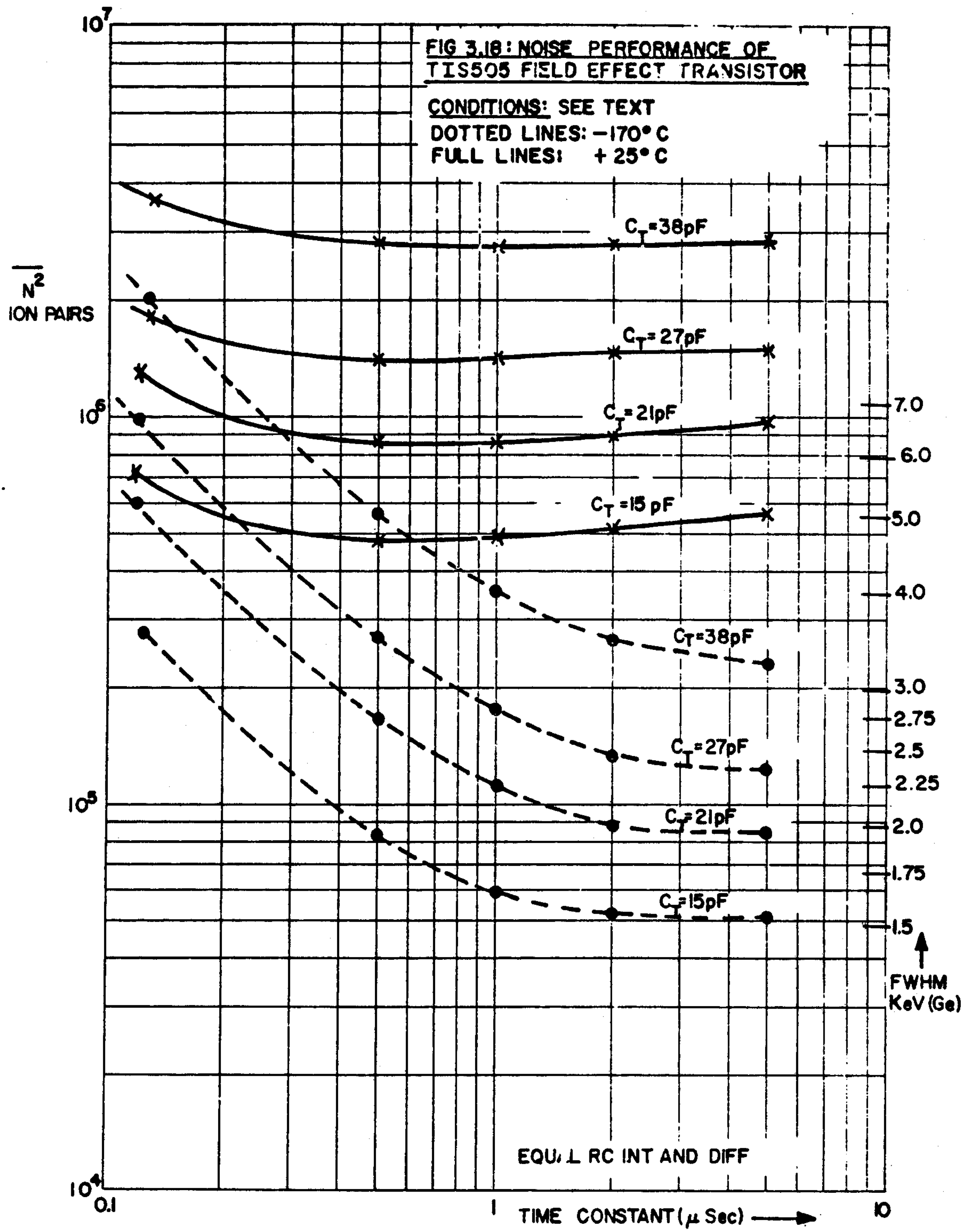

MUB-7016

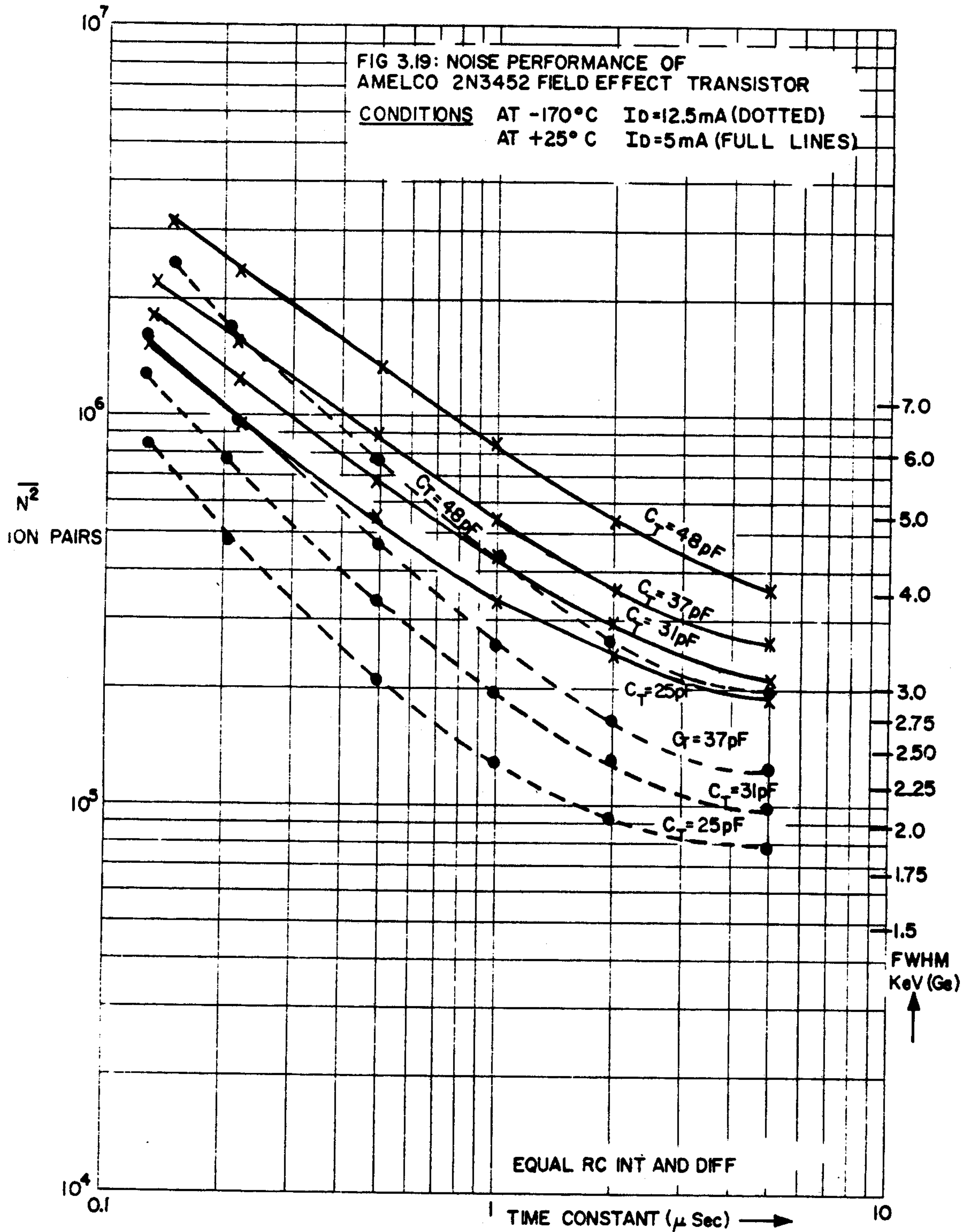
FIG 3.19: NOISE PERFORMANCE OF AMELCO 2N3452 FIELD EFFECT TRANSISTOR
CONDITIONS AT -170°C ID=12.5mA (DOTTED)
AT +25° C ID=5mA (FULL LINES)
$\overline{N^2}$ ION PAIRS
C_T=48pF
C_T=37pF
C_T=31pF
C_T=25pF
C_T=48pF
C_T=37pF
C_T=31pF
C_T=25pF
FWHM KeV (Ge)
EQUAL RC INT AND DIFF
TIME CONSTANT (μ Sec)
MUB-7017

LECTURE 4. MISCELLANEOUS DETECTOR TOPICS

Fred S. Goulding

Lawrence Radiation Laboratory
University of California
Berkeley, California

July 30, 1965

4.1 DETECTOR PULSE SHAPE

The passage of an ionizing particle or the interaction of a gamma-ray in the sensitive region of a detector releases a large number of hole-electron pairs which are separated and collected by the electric field present in the depleted region. The initial spatial distribution of the hole-electron pairs depends upon the type and energy of the radiation and, therefore, the shape of the current pulse obtained from the detector is changed by the same factors. It is also determined by the thickness of the sensitive region, by the electric field distribution within this region and by the mobilities of the charge carriers in the semiconductor at its operating temperature. The interrelation between these factors makes a general solution to the calculations of pulse shape quite impossible. We will therefore content ourselves with discussing some of the basic considerations and giving some examples of solutions for particular cases. It is instructive to first consider the signal resulting from creation of a single hole-electron pair in the sensitive volume. As the result is different for p-i-n detectors, in which the electric field is constant through the whole sensitive region, from that for p-n junctions, in which the field is a linear function of distance from the back of the depletion layer, we will deal with these two cases separately.

4.1.1 Pulse Shape Due to a Single Hole-Electron Pair in a P-I-N Detector

We will consider the situation depicted in Fig. 4.1. The parameters shown in this figure are self-explanatory and will be used here. We will assume that the detector is connected to a charge sensitive preamplifier with a feedback capacitor C_F and an open loop gain -A, which is very large. Any chrage flowing in the detector tends to produce a negative signal et the input to the amplifier but the feedback via C_F forces the amplifier input point (and therefore the detector anode) to stay almost at constant potential. The simplest way to calculate the signal is to consider the energy balance in the system. Thus, as the carriers are collected by the electric field in the detector, energy is dissipated* and, to maintain the energy stored in the detector dielectric, a charge must flow into the positive side of the detector from the external circuit. This charge flows almost entirely out of C_F giving a negative output signal from the amplifier.

We have:

$$\text{Energy W stored in the dielectric} = \frac{1}{2}\frac{Q^2}{C}$$

where Q = charge on the detector capacity C.

$$\therefore \frac{dW}{dt} = \frac{Q}{C}\frac{dQ}{dt}$$

Also work done on the electron in time dt = Force X Distance = $\frac{V^2}{W^2} \cdot q \cdot \mu_e$.

From this:

$$\frac{dW}{dt} = \frac{V^2}{W^2} \cdot q \cdot \mu_e$$

$$= \frac{Q^2}{W^2C^2} \cdot q \cdot \mu_e$$

$$\therefore \frac{Q}{C}\frac{dQ}{dt} = \frac{Q^2}{W^2C^2} \cdot q\,\mu_e$$

$$\text{i.e.,}\quad \frac{dQ}{dt} = \frac{V}{W^2} \cdot q \cdot \mu_e$$

*This energy appears as thermal vibrations in the lattice due to the electron wave interacting with the lattice.

This is the current i_e in the external circuit.

$$\therefore\ i_e = \frac{V}{W^2} \cdot q \cdot \mu e \qquad (4.1)$$

This current persists until the electron reaches the positive plate when it suddenly becomes zero. The time T_e taken for this to happen is given by:

$$T_e = \frac{W-x_o}{\mu_e} \quad \frac{W}{V} \qquad (4.2)$$

Similar equations can be derived for the signal due to hole flow:

$$i_h = \frac{V}{W^2} \cdot q\ \mu_h \qquad (4.3)$$

$$T_h = \frac{x_o}{\mu_h} \cdot \frac{W}{V} \qquad (4.4)$$

The total charge flow in the external circuit is given by:

$$Q_{TOTAL} = \frac{V}{W^2} \cdot q\ \mu_h \cdot \frac{x_0}{\mu_h} \cdot \frac{W}{V} + \frac{V}{W^2} \cdot q \cdot \mu_e \cdot \frac{(W-x_0)}{\mu_e} \cdot \frac{W}{V}$$

$$= q.$$

While this is anticipated, the author must comment that many beginners in this field find it difficult to believe that the total charge flow is not 2 q.

We note that the output signal is the integrated value of i flowing in the capacitor C_F. The resulting output signal due to the hole-electron pair is shown in Fig. 4.2 (the signal is inverted for convenience). The two components of the signal are shown and it will be obvious from this diagram that, for this type of detector, the signal due to either type of carrier is proportional to the fraction of the sensitive region crossed by that carrier. This simple situation results from the fact that the net charge residing in the sensitive region is zero end, therefore, the electric field is constant. We will shortly see that the situation is more complicated in the case of the

p-n junction detector. A complication arises in the foregoing analysis (and for p-n junction detectors) if the electric field is large enough to produce carrier velocities in the same range as thermal velocities of electrons in the lattice. This is about 10^7 cm/sec. In germanium, the velocity of an electron moving through the lattice is limited to about 10^7 cm/sec.[16] and a similar, though not so abrupt, limiting velocity exists for holes. In silicon, the velocity of carriers does not saturate as in germanium but the mobility falls fairly rapidly when carrier velocities reach the region of 10^7 cm/sec. This limitation is of some significance when considering very fast timing with thin (silicon) detectors and also when dealing with the case of germanium detectors used at 77°K. The high mobility of carriers in germanium at this temperature means that the saturation velocity is reached for electric fields in the 1000 V/cm range. This is not an unusual field in germanium detectors and the previous analysis must be applied with care to this case.

4.1.2 Pulse Shape Due to a Single Hole-Electron Pair in a p-n Junction Detector.

Fig. 4.3 depicts the situation here. The electric field is a linear function of distance from the bask of the depletion layer. Again we will consider the energy balance equations.

We have:

$$\frac{dW_e}{dt} = \frac{Q}{C} \cdot \frac{dQ_e}{dt}$$

For the electron:

$$\frac{dx}{dt} = E(x)\ \mu_e = \frac{2V}{W^2} \cdot x \cdot \mu_e$$

$$\therefore x = x_o\, e^{-\frac{2 V \mu_e t}{W^2}} \qquad (4.5)$$

The work done on the electron in time dt:

$$= \left(E(x)\right)^2 \cdot q \cdot \mu_e \, dt$$

$$= \frac{4\ V^2}{W^4} \cdot q\ \mu_e\ x_2\ dt$$

$$\therefore\ \frac{dW_e}{dt} = \frac{4\ V^2}{W^4} \cdot q \cdot \mu_e \cdot x^2.$$

Equating the two expressions for dW_e/dt we have:

$$\frac{dQ_e}{dt} = i_e = \frac{4\ V}{W^4} \cdot q \cdot \mu_e\ x^2$$

Substituting from (4.5):

$$i_e = \frac{4\ V \cdot q \cdot \mu_e\ x_o^2}{W^4}\, e^{-\frac{4\ \mu_e \cdot V \cdot t}{W^2}} \tag{4.6}$$

The total charge flow due to electrons is therefore:

$$Q_e = \int_0^t i_e\ dt$$

$$= q\ \frac{x_0^2}{W^2}\left(e^{\frac{4\ V \cdot \mu_e \cdot t}{W^2}} - 1\right) \tag{4.7}$$

The electron is collected after a time T_e given by:

$$T_e = \frac{W^2}{2\ V\ \mu_e}\ \log_e\left(\frac{W}{x_o}\right) \tag{4.8}$$

Substituting in (4.7), the total charge Q_{eo} due to the electron is given by:

$$Q_{eo} = \frac{q \cdot x_0^2}{W^2}\left\{\left(\frac{W}{x_0}\right)^2 - 1\right\}$$

$$= q\ \left(1 - \frac{x_0^2}{W^2}\right) \tag{4.9}$$

For the hole we have:

$$\frac{dx}{dt} = E\ (x\ p_h = -\frac{2\ V}{W^2} \cdot x \cdot \mu_h)$$

$$\therefore\ x = x_0 \left(e^{-\frac{2\ V \cdot \mu_h \cdot t}{W^2}} \right) \qquad (4.10)$$

Also,

$$\frac{dQ}{dt} = i_h = \frac{4\ V}{W^4} \cdot q \cdot \mu_h\ x^2 \qquad (4.11)$$

$$\therefore\ ih = \frac{4\ V \cdot q \cdot \mu_h \cdot x_o^2}{W^4}\ e^{-\frac{4\ V \cdot \mu_h \cdot t}{W^2}}$$

$$Q_h = \int_0^t i_h\ dt.$$

$$= \frac{q\ x_0^2}{W^2} \left(1 - e^{-\frac{4\ V\ \mu_h\ t}{W^2}} \right) \qquad (4.12)$$

Equation (4.12) shows that the hole collection waveform is a negative exponential and requires an infinite time to be completed. The time constant is:

$$\frac{W^2}{4\ V \cdot \mu_h}$$

We have

$$\text{Total charge due to hole} = Q_{ho} = \frac{q\ x_o^2}{W^2} \qquad (4.13)$$

$\therefore$ Total charge (electrons + holes) = q

This is expected.

Fig. 4.4 shows the pulse shape which is produced. We see that this is much more complicated than the p-i-n detector case and practical use of these

equations is very limited. However, it is interesting to calculate the time constant $\frac{W^2}{4\ V \cdot \mu_h}$ for a silicon detector made from p-type material.

We have:

$$W = 0.33\sqrt{\rho V} \times 10^{-4}$$

$$\mu_h \simeq 500\ \text{cm}^2/\text{V sec.}$$

$$\therefore \text{ Hole collection time constant} = \frac{\quad}{2000} \times 10^{-9} \text{ sec}$$

$$= \frac{\quad}{2000} \text{ n sec} \qquad (4.14)$$

If = 1000 cm

Hole T.C. = 0.5 nsec.

The electron component in the output signal is much faster than this. These results indicate the possible uses of such detetors for fast timing applications.

The very fast apparent charge collection time in a p-n junction detector introduces the possibility that other factors limit the rise time of the output signal. For example, the dense plasma of holes and electrons produced by a heavily ionizing particle must be eroded away partly by self-diffusion before the holes and electrons can be considered to be moving under the influence of the applied electric field. The significance of this is indicated by the fact that a fission fragment track might contain 10^{18} hole-electron pairs per cm^3 immediately after its formation and this is about five orders of magnitude higher than the equilibrium density of acceptors in the material. A similar situation, though not so exaggerated, exists for alpha particles. It is very likely that the ultimate timing possibilities of such semiconductor detectors will be limited by factors like this but insufficient evidence exists at the present time to determine the limit set by plasma erosion.

Another degradation of output signal occurs due to the series R, shunt capacity time constant of the detector. If the detector is made with good

low sheet resistance n^+ and p^+ layers on front and back and is operated in a punched-through mode this is not an important factor.* However, if the detector volume is only partly depleted, the series resistance of the undepleted bulk may be a serious factor in limiting the speed. As an illustration we might consider a detector made with 500 cm silicon (p-type) on a wafer thickness of 500 microns but depleted only to a depth of 100 microns. If the detector is of 1 cm^2 area, its capacity will be about 100 pF and the resistance of the 400 microns of undepleted bulk material will be 20 ohms. The resulting RC time constant is 2 nsec. The time constant for hole-collection in this detector is only 0.25 nsec - showing that rise time in a case like this may be limited by the combination of detector capacity and series resistance.

Two further possible limitations can be discussed using the example of the previous paragraph. We will suppose now that the wafer had been thinner so that the undepleted bulk was negligible. It is necessary to apply 200 Volts to this detector to deplete 100 microns. The peak electric field is 4×10^4 V/cm and, assuming a hole mobility of 500 cm^2/V sec., the hole velocity should reach 2×10^7 cm/sec. We note that the peak field is in the range where junction non-uniformity may cause small avalanching effects (called microplasma) making the device noisy. Moreover, the calculated hole velocity is larger than the 10^7 cm/sec at which the mobility falls off. The result of this is to slow down the hole collection somewhat. However, the effect is a minor one as the holes spend most of their time in the regions of lower electric field where normal mobility may be assumed.

---

*For very fast timing purposes a punch-through device made on high resistivity material is best. By applying a large over-voltage the electric field becomes constant across the device. We note that a carrier traveling at 2×10^7 cm/sec (a good value for the saturation velocity) crosses a 25 micron region in 0.1 nsec.

We see that the pulse shape obtained by collection of a single hole-electron pair in a p-n junction detector is quite complex and, moreover, the collection times are so short in thin sensitive regions that secondary effects often determine the output pulse shape. There is therefore little point in extending the topic of p-n junction detectors to deal with the complications which arise when collecting a track of ionization. However, the problem is more manageable and important in the p-i-n detector and we will now examine it for some types of radiation.

4.1.3 Pulse Shape Distribution for Gamma-rays in Germanium P-I-N Detectors at 77°K.

Gamma-rays in the energy range of commonest interest may be considered to possess a low probability of interacting in a germanium detector. Moreover, if the detector's linear dimensions are about 1 cm, the range of the electrons produced by the gamma-ray is small compared with the sensitive thickness of the detector (at 1 MeV the electron range in germanium is less than 1 mm). Therefore we may consider gamma-rays in this energy range to produce a uniform distribution of events in the detector volume and the ionization due to each event to be localized at a point. These arguments must not be applied to the case of low-energy gamma-rays where the absorption in the front region shields the beck regions giving a non-uniform event distribution, nor can they be applied to very high-energy gamma-rays where the range of electrons produced by the gamma-rays is a large fraction of the detector dimensions. These restrictions limit the validity of this discussion to the energy range of about 100 keV to 2 MeV.

Since we can now regard the ionization produced by an interaction as being localized at a point, a pulse shape like that in Fig. 4.2 will apply

to a single event uith the vertical scale being multiplied by the ratio E/ . The relative electron and hole contributions to the total signal will depend upon the exact location of the event in the detector. However, in Fig. 4.2 the hole mobility was assumed to be much smaller than the electron mobility. As seen in Fig. 1.2, the calculated hole mobility at 77°K is slightly higher than the calculated electron mobility. In practice, due to the velocity saturation phenomena in germanium at field strengths in excess of 1000 V/cm (which is commonly used for detectors), it appears that one can assume that both carriers travel at 1.5×10^7 cms/sec.* Therefore, if an ionizing event occurs at distance x_o from the negative electrode the range of pulse shapes will be as shown in Fig. 4.5. We note that the fastest pulse occurs when the event is at the middle of the sensitive region. Moreover, since we are assuming an equal probability of an event occuring at any position, pulse shapes in the range shown in Fig. 4.5 are equally probable.

The spread in pulse shape indicated by Fig. 4.5 has two possible consequences. From the point of view of energy measurements, it may cause a spread in pulse height following the shaping network of the amplifier (see section 3.4). Present limitations on the thickness of germanium detectors (~ 1 cm) which limits the maximum collection time to aoout 60 nsec and use of typical shaping network time constants in the 1 psec region have made this an unimportant ractor up to the present time. However, as thicker detectors are developed it may become significant and, if so, the effect (which is amenable to calculation) will influence the choice of optimum shaping network. A more important consequence of the spread in pulse shape, at the present time, is its effect on the fast

*This value appears to be the best fit to data we have obtained as well as being close to that measured by Prior.[16]

timing possibilities of germanium detectors. Here a timing pulse is obtained when the pulse crosses a fixed threshold level. The relative probability of the delay between the gamma-ray and the timing pulse having a value t is easy to calculate for the shape distribution of Fig. 4.5 and is shown in Fig. 4.6. Here the factor is the setting of the threshold pulse discriminator expressed as a fraction of the total pulse height. We see that the distribution of time delays is characterized by a sharp peak obtained from events in the central region of the detector and a flat distribution due to the events in the outer regions. In most practical. applications a range of gamma-ray energies occurs resulting in a further time spread. However, we have used 3 mm thick germanium detectors observing two gamma-ray lines (70 and 80 keV) with a fast coincidence resolving time between the detectors of less than 5 nsec (FWHM).

In the foregoing discussion we have made the assumption that the sensitive region of the detector was completely intrinsic so the electric field was constant through the whole volume. If this is not true, further time spread may occur. In practice many detectors appear to contain substantial regions which are poorly compensated.* These regions cause many very slow pulses which degrade energy spectra as well as coincidence resolution. T. K. Alexander[17] has used a shape discrimination system to eliminate these slow pulses.

---

*We tend to attribute this to the presence of impurities such as iron, nickel, etc. in germanium. The lithium compensates the acceptors due to these atoms at the drifting temperatures but these impurity atoms deionize well above 77°K resulting in overcompensated regions.

4.1.4 Pulse Shape Distribution for Protons and Alpha Particles Stopping in a Lithium-Drifted Silicon Detector.

This is a case where detector pulse shape can seriously influence energy resolution and it is important to be able to determine the pulse shape to evaluate its effect. We will consider here the pulse shape due to absorbtion of alpha-particles in the range 40-90 MeV incident normal to the surface gold layer of a lithium-drifted silicon detector. Ionization is produced along the entire track but its highest density is toward the end of the particle's range. The detector output signal will consist of the integral of a large number of pulse shapes like that of Fig. 4.2. No analytical solution is available for this problem. However, the author has carried out a numerical computation on a digital computer and Fig. 4.7 shows the results of the calculation for alpha-particles in a 3 mm thick lithium-drifted silicon detector with 350 V applied to it (at 25°C). This calculation is performed by dividing the detector into slices .010 cm thick, calculating the energy absorbtion in each slice using a relationship of the form Range = constant x $E^{1.73}$, and finally integrating the signals due to each slice. A similar method can be applied to other particles.

In the particular case shown in Fig. 4.7 the change in rise time which occurs for different energies causes a non-linearity in the overall energy response of the detector-amplifier combination (see Table 1.2). Moreover, the worsening of energy resolution observed in experiments at energies where the particles only just stop in the detector indicates that a statistical process involved in the length of the particle track produces rise-time

variations which thereby cause a spread in pulse height ac the output of the amplifier system.

4.2 RADIATION DAMAGE IN DETCTORS

Except in the case of some minor applications of detectors as radiation dosimeters the only useful interactions between radiation and the detector material are those producing hole-electron pairs in the material. In this case the normal equilibrium of the material is restored in a very short time and we use only the transient effect for measurements. However, radiation in its many forms can interact with atoms in the lattice structure and displace them from their lattice sites. Each such interaction produces at least one vacancy and an interstitial atom in the lattice. This vacancy-interstitial pair is known as a Frenkel pair or Frenkel defect. In general, the atom ejected from its lattice site carries enough energy to displace further atoms and more than one Frenkel pair is produced by an interaction. The quantity of defects produced by a single interaction and the probability of occurrence of a damaging interaction depends upon the type and energy of the radiation. Dearnaley treats this problem in some detail in his book[18] and we will use his results in this discussion.

4.2.1 Damage Mechanism

The discussion which follows will deal with collisions between an incoming particle and the semiconductor atoms. Gamma-rays interact in the material to produce electrons with energies ranging up to the gamma-ray energy and, therefore, the damage caused is similar to that of fast electrons. Different types of particles react (with the atoms which constitute the lattice) in different ways and this causes the amount and character of the damage to differ considerably. Fast neutrons have very low probability of

producing direct hits with silicon* atoms but the average energy acquired by the silicon atoms from the collisions is quite high. The resulting energetic silicon atom produces many secondary defects and the overall damage to the material is characterized by small highly damaged regions separated by considerable amounts of undamaged material. In contrast to this, heavy charged particles interact with silicon atoms by Rutherford scattering (mutual electrical repulsion) so there are large numbers of low energy exchanges and very few silicon atoms acquire high enough energies to produce substantial numbers of secondary defects. Damage by fast electrons is influenced largely by the fact that a silicon atom can acquire little energy when an electron collides with it. Therefore damage is limited almost entirely to the few silicon atoms which acquire sufficient energy to be displaced from the lattice. For low electron energies (< 250 keV in Si; < 600 keV in Ge) no collision can give sufficient energy to a lattice atom to displace it. Measurements of the energy required to displace a silicon atom indicate that 25 to 30 eV is necessary.

The case of slow neutron damage is a little different from those discussed above. Here the capture of a neutron by Si^{30} (4% of silicon) produces P^{31} and a -particle whose energy ranges up to 1.5 MeV. Damage of the Frenkel defect type is produced by the electrons as in the previous paragraph. However, the phosphorous atoms now act as donors in the lattice and the bulk resistivity changes. This can be considered to be damage or a desirable result depending upon its effect on detector performance.** Fortunately the cross-section for this process is small.

---

*We will deal only with silicon in this discussion. Radiation damage in germanium detectors used only for gamma-rays appears likely to be small. However, germanium detectors will be very susceptible to damage if used in a significant flux of neutrons. The effects of the damage may not be evident, however, as long as the detector is maintained at a low temperature where diffusion of lithium and vacancies is negligible.

**The production of P^{31} by slow neutron bombardment has been used as a method of compensating p-type material to produce high resistivity silicon.[20]

A case which defies analysis is that of fission fragment damage. The intense damage spike produced by the entry of highly charged heavy particles and deposition in the lattice of radioactive nuclei is too complicated a process to permit detailed understanding. However, in p-n junction detectors, it is known that the damage tends to produce more intrinsic material than was present before irradiation. This presumably results from the production of donors and acceptors near the middle of the band-gap of the material.

From these general considerations we conclude that the most important types of damage to the nuclear spectrocopist, not concerned with heavy ion or fission fragment research, are likely to be those due to fairly heavy charged particles (such as protons or alpha particles) and to fast neutrons. The cross section for fast neutron collisions is about 3×10^{-22} cm^2 (corresponding to a mean free path of about 0.5 cm) and the energy distribution of Si recoils is flat up to E_{max} where E_{max} is given by:

$$E_{max} = 0.133\ E_n \qquad (4.15)$$

The average energy of the recoils is therefore half this value. The energy of the silicon recoil atom is partly expended in producing ionization and partly in producing secondary defects. As long as the silicon nucleus is moving at high velocity it will be stripped of some of its atomic electrons and therefore behave as a charged particle. As it slows down it will become uncharged by capturing electrons. The threshold energy of an uncharged silicon atom to produce ionization is 7 keV and therefore the minimum number of defects per neutron collision (assuming $E_{RECOIL} > 7$ keV) is $7000/E_d$ where E_d is the energy required to displace a silicon atom.* This means

*Very little of the silicon atoms energy is likely to be lost to vibrational modes of the lattice as the wavelength equivalent of the silicon atom is much smaller than the lattice dimensions.

that each neutron collision produces a minimum of about 300 Frenkel pairs. Depending upon the fraction of the primary silicon atom's recoil energy used up in ionizing collisions before it slows down to the 7 keV level the number of Frenkel pairs produced can range from 300 to about $\frac{E_{max}}{2\ E_d}$. If E_{max} = 1 MeV this upper limit is well over 1000 defects. It is likely that most of the energy above 7 keV will be lost by ionizing collisions and, for the moment, we will assume that 500 defects are produced per fast neutron collision. 10^{10} neutrons/cm^2 will then produce about 2×10^9 primary recoils in a 0.1 cm thick (1 cm^2) slab of silicon and 10^{12} total Frenkel defects will be produced in the material as a result of this bombardment.

In the case of charged particles, such as alpha-particles, the mean energy acquired by the primary silicon recoils is low but the number of primary recoils is large. Dearnaley has analyzed this situation and Fig. 4.3 shows his results for alpha-particles and protons. Integration of the curve to determine the total number of defects produced by a 40 MeV alpha-particle shows that it leaves about 400 defects along its track. This means that 10^{10} such alpha-particles will leave about 4×10^{12} defects in a 0.1 cm thick piece of silicon. This is about the same number as was calculated for the fast neutron case but the defects have a different spatial distribution in the material.

4.2.2 Consequences of Damage in p-n Junction Detectors

A confusing mass of literature exists on the results of radiation damage to detectors. Most of the experimental data has been obtained under poorly controlled conditions in which the measurement of damage was a secondary objective in a nuclear experiment. Moreover the consequences of irradiation

depend on the type of detector and they may depend upon details of the manufacturing process. To provide a logical interpretation of the results some restrictions must be placed upon the scope of the following discussion. In particular we will not discuss surface barrier detectors as the lack of knowledge of the nature of the barrier makes it difficult to assess the likely effect of radiation in the barrier itself. There is evidence that the barrier is damaged by quite small doses of fission fragments ($\sim 10^7/cm^2$). We will further restrict the discussion by eliminating consideration of any deleterious effects produced by radiation in the surface layer at the edge of the junction. There is evidence that surface properties can be affected in certain radiation environments but the effects are complex and are quite unimportant in the case of detectors used for spectroscopy.

These restrictions limit us to considering the coasequeaces of bulk damage of the Frenkel defect type in silicon p-n junction and lithium drifted silicon detectors. It is necessary to realize at the outset that the probable consequences of damage to a detector are directly related to the ratio of the number of active acceptor (or donor) atoms in the bulk to the number of defects produced by the radiation. If few defects are produced compared with the acceptor concentration,the effect of the damage on the detector properties is likely to be small. A consequence of this is that p-n junction detectors - particularly those made with low resistivity bulk material - are much less prone to damage than lithium-drifted detectors. One might argue that this is, in fact, a consequence of the thickness of the detector which is, of course, related to the resistivity.

From Fig. 1.3 we see that the acceptor concentration in the bulk of a detector made from 1000 ohm cm p-type silicon is about 2×10^{13} atoms/cm^3. We would therefore be surprised if a defect level close to this could not be tolerated. According to Dearnaley's calculations this will correspond to the damage produced by about 10^{11} alpha-particles (40 MeV), 10^{11} fast neutrons, 5×10^{11} protons (10 MeV) or 10^{14} fast electrons. Here we are assuming that each defect finally behaves as an acceptor or donor. In fact, the effects of damage become evident at just about these doses. However, the details of the damage process and its precise effect in detector characteristics are not easy to explain. In one group of detectors[21] made from p-type bulk material the effect of electron irradiation was to increase the bulk resistivity but the effect of proton irradiation was the reverse. In the first case, the damage did not anneal out over a long period of time but it did so to a big extent in the second case. Any explanation for these results must postulate the formation of different sets of levels due to the defects or due to their migration through the lattice. Pairing of vacancies and oxygen atoms has been postulated as one factor in this process. Presumably the striking difference between the effects of electrons and protons must be associated with the different densities of defects in the "spikes" produced by the two types of particles. One is tempted to explain the recovery effect in the proton case by a partial re-association of vacancies and interstitials in the rather dense damage track. If this is so, a similar recovery might be expected after alpha-particle or fast neutron damage. To my knowledge, detailed measurements on this have not been reported.

The use of p-n junction detectors in fission physics research has been one of the most important areas of application of detectors for several years. It has therefore been important to consider ways to reduce the sensitivity of

these detectors to fission fragment damage. P-N junction detectors made on high resistivity p-type material (e.g., 2000 ohm cm) show severe damage effects after doses of 10^7 to 10^8 fragments/cm^2. As we might expect, reduction of the bulk resistivity to 400 ohm cm has increased the useful range into the 10^8 to 10^9 fragments/cm^2 range. Furthermore, Gibson[22] has reported excellent radiation damage behaviour in thin punched-through detectors operated at voltages much larger than those required to deplete the thickness of the wafer. This might be anticipated since the detector would be expected to operate reasonably well until the donor* (or acceptor) density introduced by the damage process was high enough to prevent the punch-through condition.

Apart from the effect of damage on the bulk resistivity of the detector material (which causes electric field changes), the levels introduced in the forbidden gap provide recombination and generation centers. Consequently the detector leakage current tends to increase and significant amounts of charge may disappear during the charge collection process. Since these effects may not be uniform in the whole sensitive volume of the detector, worsening of energy resolution and the appearance of multiple peaks in the amplitude spectrum are common signs of substantial radiation damage.

4.2.3 Consequences of Damage in Lithium-Drifted Silicon Detectors.

From the considerations outlined in the previous section it will be obvious that these detectors are more sensitive to damage than the p-n junction detectors. In our experience the worst effect of the damage is to prevent total depletion of the detector thickness by the applied voltage.

*There is evidence that fission fragment damage at least in p-type material tends to make the material change in an n-type direction.

We will consider a 3 mm thick silicon detector with 300 V applied to it. We can easily show that this will only just be depleted if 2×10^{10} acceptors/cm^3 are introduced uniformly through the material. In 3 mm thickness this means that about 10^{10} acceptors/cm^2 are permissable. From section 4.3.1, we can see that 10^{10} neutrons/cm^2 produce about 3×10^{12} defects in 3 mm of silicon. Alternatively 10^{10} 40 MeV alphas/cm^2 produce about the same number of defects. We might therefore expect signs of damage* to occur at neutron or alpha doses of about 10^8/cm^2. Results in agreement with this conclusion have been reported by Mann and Yntema[23].

Our own experimental observations on damage in lithium-drifted silicon detetors induced during nuclear reaction experiments in the bombarding particle energy range from 20 to 120 MeV are of' interest in throwing some light on the damage process. In summary these results are as follows:

(a) For practical purposes, damage in such scattering experiments is almost entirely due to fast neutrons. These neutrons originate at the target, collimating slits, and in the carbon absorber of the Faraday-cup. Clear proof that damage is due to neutrons is afforded by the observation that damage is not confined to the region of the collimating slit image in the detector.

(b) The dominant consequence of the damage is the appearance of a dead layer at the entry window of the detector. Increasing the applied voltage can correct this up to the limit at which edge breakdown causes substantial noise.

---

*It seems likely, and is experimentally observed, that the failure to deplete the material, with consequent appearance of a dead layer at the entry face of the detector, is the most impor tant consequence of damage. Leakage current and charge loss during collection are negligible.

(c) After irradiation, the effects of the damage increase by a large factor over a period of several weeks. We deduce from this that the vacancies/interstitial pairs have very little direct effect on the electrical behavior of the detector. However, migration of the vacancies and lithium atoms may cause lithium precipitation at the vacancies in due course. Thus, the donors are slowly removed and the material becomes uncompensated. A consequence of this is that detectors show no signs of damage during experiments until they have received neutron doses much larger than the $10^8/\text{cm}^3$ mentioned earlier.

(d) No increase in leakage due to either surface or bulk effects is noted at the radiation levels at which the previously mentioned effects occur.

(e) No shift of peaks in spectra is observed, nor does the energy resolution change until the dead layer appears.

(f) In fast coincidence experiments a change in timing is the first apparent effect of radiation damage. In a sensitive experiment this can be observed for a total dose an order of magnitude smaller than that at which any dead layer is seen. The change in timing results from electric field lines terminating on radiation produced acceptors thereby reducing the electric field in the region toward the back of the detector.

While some workers have reported cases where the characteristics have been recovered by redrifting the lithium, our results, if correctly interpreted, offer little hope of any substantial improvement in the radiation sensitivity of lithium-driited detectors. Almost perfect material is required for thick detectors and an unfortunate consequence of radiation damage is that

we no longer have adequate material. Repurification of the mateial and recrystallization may well be the only solution to damage in this case.

ACKNOWLEDGEMENTS

Many people have contributed ideas and effort to these notes. In particular, I should like to thank W. Hansen, R. Lothrop, M. Roach, B. Jarrett, D. Landis, R. Pehl, and S. Antman for spending valuable time discussing various aspects of the lectures. My thanks are also due to several experimenters in the Nuclear Chemistry Department of the Lawrence Radiation Laboratory for their stimulation and constant interest in developing and using detectors. Without their active support little of this work would have been possible. Finally thanks are due to Leo Schifferle and Mary Thibideau for their constant help in preparing the script and figures.

This work was carried out as part of the program of the Nuclear Chemistry Instrumentation Group of the Lawrence Radiation Laboratory supported by A.E.C. contract No. W-7405-eng-48.

LECTURE 4. FIGURE CAPTIONS

Fig. 4.1 Collection of Hole-electron Pair in a p-i-n Detector (No Velocity Saturation Case)

Fig. 4.2 Signal Output Due to a Single Electron Hole Pair in a p-i-n Detector.

Fig. 4.3 Collection of Hole-Electron Pair in a P-N-Junction (No Velocity Saturation Case)

Fig. 4.4 Signal Output due to a Single Electron-Hole Pair in a P-N Junction Detector.

Fig. 4.5 Expected Range of Pulse Shapes from p-i-n Germanium Detector at 77°K. (Assuming V > 1000 Volts/cm)

Fig. 4.6 Distribution in Triggering Delays of a Discriminator set to -Peak Pulse Amplitude from a Germanium Detector.

Fig. 4.7 Detector Pulse Shape for Alphas
(Silicon Detector W = 3 mm,)
V = 350 V,
T = 25°C.

Fig. 4.8 Frenkel Defect Production by Alphas and Protons (Silicon) (After Dearnaley)

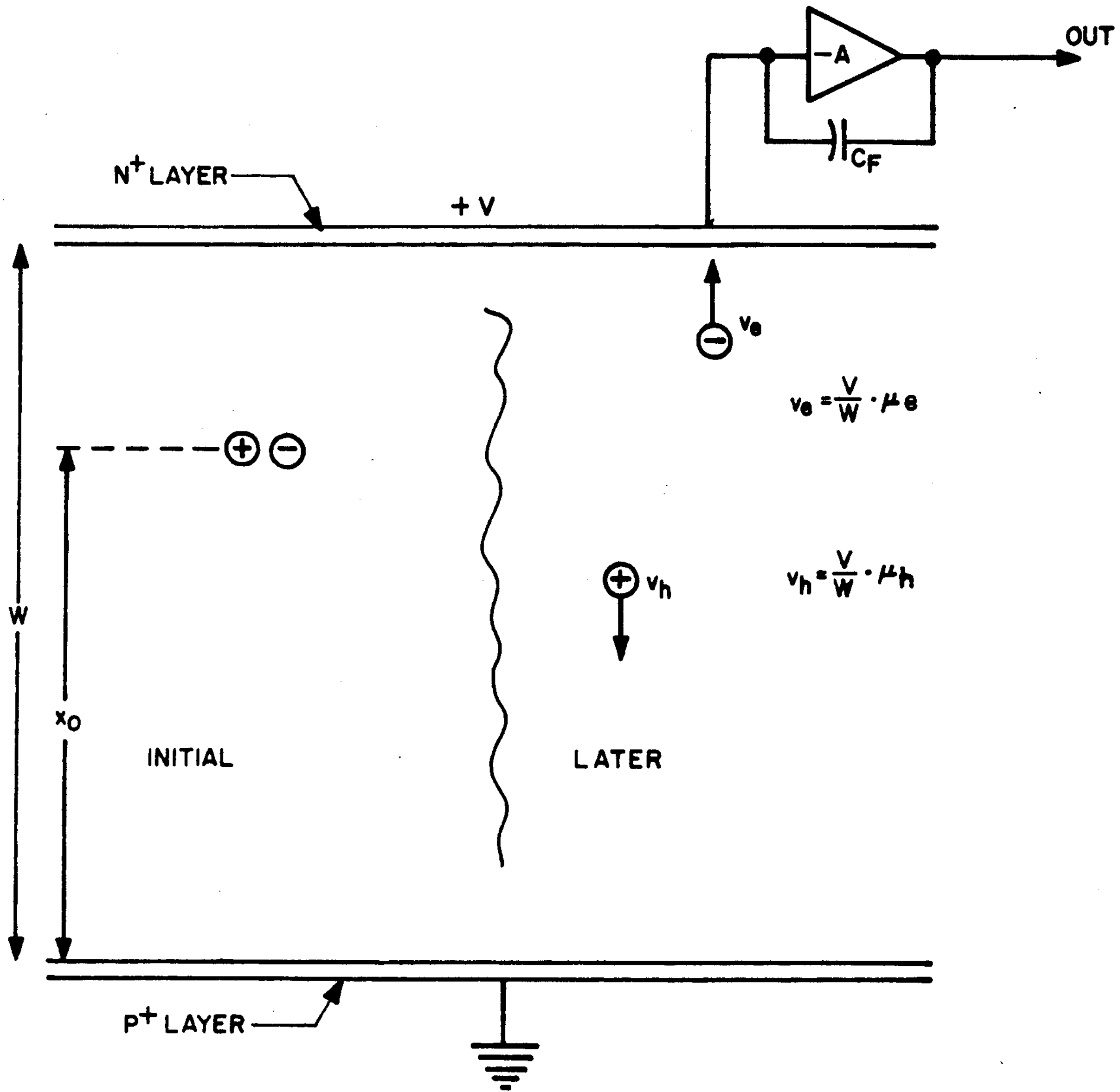

FIG 4.1
COLLECTION OF HOLE-ELECTRON PAIR IN A P-I-N DETECTOR (NO VELOCITY SATURATION CASE)

MUB-7018

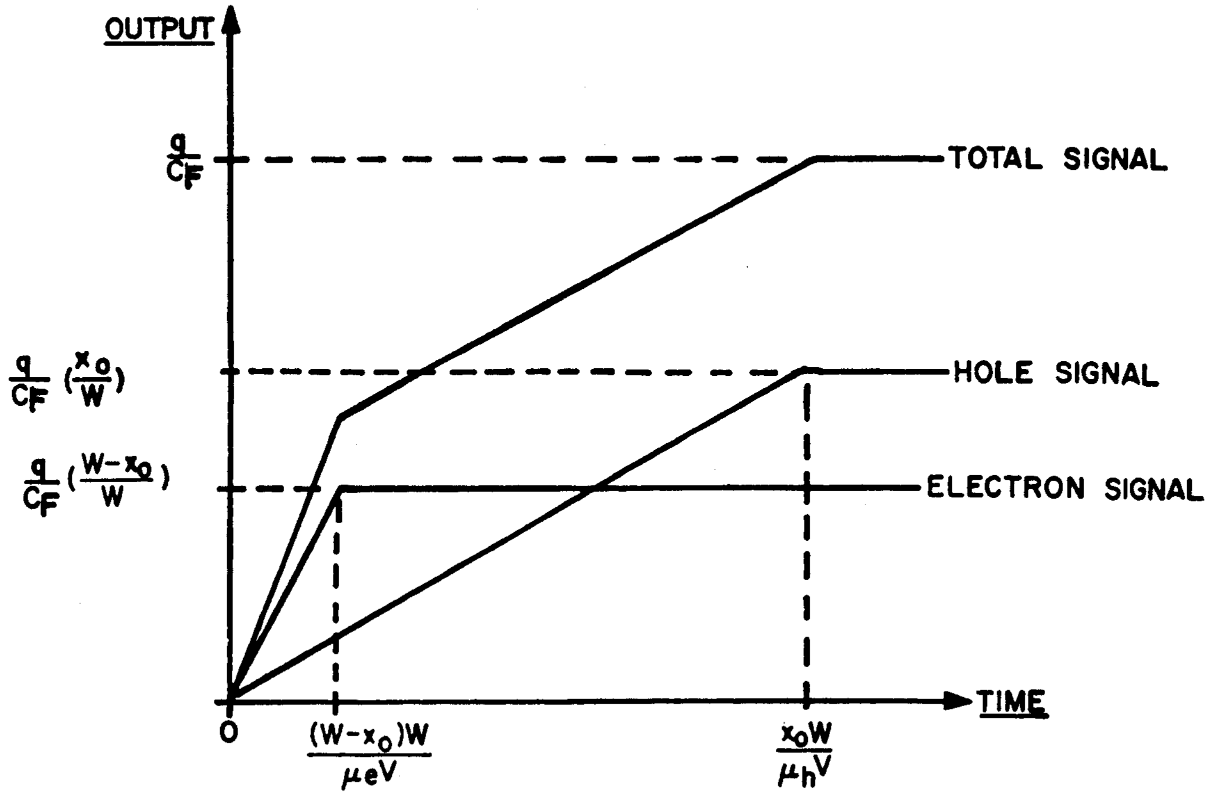

FIG 4.2 SIGNAL OUTPUT DUE TO A SINGLE ELECTRON HOLE PAIR IN A P-I-N DETECTOR

MUB-7019

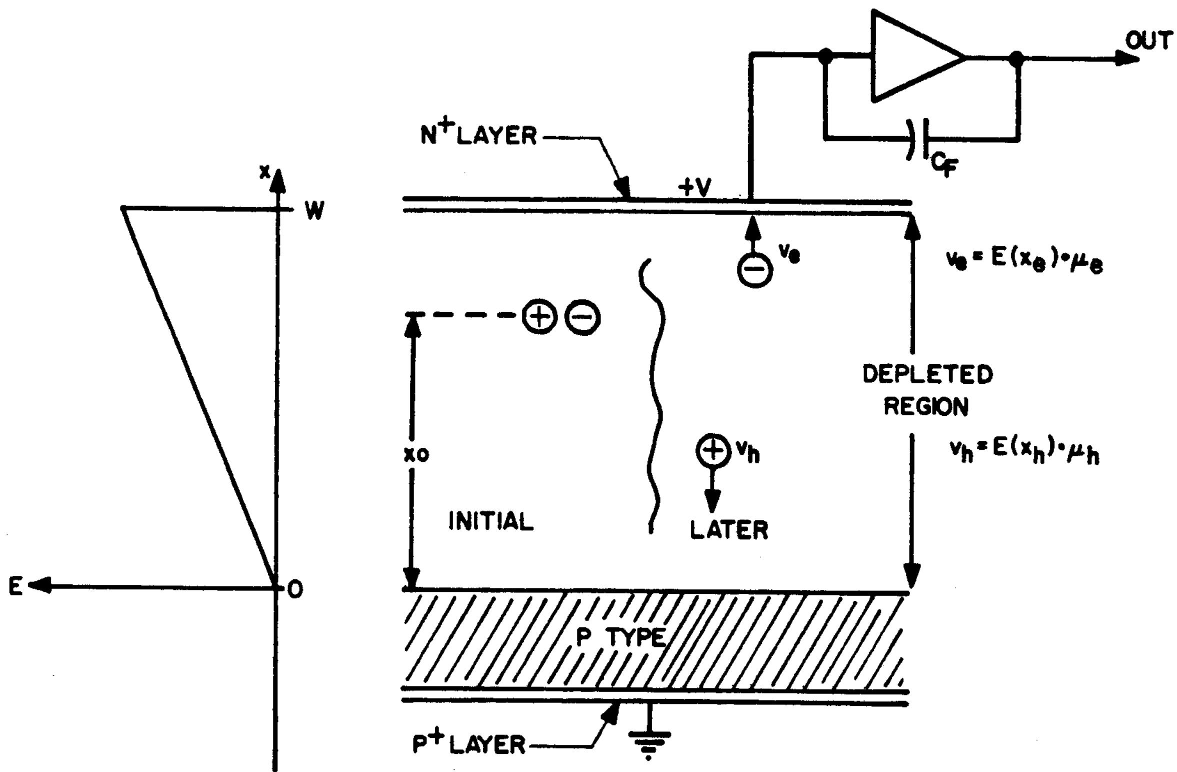

FIG 4.3
COLLECTION OF HOLE-ELECTRON PAIR IN A P-N JUNCTION (NO VELOCITY SATURATION CASE)

MUB-7020

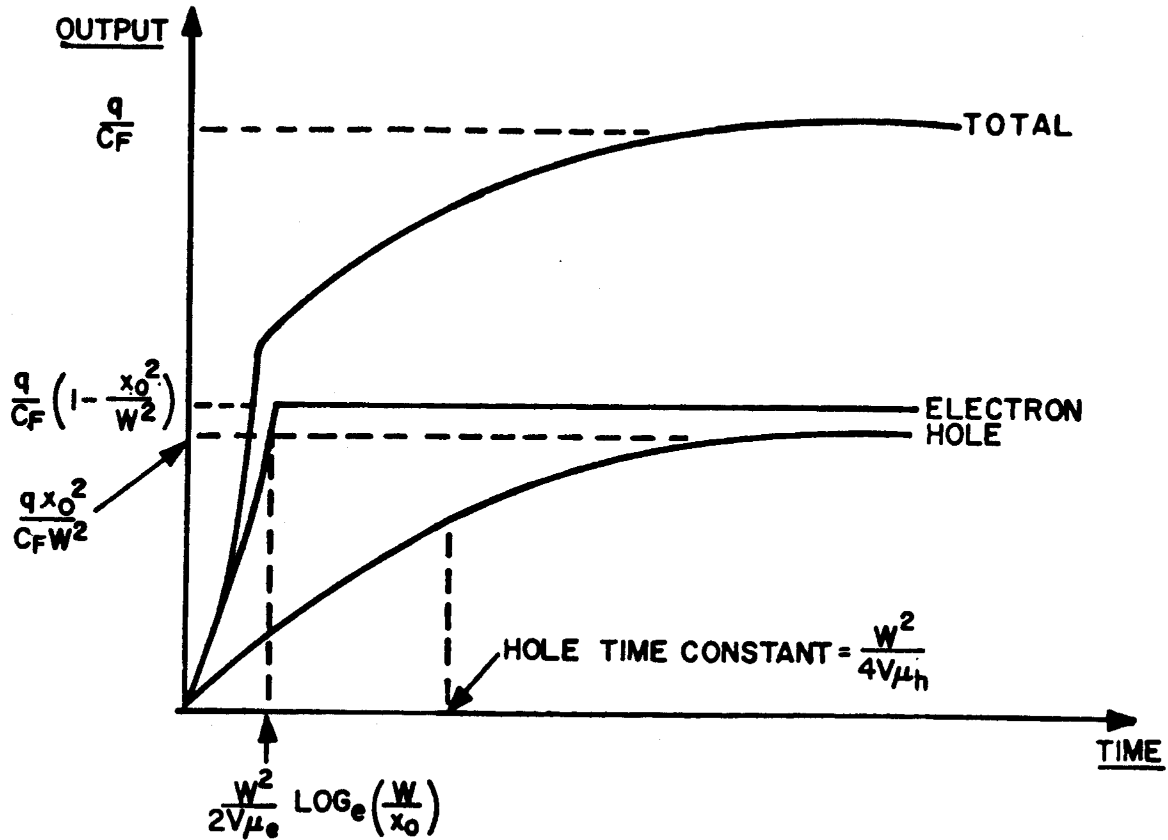

FIG 4.4
SIGNAL OUTPUT DUE TO A SINGLE
ELECTRON-HOLE PAIR IN A P-N JUNCTION DETECTOR

MUB-7021

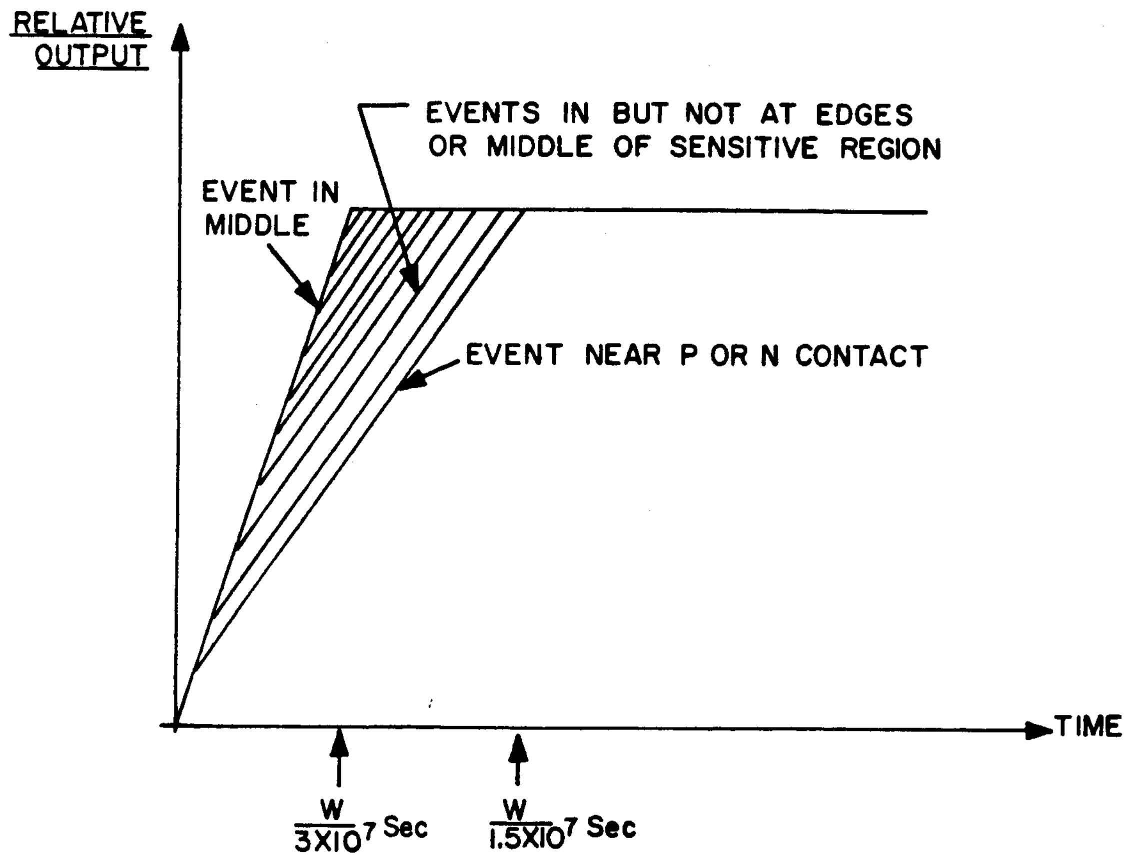

FIG 4.5
EXPECTED RANGE OF PULSE SHAPES FROM P-I-N GERMANIUM DETECTOR AT 77°K (ASSUMING V > 1000Volts/cm)

MUB-7022

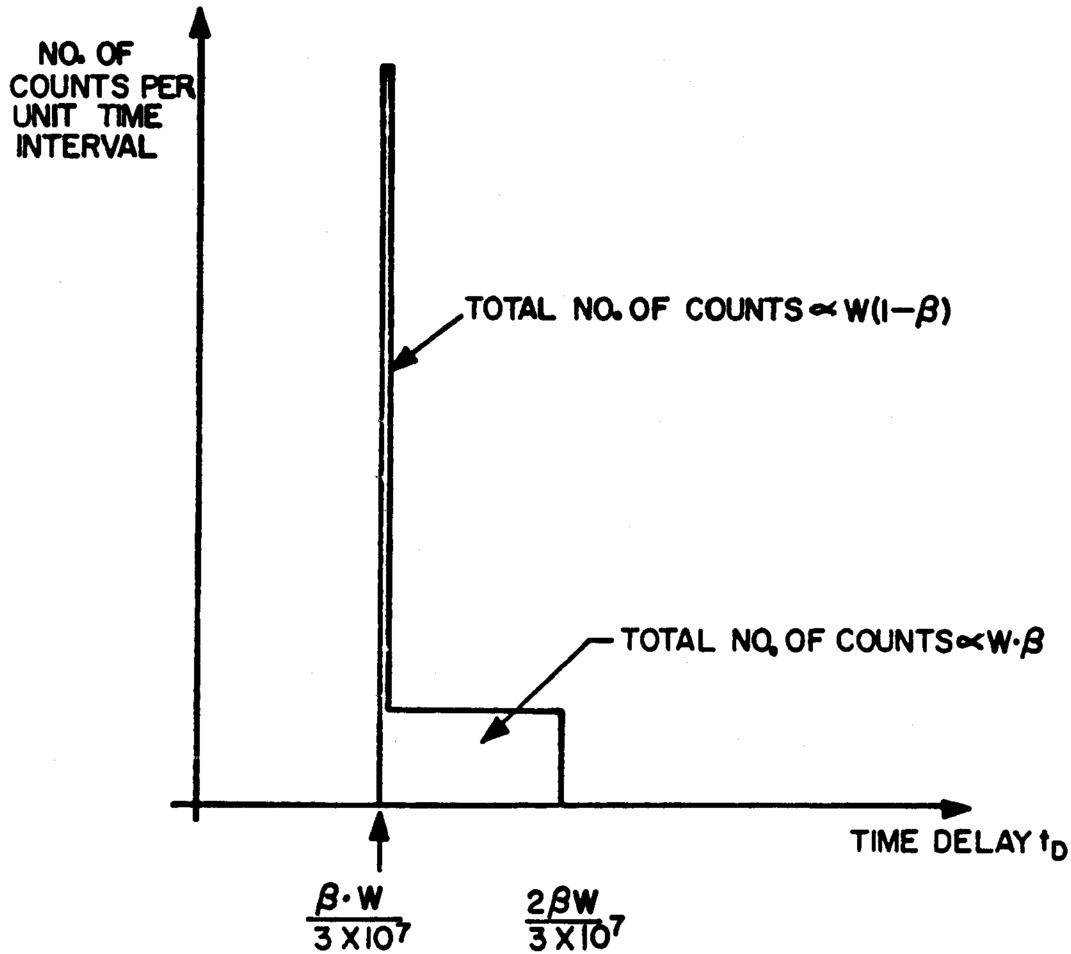

FIG 4.6
DISTRIBUTION IN TRIGGERING DELAYS OF A DISCRIMINATOR SET TO β• PEAK PULSE AMPLITITUDE FROM A GERMANIUM DETECTOR

MUB-7023

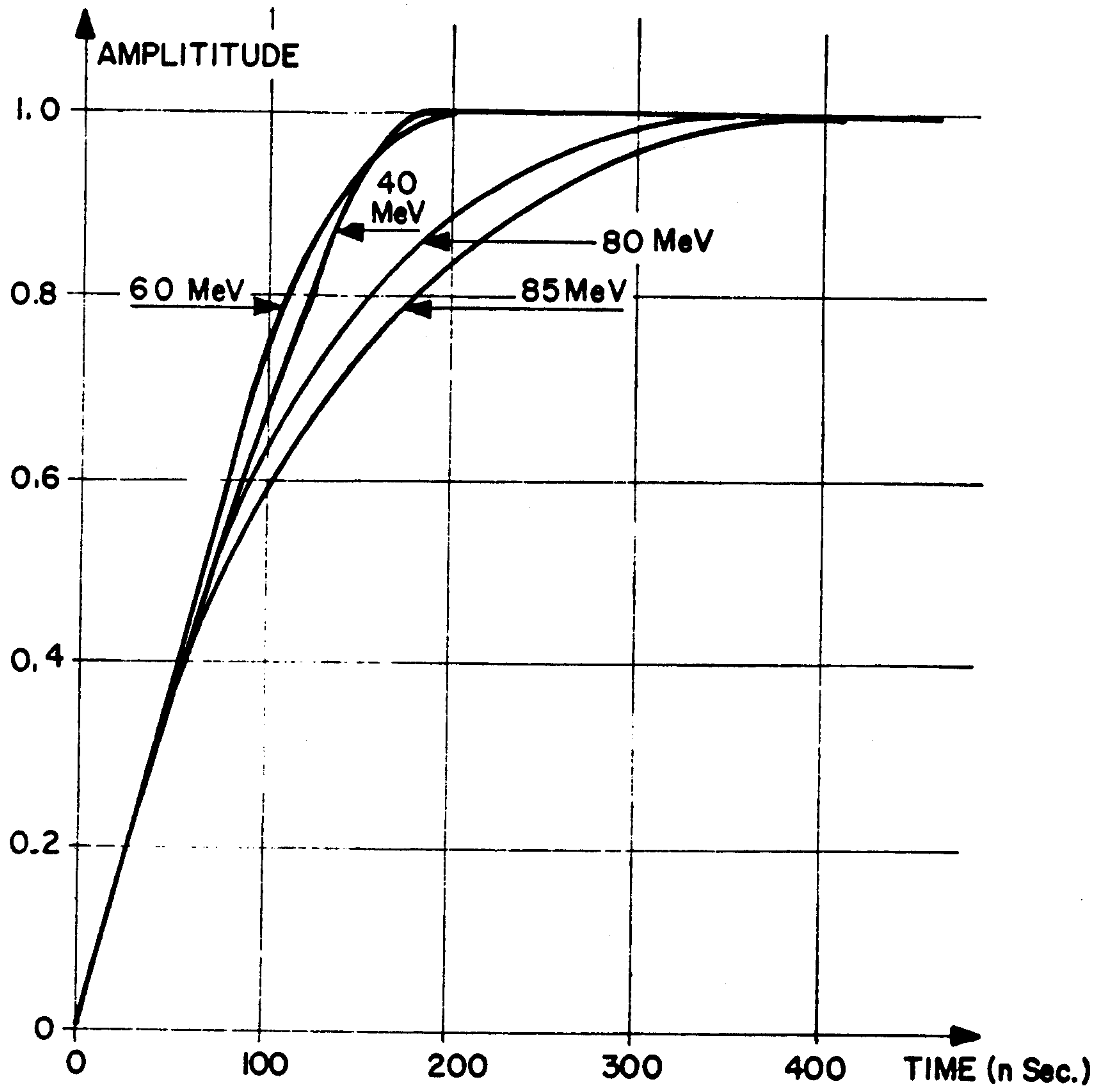

FIG 4.7
DETECTOR PULSE SHAPE FOR ALPHAS
(SILICON DETECTOR W=3mm, V=350V, T=25°C)

MUB-7024

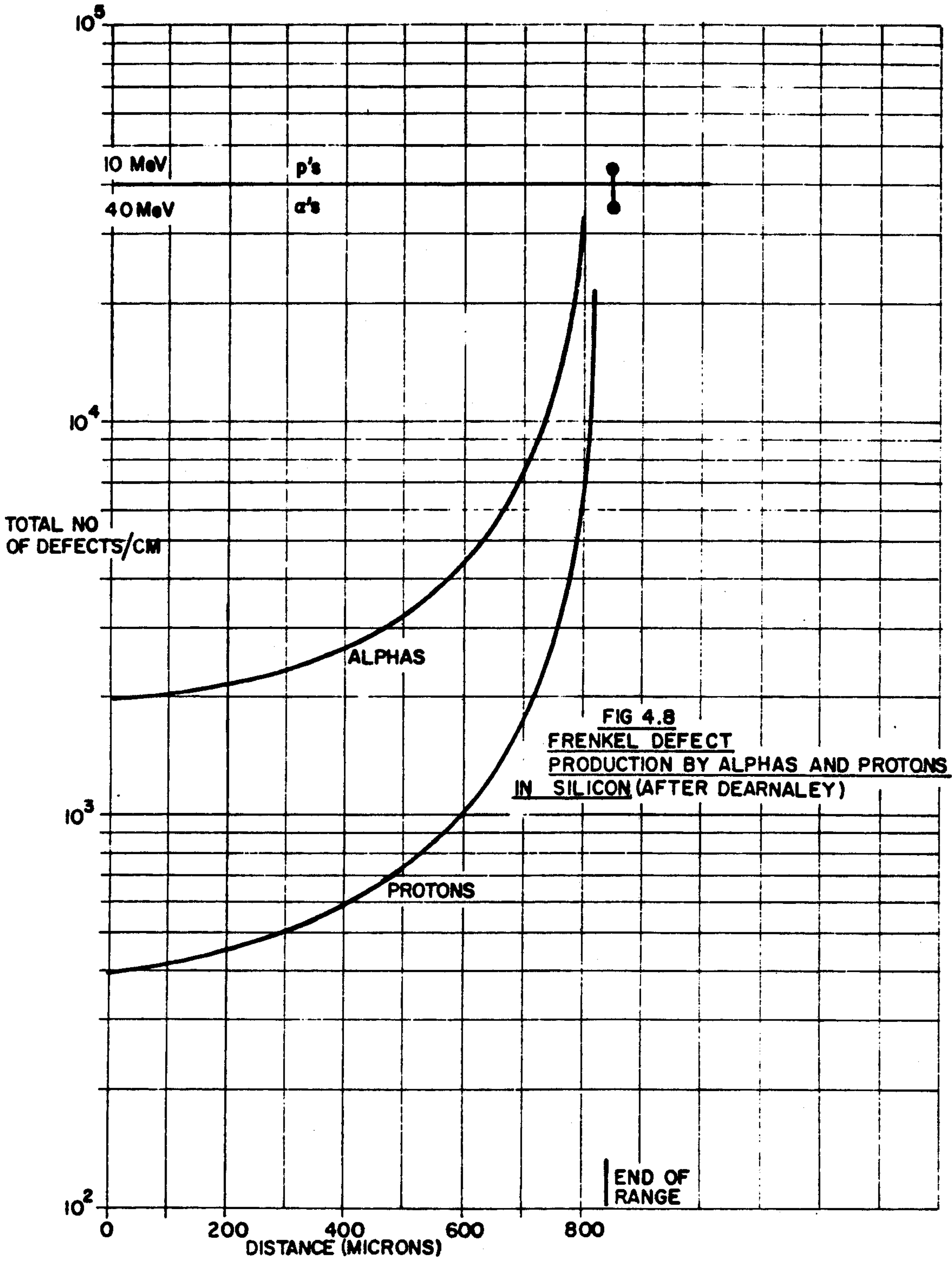

FIG 4.8
FRENKEL DEFECT
PRODUCTION BY ALPHAS AND PROTONS
IN SILICON (AFTER DEARNALEY)

MUB-7025

REFERENCES

1. V. Fano, Phys. Rev. **70**, 44 (1946).

2. V. Fano, Phys. Rev. **72**, 26 (1947).

3. J. B. Birks, Theory and Practice of Scintillation Counting (Pergamon, MacMillan, Co., New York, 1964) p. 662.

4. P. Iredale, Nuclear Inst. & Methods **11**, 336 (1961).

5. P. Thieburger, et al., Proc. of Symposium on Nuclear Instruments, Harwell, Sept., 1961 (Academic Press) p. 54.

6. W. Shockley, Proc. IRE **46**, 973 (1958).

7. T. M. Buck, Semiconductor Nuclear Particle Detectors, N.R.C. Pub. #871, p. 111 (1961).

8. F. S. Goulding, W. L. Hansen, N.R.C. Pub. #871, p. 202 (1961).

9. W. L. Hansen, F. S, Goulding, Nuclear Instr. & Methods **29**, 345 (1964).

10. R. Deshpande, Solid State Electronics **8**, 313 (1965).

11. H. Reiss, C. S. Fuller & F, J. Morin, Bell System Tech, Jour. XXXV, 535 (1956).

12. E. M. Pell, N.R.C. Pub. #871, p. 136 (1961).

13. W. L. Hansen, B. Jarrett, Nuclear Instr. & Methods **31**, 301 (1964).

14. F. S. Goulding, W. L. Hansen, IEEE Trans. on Nucl. Sci. NS-11, 286 (1964).

15. A. J. Tavendale, IEEE Trans. on Nucl. Sci, NS-11, 191 (1964).

16. A. C. Prior, J. Chem. Phys, Solids **12**, 175 (1960).

17. T. K. Alexander, et al., Phys. Rev. Letters **13**, 86 (1964).

18. G. Dearnaley, D. C. Northrop, Semiconductor Counters for Nuclear Radiations (John Wiley & Sons, Inc., New York, 1963).

19. (Not Used)

20. J. Messier, et al., IEEE Trans. on Nucl. Sci. NS-11, 276 (1964).

21. R. E. Scott, IEEE Trans. on Nucl. Sci. NS-11, 206 (1964).

22. W. M. Gibson, Private Communication.

23. H. M. Mann & J. L. Yntema, IEEE Trans. on Nucl. Sci. NS-11, 201 (1964).

24. W. Van Hoosbroeck, Private Communication.

25. A. Van der Ziel, Proc. IRE **50**, 1808 (1962).

26. A. Van der Ziel, Proc. IRE **51**, 461 (1963).

27. O. Meyer, Nuclear Instr. & Methods **33**, 164 (1965).

28. T. W. Nybakken, V. Vali, Nuclear Instr. & Methods **32**, 121 (1965).